Bachelor project

Study area	**Healthcare**
Bachelor	**Biomedical Laboratory Science**
Option	**Pharmaceutical and Biological Laboratory Science**
Academic year	**2020-2021**
Student	**Jonas Castelein**

Theme

The anti-inflammatory effect of mesenchymal stem cell-derived extracellular vesicles in Niemann-Pick disease type C1 pathology

Work placement

Inflammation Research Center VIB-UGent Vandenbroucke Lab – Barriers in inflammation

Howest – University of Applied Sciences
Rijselstraat 5 – 8200 Brugge – T 050 38 12 77 – F 050 38 11 71
brugge@howest.be – www.howest.be

Bachelor project

Study area	**Healthcare**
Bachelor	**Biomedical Laboratory Science**
Option	**Pharmaceutical and Biological Laboratory Science**
Academic year	**2020-2021**
Student	**Jonas Castelein**

Theme

The anti-inflammatory effect of mesenchymal stem cell-derived extracellular vesicles in Niemann-Pick disease type C1 pathology

Work placement

Inflammation Research Center VIB-UGent Vandenbroucke Lab – Barriers in inflammation

Howest – University of Applied Sciences
Rijselstraat 5 – 8200 Brugge – T 050 38 12 77 – F 050 38 11 71
brugge@howest.be – www.howest.be

Declaration of approval

The work placement company offers modalities to execute the bachelor project and ensures process coaching, but does not take any responsibility for the final product.

External bachelor project supervisor
Lien Van Hoecke

Internal bachelor project supervisor
Paco Hulpiau

Student
Jonas Castelein

Foreword

As a third-year student of the bachelor education 'Biomedical Laboratory Science', my final semester is devoted to an internship with a bachelor's thesis linked to it. I performed my internship at the Vandenbroucke lab at the Center of Inflammation Research at VIB-UGent. I was very lucky to be part of such a young, dynamic and enthusiastic team. From the first day, they made me feel welcome.

First of all, I would like to thank Lien, my external supervisor. This thesis wouldn't be what it is now without her guidance, support and advice. I also thank her for the techniques she taught me and for the work-related and not work-related talks between the experiments. She found a way to challenge me and make me grow as a lab technician and as a person. I also want to thank Griet, my 'stand-in' external supervisor when Lien was absent. I also learnt a lot from her and a day of laughter is always guaranteed when you work with her.

I would also want to thank Junhua. He did the imaging for all the stainings and I can assure you there were many. My thanks also go to professor Roosmarijn 'Roos' Vandenbroucke for letting me do my internship and student job in her lab and for giving me advice on the layout of this thesis. I am also grateful for my colleagues from the Vandenbroucke lab and other groups. Due to them, I learnt so many more skills and time flew by so much faster than I could imagine.

I would like to thank the lecturers from the bachelor education 'Biomedical Laboratory Science' for teaching me the past three years. In particular, thank you to Mr Hulpiau and Mr Quartier for arranging this internship and to guide me through it.

Last but not least, I would like to thank my family and my friends for supporting and motivating me.

So, with these words I would like to present you my bachelor thesis. I hope this work may learn you something and may inspire you in any kind of way.

Jonas Castelein

Abstract

Niemann-Pick disease type C1 (NPC1) is a lysosomal storage disorder caused by loss-of-function mutations of the *Npc1*-gene. The disease has many clinical features, including inflammation. Despite many years of research, a cure for this disease is not available. This bachelor thesis aims to investigate the anti-inflammatory effect of mesenchymal stem cell-derived extracellular vesicles (MSC-EVs) on NPC1 pathology. The ultimate purpose of this research is to understand the disease better and to take the first steps into finding a possible cure. For this, two separate groups of $Npc1^{-/-}$ mice are treated with MSC-EVs fraction 16.3 or MSC-EVs fraction 41.5, delivered by an external lab (from the University Hospital of Essen). Furthermore, $Npc1^{+/+}$ as well as $Npc1^{-/-}$ mice are given four intravenous injections with either a buffer or platelet-derived extracellular vesicles (EVs) as a control.

The mice are weighed before each injection. The weight gain of mice treated with MSC-EVs 41.5 is remarkable higher than the other groups. Approximately two weeks after the first injection, the mice are sacrificed. Bio-Plex is performed on both cerebrospinal fluid (CSF) and serum to determine the concentration of specific chemo- and cytokines. The results show a difference in cytokine levels between $Npc1^{+/+}$ and $Npc1^{-/-}$ mice. Furthermore, it can be derived that treatment with MSC-EV 41.5 can revert the phenotype of $Npc1^{-/-}$ mice to the phenotype of $Npc1^{+/+}$ mice. In serum, the concentration of interleukin (IL)- 12 is decreased to normal levels in mice treated with MSC-EVs 41.5. On the other hand, no differences in the concentration of keratinocyte-derived chemokine (KC) are seen between the groups. However, the concentration of KC in CSF of mice treated with MSC-EV 41.5 is decreased compared to treatment with MSC-EV 16.3.

Also, qPCR is performed on the liver, lung, spleen and different brain regions. In general, $Npc1^{+/+}$ mice show lower expression levels of chemo- and cytokines compared to $Npc1^{-/-}$ mice. Additionally, the relative expression of tumour necrosis factor (*Tnf)*, *Il-1β*, C-C motif chemokine ligand (*Ccl) 2*, *Ccl3*, *Ccl5* and C-X-C motif chemokine ligand (*Cxcl) 10* of $Npc1^{-/-}$ mice treated with MSC-EV 41.5 is decreased to levels of $Npc1^{+/+}$ mice. In some cases, T-test shows a significant difference between $Npc1^{+/+}$ control mice and $Npc1^{-/-}$ mice treated with MSC-EV 16.3, but also between $Npc1^{-/-}$ control mice and $Npc1^{-/-}$ mice treated with MSC-EV 41.5. Inducible nitric oxide synthase (*Inos)* and 'nuclear factor of kappa light polypeptide gene enhancer in B-cells inhibitor, alfa' *(Ικba)* don't show any pattern in any of the investigated tissues. *Il-4* and *Il*-6 show this pattern in the prefrontal cortex and the prefrontal cortex and olfactory bulb respectively.

Finally, immunohistochemistry (IHC) is performed. The stainings show mostly a difference between $Npc1^{+/+}$- and $Npc1^{-/-}$ mice, but not between treatment with MSC-EV 16.3 or 41.5. Only 'glial fibrillary acidic protein' (GFAP)-staining (except for the cortex-region) and 'ionized calcium-binding adapter molecule 1' (Iba1)-staining (only in the cortex-region) do show a difference between $Npc1^{+/+}$- and $Npc1^{-/-}$ mice.

Ultimately, it can be concluded that of the two MSC-EV fractions that have been tested, only fraction 41.5 has an anti-inflammatory effect on NPC1 pathology. Possible further experiments can be a repeat of the experiment, but the sampling could take place a few weeks later so that possible changes in immune cells and cellular processes have time to develop. Also, IHC could be performed on the peripheral organs to see whether MSC-EV 41.5 can normalize the morphology.

List of abbreviations and symbols

®	Registered trademark
ABC	Avidin-biotin complex
ACAT	Acyl-coenzyme A: cholesterol acetyltransferase
Alix	Apoptosis-linked gene-2 interacting protein X
BBB	Blood-brain barrier
BCSF	Blood-cerebrospinal fluid barrier
BSA	Bovine serum albumin
CB	Cerebellum
CCL	C-C motif chemokine ligand
cDNA	Complementary DNA
CNS	Central nervous system
CSF	Cerebrospinal fluid
C_t	Threshold cycle-value
Cxcl10	C-X-C motif chemokine ligand 10
DABCO	1,4-diazabicyclo[2,2,2]octane
DAPI	4’,6-diamidino-2-phenylindole
DCX	Doublecortin
ECR	Evolutionary constrained region
ELISA	Enzyme-linked immunosorbent assay
EMA	European Medicines Agency
ER	Endoplasmic reticulum
EV	Extracellular vesicle
EV PL	Platelet-derived extracellular vesicles
GADPH	Glyceraldehyde-3-phosphate dehydrogenase
GAR	Goat anti-rabbit
GFAP	Glial fibrillary acidic protein
Gramd1b	Glucosyltransferases, Rab-like GTPase activators and myotubularins domain containing 1b
H_2O_2	Hydrogen peroxide
HCl	Hydrochloric acid
HIER	Heat-induced epitope retrieval
HKG	Housekeeping gene
HPRT	Hypoxanthine-guanine phosphoribosyltransferase
IκBα	Nuclear factor of kappa light polypeptide gene enhancer in B-cells inhibitor, alfa
Iba1	Ionized calcium-binding adapter molecule 1
IF	Immunofluorescence
IFN_γ	Interferon-gamma
IHC	Immunohistochemistry
IL	Interleukin

iNOS	Inducible nitric oxide synthase
KC	Keratinocytes-derived chemokine
LDL	Low-density lipoprotein
MCS	Membrane contact site
MLN64	Metastatic lymph node 64 protein
MSC-EV	Mesenchymal stem cell-derived extracellular vesicles
n	Sample size
NGS	Normal goat serum
NK	Natural killer
NLRP3	Nod-like receptor family pyrin domain containing 3
NPA	Niemann-Pick disease type A
NPB	Niemann-Pick disease type B
NPC	Niemann-Pick disease type C
NPD	Niemann-Pick disease type D
NTD	N-terminal domain
OB	Olfactory bulb
ORD	Oxysterol-binding protein-related domain
ORP5	Oxysterol-binding protein-related protein 5
PAP	Pulmonary alveolar proteinosis
PBS	Phosphate-buffered saline
PBT	Phosphate-buffered saline with Triton X-100 and normal goat serum
PFC	Prefrontal cortex
PH	Pleckstrin homology
PIER	Protease-induced epitope retrieval
PVA	Poly-vinyl alcohol
qPCR	Quantitative polymerase chain reaction
RPL	Ribosomal protein L
RT-PCR	Reverse transcription-polymerase chain reaction
Smpd1	Sphingomyelin phosphodiesterase 1
SSD	Sterol sensing domain
StAR	Steroidogenic acute regulatory protein
STARD3	Steroidogenic acute regulatory protein-related lipid transfer domain containing 3
TGN	Trans-Golgi network
™	Trademark
TNF	Tumour necrosis factor
TSA	Tyramide signal amplification
UBC	Ubiquitin C
VSGP	Vertical supranuclear gaze palsy

Glossary

Allelic variant	A different allele of one gene.
Anchored oligo(dT) primer	Sequences that consist of thymine residues, but contains one other residue at the 3' end.
Apoptosis	The cellular process of programmed death.
Ascites	The accumulation of fluid in the peritoneal cavity.
Ataxia	A reduction of the voluntary movement of the muscles.
Autophagy	A cellular pathway in which cells break down components and organelles that are damaged or aged.
Axonal spheroid	Swelling of the axons due to alterations of the myelin sheath.
Cataplexy	A triggerable, sudden episode of muscle weakness while the person is fully conscious.
Ceramide	A group of lipids that consists of sphingosine and a fatty acid.
Chemokines	A group of cytokines that can induce chemotaxis of immune cells to a site of infection.
Cholestatic icterus	A pathological disorder in which an obstruction in the bile duct causes the accumulation of bile (and bilirubin) in the body.
Conformation	The way a protein is folded into space, affected by interactions between amino acids.
Cytokines	A group of proteins released by different cells as a response to an activating stimulus, that at their turn can activate the immune system by binding to receptors.
De novo synthesis	The formation of complex biomolecules out of simple molecules.
Dysarthria	A speech disorder caused by weakened, damaged or paralysed muscles.
Dysphagia	The neurological disorder of swallow difficulties.
Dyspraxia	A developmental disorder with the inability to plan and perform motor skills.
Dystonia	A movement disorder due to overactive muscles.
Effective circulating volume	The amount of blood in the arteries that actually perfuses tissues.
Endocytosis	A cellular process whereby molecules are brought into the cell by engulfment with the cell membrane.
Exocytosis	A cellular process whereby molecules within a cell vacuole leave the cell by fusion of the vacuole membrane with the plasma membrane.
Exon	The part of a gene that encodes amino acids.

Founders' effect	The influence of ancestors on the genetic variation of the population that consists of their offspring.
Glycocalyx	A layer of polysaccharides around the cell membrane of eukaryotic cells.
Hemochromatosis	A liver disorder characterized by the accumulation of iron in the body.
Hepatomegaly	An enlargement of the liver.
Hepatosplenomegaly	An enlargement of the liver and the spleen.
Hexamer primer	Random sequences of six nucleotides that can bind at multiple points along the RNA transcript.
Housekeeping gene	A gene whose expression is equal in all cell types.
Hydrops	A pathological situation with an accumulation of fluids in body cavities.
Hypoproteinaemia	A shortage of proteins in the blood.
Hypotonia	A disorder characterized by low muscle tone.
Insomnia	Sleeplessness.
Interstitial disease	A group of disorders causing lung fibrosis.
Leukodystrophy	An umbrella term for disorders affecting the white matter of the brain.
Membrane contact site	A region where the membranes of two organelles are positioned at approximately 5 to 30 nm of each other.
Narcolepsy	A neurological disorder in which patients have sudden attacks of sleep and aren't able to regulate their sleep pattern.
Necrosis	The process of tissue death.
Neurodegeneration	The decrease of neurological structures, such as nerve cells, and functions.
Purkinje cell	A neuronal cell in the cortex of the cerebellum.
Pyramidal signs	Clinical features (such as spasticity, weakness) that are caused by alterations in the tract that regulates voluntary movements.
Single nucleotide polymorphism	A one nucleotide mutation within a gene.
Sphingolipid	A group of lipids of which the fatty acids are derived from sphingosine, an alcohol with an amino group, two hydroxyl groups and a total of eighteen carbon atoms.
Splenomegaly	An enlargement of the spleen.
Tachypnea	A too high respiratory rate.
Transposon	A chromosomal segment that can change its position within the genome.
Truncation	The shortening and formation of a non-functional protein due to nonsense mutations.

Ubiquitination	The addition of a ubiquitin molecule to a protein that is about to get degraded.
Vertical supranuclear gaze palsy	A neurological disorder in which the vertical eye movement is limited or impossible.

List of figures and tables

List of figures

List of tables

Table of contents

Introduction

The first patient diagnosed with Niemann-Pick disease was examined in 1914 by Albert Niemann. Ludwig Pick was the first person to describe the pathology of the disease in multiple papers in the late 1920s and 1930s (Pick, 1926, 1927, 1933). Five types of Niemann-Pick disease have been described based on the genetic cause and symptoms: type A, type B, type C1, type C2 and type D. Niemann-Pick disease type A (NPA) and Niemann-Pick disease type B (NPB) are caused by autosomal recessive inherited mutations in the sphingomyelin phosphodiesterase 1 (*Smpd1*) gene. Niemann-Pick disease type C (NPC) has an estimated incidence of 1/120 000 to 1/150 000 live births in Western Europe. This type is caused by loss-of-function mutations in the *Npc*1 (95 % of the cases, leading to NPC1) and *Npc2* genes (5 % of the cases, leading to NPC2) respectively. Niemann-Pick disease type D (NPD) has been described by most patients in Nova Scotia (Canada). This was first described as a fifth form, but mutation analysis showed a point mutation in the *Npc1* gene (G3097T) resulting in a substitution of glycine to tryptophan. Now it is considered an allelic variant of type C1 which is clinically not distinguishable. In this thesis, the focus is on NPC1. (Chang et al., 2005; Dipharma SA, n.d.; Greer et al., 1998; Lamri et al., 2018; *Niemann-Pick Disease*, 2020)

NPC is an autosomal recessive inherited lipid storage disorder. The disease leads to neurodegeneration. NPC is characterised by the accumulation of unesterified cholesterol among other lipids in the late endosomes and lysosomes. These accumulations lead to several visceral and/or neurological pathologies. The disease is caused by loss-of-function mutations in the *Npc1* or *Npc2* gene. As these genes fulfil an important role in the intracellular transport of cholesterol, loss-of-function mutations cause impaired intracellular cholesterol trafficking. (Chang et al., 2005; Vanier, 2010)

The NPC-related clinical symptoms vary according to the age of onset and differ from patient to patient. Early-infantile (2 months – 2 years of age), infantile (2-6 years), juvenile (6-15 years) and adult (>15 years) forms of the disease have been described. None of the symptoms on their own is specific to the disease. It is the combination of different manifestations that is indicative of NPC. In general, neurological and systemic symptoms are distinguished. Since the disease presents with a broad heterogeneous clinical spectrum, the involved disease mechanisms are still incompletely understood. This makes finding a good treatment very difficult. (Lamri et al., 2018; Mengel et al., 2013; Vanier, 2010)

Despite decades of research, there is no cure for NPC available because too little is known about the disease. Therefore, treatment of NPC1 focuses on the alleviation of symptoms. (Dipharma SA, n.d.; Platt et al., 2016; Vanier, 2010)

Administration of mesenchymal stem cell-derived extracellular vesicles (MSC-EVs) in clinical trials showed anti-inflammatory. Therefore, in this research project, several MSC-EVs delivered by an external lab will be administered in *Npc1*$^{-/-}$ mice to examine the anti-inflammatory effect on the NPC1 pathology. The ultimate goal of this project is to understand the disease better so that better treatment can be found for the thousands of people suffering and dying from the disease. (Tsiapalis & O'Driscoll, 2020)

In the first part of this report, a theoretical background covering the Niemann-Pick disease type C1 will be given. Hereby the different types of the disease will be mentioned. Next, the focus will be on the molecular background and the clinical features of NPC. In the second half of the report, the practical part will be introduced with the methodology followed by a chapter that is dedicated to the elaboration of the conducted experiments and their results and discussions.

This research is performed at the Vandenbroucke lab at VIB-UGent Center for Inflammation Research. Vandenbroucke lab investigates the effects of systemic inflammation and neuroinflammation on the blood-brain barrier (BBB) and blood-cerebrospinal fluid barrier (BCSF). The research can be summarized in the following questions:

1 What role do key molecules play in the activated detrimental process at the BBB and BCSF upon inflammation? Here, the focus lays upon barrier integrity, extracellular vesicles (EVs) and acute phase response.
2 Is the *choroid plexus* 'the missing link' in the body-to-brain axis?
3 Can the BBB of BCSF be used as a delivery route to the brain?

The first question comprises the research question of this thesis. (*Vandenbroucke Lab Research | VIB Labs*, n.d.)

1 Niemann-Pick disease

Niemann-Pick disease is a rare, autosomal recessive disease characterized by an accumulation of several lipids in late endosomes and lysosomes. The disease can result in visceral but also neurological disorders. In this chapter, the different types of Niemann-Pick disease will be covered with a specific focus on NPC, as this type is the main focus of this thesis project. (Hammond et al., 2019; Vanier, 2010)

1.1 Types of Niemann-Pick disease

Niemann-Pick disease can be classified into five types: A, B, C1, C2 and D. This classification is based on the genetic cause and symptoms. (Vanier, 2010)

Type A and B are caused by autosomal recessive mutations in the *Smpd1* gene leading to an aberrant sphingomyelinase activity. This enzyme is located in the lysosomes where it has an important role in the degradation of the membrane by degrading sphingolipids into ceramides. Therefore, mutations in the *Smpd1* gene lead to accumulation of sphingomyelin in the lysosomes. NPA can be distinguished by its severe clinical symptoms leading to early-infantile death. These symptoms include hepatosplenomegaly, lung damage, a cherry-red spot on the retina and severe neurological damage. Where type A mostly has an impact on neurological involvement, the symptoms of NPB manifest themselves viscerally, with less severe symptoms. Moreover, a slower progression of the disease has been described for NPB. (Gabandé-Rodríguez et al., 2014; Irun et al., 2013; McGovern et al., 2017; Vanier, 2013)

NPC1 and NPC2, just like NPA, are typified by neurological deterioration, but follow a subacute course and are therefore less ruthless than type A. The slower course is also a characteristic of type C. Additionally, visceral involvement takes place, resulting in hepatosplenomegaly and sometimes lung damage. These visceral symptoms don't always show up. Type C has another cause than type A and B, namely a loss-of-function mutation in the *Npc1* or *Npc2* gene. NPC1 pathology is extensively described below. (Vanier, 2010)

NPD is an example of a disease that mainly appears in *Nova Scotia*-individuals and their offspring due to the founders' effect. Mutation analysis showed that NPD is caused by a specific point mutation (G3097T) in the *Npc1* gene. Therefore, it is proven that type D is considered to be an allelic variant of type C more than a fifth variant. Type C and type D are clinically not distinguishable. (Greer et al., 1998; Vanier, 2010)

1.2 Molecular background of Niemann-Pick disease type C

Like mentioned before, NPC is an autosomal recessive disease caused by a mutation in the *Npc1* or *Npc2* gene. 95 % of the NPC-cases are due to a mutation in the *Npc1* gene on chromosome 18q11.2 and lead to NPC1. 5 % of the NPC-cases are due to a mutation in the *Npc2* gene that is located on the long arm of chromosome 14 at position 24.3. Both genes are functional in cholesterol metabolism. Mutations in one of the two genes lead to impaired trafficking of cholesterol and glycosphingolipids. Moreover, the loss of one protein cannot be compensated by the other. In this chapter, both proteins will be discussed independently, followed by discussing their role in the intracellular trafficking of cholesterol. (Dardis et al., 2020; Pacheco & Lieberman, 2008; Vanier, 2010; Xu et al., 2019)

1.2.1 NPC1

NPC1 is a protein comprising 1278 amino acids. The protein is localized to the limiting membrane of the late endosomes and lysosomes and is only present in cells with low-density lipoprotein (LDL)-uptake. NPC1 fulfils a significant role in the transport of cholesterol to the endoplasmic reticulum (ER). The site on the membrane of the lysosome or late endosome that contacts other organelles, such as the ER, is called the membrane contact site (MCS). NPC1 localizes in particular to these MCSs where it can interact with 'glucosyltransferases, Rab-like GTPase activators and myotubularins domain containing 1b' (Gramd1b) among other proteins to stabilize the MCS. Gramd1b is a sterol-transfer protein that is localised on the ER membrane. Scientist observed a reduction of MCS in *Npc1* depleted cells. On the other hand, cells with an *Npc1* overexpression showed an expansion in MCS. (Chang et al., 2005; Höglinger et al., 2019; Martello et al., 2020; Xu et al., 2019)

The NPC1 protein (Figure 1-1) consists of thirteen transmembrane domains and three luminal loops. Some of the domains are very important for the protein. The first one is the sterol sensing domain (SSD). This area has a significant role in multiple processes, like cholesterol homeostasis, intracellular communication and uptake of dietary cholesterol. A functional SSD is important to maintain a functional NPC1 protein. (Chang et al., 2005; Du et al., 2011)

Another important domain is the cysteine-rich domain (Figure 1-1). This domain carries up to 45 % of the mutations affecting the *Npc1* gene. The function of this domain is not completely understood yet, but the suggestion is that the eight cysteines in this domain form several disulfide bonds which stabilize the protein. (Li et al., 2017)

The second luminal loop (Figure 1-1) is the domain on the NPC1 protein that can bind with NPC2 prior to the transfer of cholesterol. Cholesterol can bind to the N-terminal domain (NTD) of NPC1. This binding happens in an opposite orientation compared to the binding between cholesterol and NPC2. (Du et al., 2011; Xu et al., 2019)

Most single nucleotide polymorphisms, especially in the SSD, lead to a change in conformation of the protein with loss of function as a consequence. Nevertheless, some mutations, like D787N, don't have devastating consequences for the protein, so the protein retains its function. (Du et al., 2011)

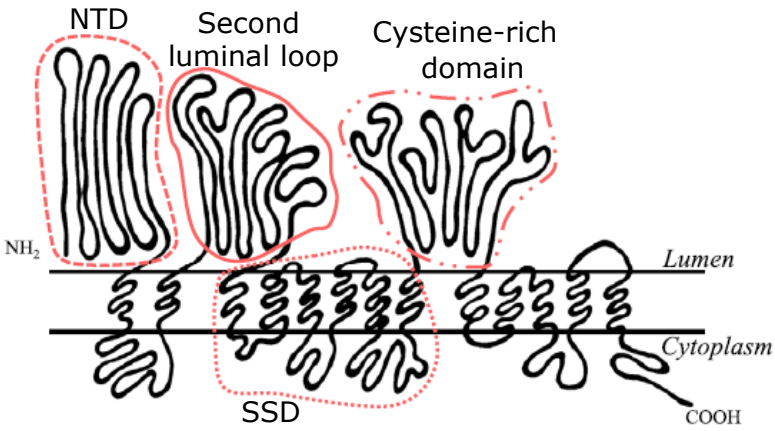

Figure 1-1 Schematic overview of the NPC1 protein. NTD (dashed line), second luminal loop (full line), SSD (dotted line) and cysteine-rich domain (dash-dotted line) are indicated. (Hammond et al., 2019)

1.2.2 NPC2

NPC2 is a small, flexible and soluble protein. It is present in the lumen of lysosomes and late endosomes where it is transported to after transcription and translation. Binding with mannose-6-phosphate is needed for cholesterol to be taken up by these organelles. Unlike NPC1, NPC2 is present in all kind of cells and a few secretory fluids, suggesting that it has more functions than binding and transferring cholesterol. Researchers suggest that NPC2 also plays a role in the innate immune system. (Hammond et al., 2019; Xu et al., 2019)

NPC2 has four evolutionary constrained regions (ECRs) (Figure 1-2). The fourth ECR, also indicated as ECR D, is responsible for binding cholesterol with high affinity. Mutations that affect this protein, involve mostly the cholesterol-binding domain. (Hammond et al., 2019; Vanier, 2010; Xu et al., 2019)

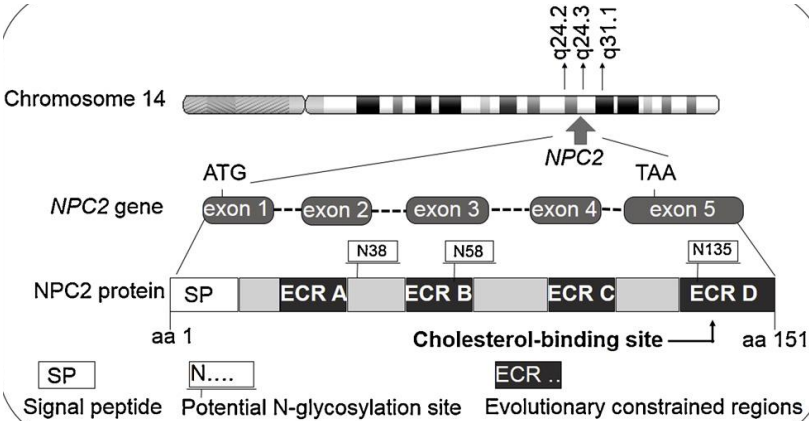

Figure 1-2 Schematic overview of the Npc2 gene and NPC2 protein (Xu et al., 2019)

The NPC2 protein has multiple electrostatic charges on its surface (Figure 1-3). It is suggested that these charges are important for the binding of NPC2 and cholesterol. Since NPC2 is a flexible protein, it can respond differently to various mutations by adapting its conformation. Not only the kind of mutation is important, but also how NPC2 changes its conformation. Mutations that make the non-polar area near the cholesterol-binding cavity smaller or disappear have a bigger impact than mutations that have a minimal effect on the electrostatic surface. (McCauliff et al., 2015)

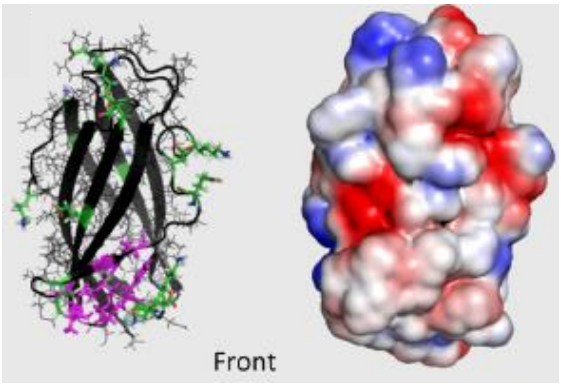

Figure 1-3 Structural presentation of the NPC2 protein. Left: cartoon-and-sticks display with cholesterol binding site indicated with magenta sticks. Right: surface display with electrostatic charges indicated (red = negative charge; blue = positive charge; white = uncharged). (McCauliff et al., 2015)

1.3 Cholesterol metabolism

NPC1 and NPC2 are two proteins that are part of intracellular cholesterol trafficking. Mutations in these proteins lead to impaired intracellular cholesterol trafficking and accumulation of cholesterol among other lipids. This chapter starts with an overview of the normal intracellular trafficking of dietary cholesterol (Figure 1-4 A), followed by the impact of *Npc1*- mutations (Figure 1-4 B) on the metabolism. (Chang et al., 2005; Du et al., 2011; Martello et al., 2020)

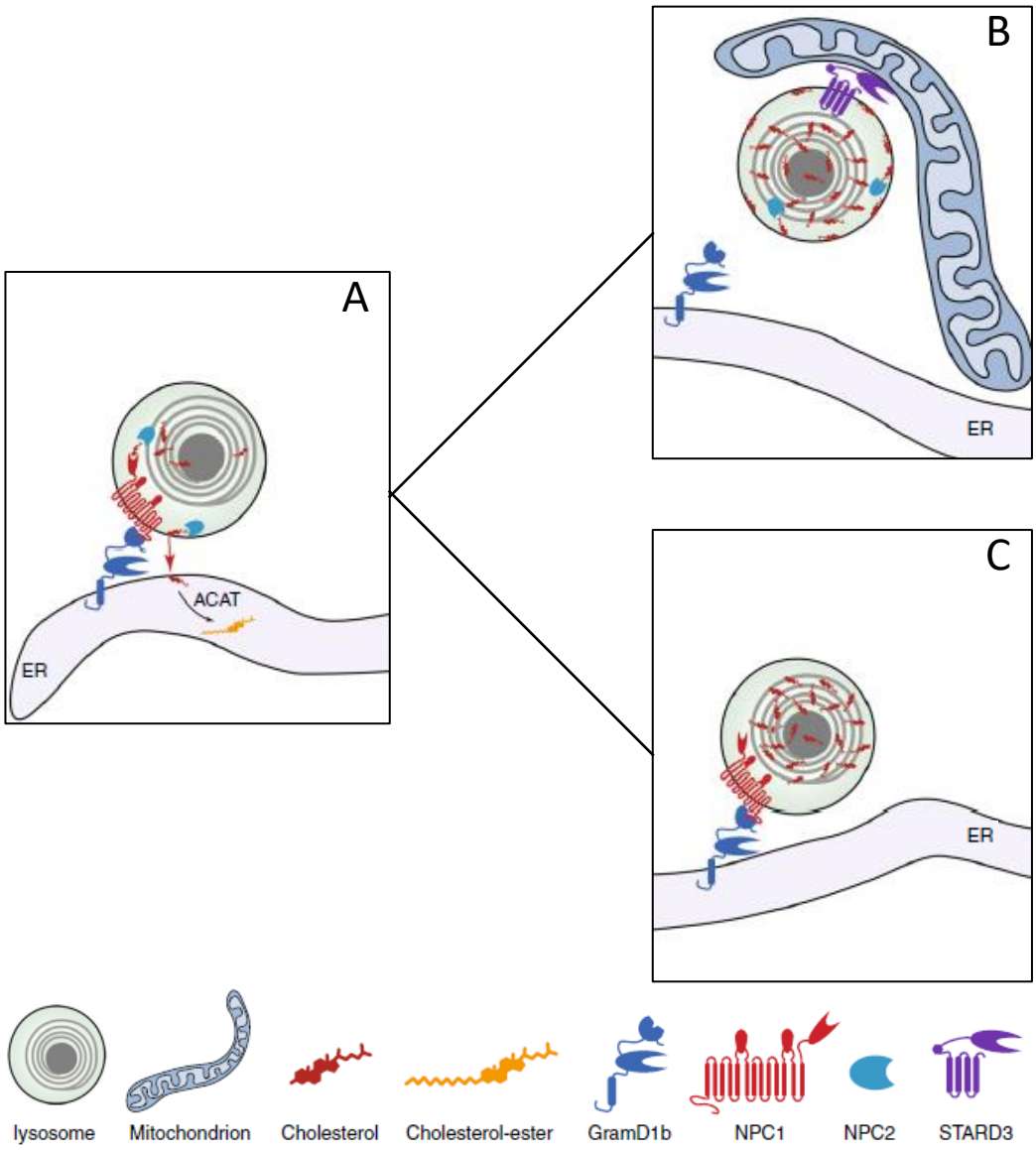

Figure 1-4 Schematic overview of the normal intracellular cholesterol metabolism (A), impaired cholesterol metabolism due to Npc1-mutation (B) and impaired cholesterol metabolism due to Npc2-mutation (C). (Höglinger et al., 2019)

1.3.1 Normal metabolism

Cholesterol has an important function in membrane rigidity, fluidity and permeability. The major source of cholesterol is the *de novo* synthesized cholesterol from the ER. Another source is dietary cholesterol that is important to regulate the *de novo* synthesis. (Du et al., 2011; Martello et al., 2020)

Dietary cholesterol is absorbed from the gut into the blood. Because of the first passage effect, cholesterol is delivered to the liver. In the liver, it is packaged into lipoprotein particles to form LDL-cholesterol. The apolipoprotein B-100, present in LDL-cholesterol, is a ligand to bind to the LDL-receptor on the cell membrane. LDL-cholesterol enters the cell through endocytosis and an early endosome is formed. The early endosome transforms into a late endosome by incorporating some proteins (such as NPC1) into its membrane. The late endosome either melts together with a lysosome or goes directly to the ER. (Chang et al., 2005; Höglinger et al., 2019; Martello et al., 2020)

Within the lysosome, cholesterol is released out of LDL-cholesterol by acid lipases. The released, unesterified cholesterol binds with the NPC2 cholesterol-binding cavity and is transferred to the sterol-binding domain at the NTD of NPC1. NPC1, localized at the MCS, manages to transfer cholesterol through the glycocalyx of the lysosome to the limiting membrane. To stabilize the MCS and to maintain a smooth transfer, NPC1 interacts with Gramd1b. (Figure 1-4 A) (Chang et al., 2005; Du et al., 2011; Martello et al., 2020)

Different proteins play an important role in transferring cholesterol from the lysosomes to the ER. Researchers suggest not all of these proteins have been identified yet. One known protein is oxysterol-binding protein-related protein 5 (ORP5). This protein has a pleckstrin homology (PH) domain at the NTD that can bind with different kinds of membranes. An oxysterol-binding protein-related domain (ORD) can be found at the C-terminal end as well as a transmembrane domain with which ORP5 is anchored into the ER-membrane. The ORD of ORP5 is capable of binding cholesterol and oxysterol. *In vitro* studies of the ORP5 protein showed that this protein transfers cholesterol *in vitro* from the lysosomes to the ER membrane. Other putative proteins collaborate in this transfer. Since it is NPC1 that delivers cholesterol to ORP5, the function of ORP5 depends on a functional NPC1-protein. (Du et al., 2011)

Within the ER, cholesterol is esterified by acyl-coA: cholesterol acetyltransferase (ACAT). After esterification, cholesterol is transferred to the Golgi-apparatus where it is packed into vesicles and undergoes exocytosis into the blood circulation. (Chang et al., 2005; Höglinger et al., 2019)

Instead of being transferred to the ER where cholesterol has mainly a regulatory function (synthesis of steroid hormones, bile acids etc.), cholesterol can also be transferred to the plasma membrane to fulfil a structural function by maintaining the membrane rigidity. (Du et al., 2011; Xu et al., 2019)

1.3.2 Metabolism in Niemann-Pick disease type C1

NPC1 has an essential role in the egress of cholesterol from the late endosomes/lysosomes to the ER. Loss-of-function mutations lead to an accumulation of cholesterol in the lumen (Figure 1-4 B). Because the egress is blocked, no esterification can take place and no cholesterol-ester can leave the cell. Accumulation of cholesterol also interferes with the transport of endosomes to the trans-Golgi network (TGN). Endosomes are important in providing receptors, enzymes and bacterial toxins to the TGN. As a result, normal cell function is disturbed. (Du et al., 2011)

Research also showed an elevation in cholesterol concentration in mitochondria of *Npc1* depleted cells. Further investigation of this phenomenon revealed that metastatic lymph node 64 protein (MLN64), also known as 'steroidogenic acute regulatory protein (StAR) related lipid transfer domain containing 3' (STARD3), can transport cholesterol from the late endosomes to the mitochondria. The mechanism behind this transfer still needs to be revealed. Certain is that both MLN64 and NPC2 need to be present. (Figure 1-4 B) (Balboa et al., 2017; Martello et al., 2020)

1.4 Clinical features of Niemann-Pick disease type C

NPC has an impact on basically every organ as almost every cell is affected by the impaired cholesterol trafficking leading to accumulation. However, some organs show worse clinical features than others. This chapter focuses on these clinical features and discriminates between systemic and neurological involvement. (Figure 1-5) (Bi & Liao, 2010)

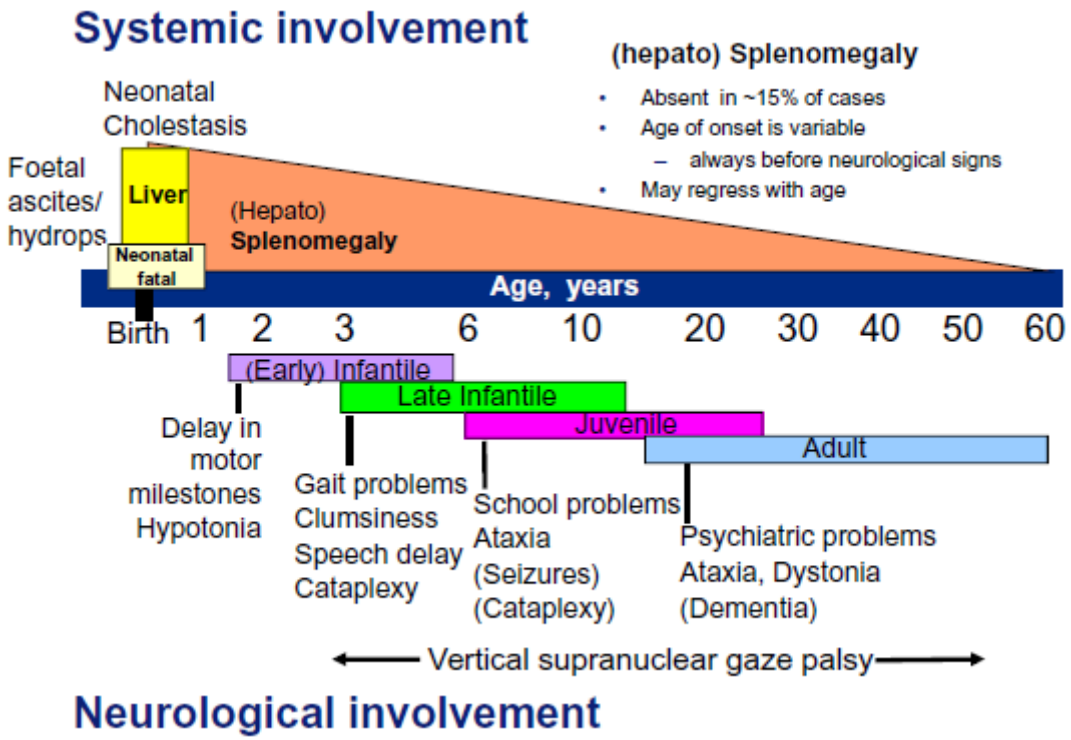

Figure 1-5 Overview of the systemic and neurological involvement of NPC (Vanier, 2010)

1.4.1 Systemic features

Systemic features are not always present in NPC pathology, but when they are present, they are always onset of the neurological symptoms. This chapter will be limited to the liver, spleen and lungs as these organs are the most affected peripheral organs. In the result part of this thesis, these organs will also be discussed. (Vanier, 2010)

1.4.1.1 Liver and spleen

The liver is the most affected peripheral organ in NPC1 pathology. The explanation is that one of the most important roles of the liver is to take LDL-cholesterol out of circulation. Therefore, there is a higher supply of cholesterol to the hepatocytes leading to more accumulation. This increasing accumulation leads to one of the most abundant systemic features, namely hepatomegaly. Splenomegaly often occurs simultaneously with hepatomegaly and is caused by the vacuolization of macrophages due to the accumulation of lipids. Hepatomegaly is also a cause of hydrops that is often seen in foetuses. Another cause of foetal hydrops could be hypoproteinaemia due to liver failure. (Karten et al., 2009; Kattner et al., 1997; Maeda et al., 2019)

Next, the accumulation of cholesterol in the liver can also cause intrahepatic cholestasis. The feature mostly affects neonates and results in the death of about 10 % of those suffering the disease. As these patients rarely show neurological features yet, they are often misdiagnosed with other liver diseases, such as hemochromatosis. (Hildreth et al., 2017; Karten et al., 2009; Kumagai et al., 2019)

Another hepatic feature in NPC pathology is hepatitis. The link between NPC and hepatitis is not well understood yet but some researchers hypothesize that the accumulation of lipids damages the lysosomal integrity. Because of that, the content of the lysosomes (proteolytic enzymes among them) is released into the cytosol, leading to cell death. Macrophages are attracted to the site of apoptosis and release tumour necrosis factor (TNF). This latter cytokine, in turn, enhances apoptosis and necrosis. (Idriss & Naismith, 2000; Rimkunas et al., 2009)

Lysosomal disruption is also considered to be a trigger to activate the 'Nod-like receptor family pyrin domain-containing 3' (NLRP3) inflammasome. This inflammasome induces the formation of a complex that creates caspase-1. Caspase-1 is needed to induce necrotic cell death and synthesis of interleukin (IL)-1β. This cytokine induces many processes such as macrophage stimulation and activation of lymphocytes. (Justiz Vaillant & Qurie, 2021; Lima et al., 2013)

Foetal ascites mostly affects foetuses with NPC. This feature is caused by portal hypertension due to liver disease. Portal hypertension, in turn, causes vasodilatation and a reduction in effective circulating volume. The kidneys react by increasing the renal reabsorption and the cardiac output. The combination of hypertension and increased reabsorption causes leakage of fluids in the peritoneal cavity, which leads to ascites. (Piano et al., 2018)

1.4.1.2 Lungs

Alveolar type II cells produce surfactant, a solution consisting of lipids and proteins to reduce the surface tension of the alveoli. This surfactant is stored in lamellar bodies that undergo exocytosis to release the surfactant to the alveolar surface. In normal cases, 5 to 10 % of the surfactant consists of cholesterol. Lamellar bodies are lysosome-like organelles that also contain NPC1 and NPC2 proteins. Consequently, there is also an accumulation of cholesterol in lamellar bodies within NPC1 pathology, leading to higher concentrations of cholesterol in the surfactant and an accumulation of surfactant itself. This is called pulmonary alveolar proteinosis (PAP). The increased amount of cholesterol in the surfactant possibly leads to aberrant function of the fluid and therefore to acute respiratory distress syndrome. (Roszell et al., 2012, 2013)

Patients with pulmonary involvement in NPC often suffer from interstitial disease, with typical symptoms like wheezing, crackles and tachypnea. The interstitial disease could be caused by an accumulation of NPC-affected macrophages in the alveoli. (Staretz-Chacham et al., 2018)

Pneumonia is also occurring in NPC patients. The theory is that the increase of macrophages filled with lipids is causing pneumonia, which is called lipoid pneumonia. As some patients with NPC have difficulties with swallowing (see 1.4.2), food and fluids may end up in the lungs. This causes aspiration pneumonia. As with every inflammation reaction, pneumonia is associated with an immune reaction with immune cells (macrophages …), chemo- and cytokines (TNF, IL-1β …) as described in 1.4.1.1. (von Ranke et al., 2016; Walterfang et al., 2012)

1.4.2 Neurological features

NPC also impacts the central nervous system (CNS) and leads to neurodegeneration. The ultimate link between NPC1 and neurodegeneration is not fully understood yet. This chapter is dedicated to the neurological features that are the consequences of NPC. To start, the cause of the most common neurological features will be explained. After that, the classification based on the neurological onset of the disease will be discussed. Finally, neuroinflammation as a consequence of NPC1 will be mentioned. In the result part, the focus will be on the (prefrontal) cortex, olfactory bulb, cerebellum, hippocampus and *corpus striatum*. (Hovakimyan et al., 2013; Vanier, 2010)

1.4.2.1 Neurological features in general

The only source of cholesterol for the brain is *de novo* synthesized cholesterol. The largest pool resides in myeline, while astrocytes (glial cells) are the most important source in the adult brain. Cholesterol has a protective function in the brain. Deficiencies in the cholesterol egress lead to neurodegeneration. The neurological features mostly include gait ataxia, dysarthria, dementia and seizures. (Fiorenza et al., 2018; Karten et al., 2009)

As cholesterol is continuously made in the brain, albeit at low rates, and homeostasis needs to be maintained, the excess of cholesterol is removed from the brain. In the cerebellar cortex, hippocampus and thalamus, cholesterol is converted into 24-hydroxycholesterol which can pass the BBB. As cholesterol egress is blocked in NPC, the excess can't be removed from the brain. This alteration is expected to cause aberrant neuronal function. (Karten et al., 2009)

Based on the above findings, NPC1 pathology has consequences on different brain regions and cells. Studies have shown shorter axons in *Npc1*-deficient neurons. Furthermore, studies in *Npc1*$^{-/-}$ mice have shown losses in Purkinje cells of the cerebellum, hypomyelination, axonal spheroids and abundancy of with cholesterol accumulated astrocytes in selective brain regions. Neuronal losses also occur in mostly the cerebellum, midbrain, pons, thalamus and prefrontal cortex. Furthermore, alterations in the concentration of neurotransmitters have been detected in specific brain regions which can cause seizures. (Karten et al., 2009; McCauliff et al., 2015)

As an increase in autophagy has been observed in several neurodegenerative diseases, the suggestion is that this process also is important in NPC pathology. Autophagy is a basal phenomenon, meaning that it is important for the normal function and development of the CNS. It can be induced in stressful situations, like starvation. Studies have shown that there is an increase in autophagy in NPC. However, the supply of damaged and aged structures is too much for the pathway to handle. This leads to autophagic stress or death. (Pacheco & Lieberman, 2008)

1.4.2.2 Classification by neurological onset

Several studies have been performed to obtain more information about the impact of NPC on the CNS. Because of these studies, it is possible to make a classification based on the age of neurological onset (which can differ from the perinatal period to over 60 years of age). This classification distinguished five groups: (i) perinatal presentation, (ii) early infantile period (2 months – 2 years), (iii) late infantile period (2 – 6 years), (iv) juvenile period (6 – 15 years) and (v) adolescents and adults (> 15 years). (Vanier, 2010)

In Table 1-1 the different groups of NPC are shown together with their systemic and neurological features and the estimated lifespan. It is important to emphasize that none of the features is specific to the disease and that the manifested features can differ from patient to patient. (Geberhiwot et al., 2018; Vanier, 2010).

Table 1-1 The different groups of NPC with their systemic features, neurological features and estimated lifespan (Geberhiwot et al., 2018; Vanier, 2010)

Group	Systemic features	Neurological features	Estimated lifespan
Perinatal presentation	Foetal ascites, foetal hydrops, neonatal cholestatic icterus, hepatosplenomegaly and PAP	None	6 months
Early infantile period	Hepatosplenomegaly	Motor delay, hypotonia, loss of acquired motor skills, mental regression, spasticity, intention tremor, leukodystrophy, cerebellar atrophy	5 years
Late infantile period	Hepatosplenomegaly	Language delay, gait problems, ataxia, vertical supranuclear gaze palsy (VSGP), cataplexy, motor delay, seizures, dysphagia, dysarthria, dementia, pyramidal signs, spasticity, swallowing problems	7-12 years
Juvenile period	Splenomegaly	School problems, dyspraxia, VSGP, cataplexy, narcolepsy, ataxia, dysarthria, dysphagia, dystonia, spasticity, pyramidal signs, swallowing problems,	Variable, often 30 years or more
Adolescents and adults	Slight splenomegaly	VSGP, psychiatric signs, cerebellar ataxia, dysarthria, cognitive dysfunction, dystonia, dysphagia	Variable

1.4.2.3 Neuroinflammation

Microglia are phagocytic immune cells present in the CNS. These cells become activated when injury and inflammation occur. They can phagocyte death cells while secreting pro-inflammatory cytokines, nitric oxide and reactive oxygen species. Moreover, microglia also secrete neuroprotective molecules, such as anti-inflammatory cytokines. (Karten et al., 2009)

Studies in mice with neurodegenerative diseases other than NPC have shown alterations in microglia activation. An increased number of activated microglia has been reported in several brain regions. Furthermore, increased levels of mRNAs encoding *Tnf* and other genes in the TNF signalling pathway, such as C-C motif chemokine ligand (*Ccl) 2* and *Ccl5*, have been detected. Studies in *Npc1*-deficient mice reported the same findings. However, the exact role of microglia in NPC is not completely understood yet. (Karten et al., 2009; KEGG PATHWAY: TNF Signaling Pathway - Reference Pathway, n.d.)

As mentioned in 1.4.2.1, glial cells have an important role in the brain. Besides microglia, astrocytes also become activated in NPC-pathology. Astrocytes have several functions such as neuronal development and control of the BBB. Studies have shown an increase of the glial fibrillary acidic protein (GFAP), which is a marker for reactive astrocytes, in all brain areas in *Npc1*$^{-/-}$ mice. Moreover, these astrocytes have been shown to secrete increased amounts of IL-6. This is a cytokine that induces differentiation of B-cells and stimulates acute-phase proteins. The exact consequences of the increase of reactive astrocytes are not fully understood yet. Scientists suggest that it contributes to the disease progression more than having a protective function. (Burda & Sofroniew, 2014; Justiz Vaillant & Qurie, 2021; Karten et al., 2009)

Studies have also shown that the complement system does not have a significant influence on the brain inflammation that occurs within NPC1 pathology. (Cologna et al., 2014)

1.5 Treatment

Despite the many studies and clinical trials, a cure for NPC isn't available yet. Miglustat is the only drug approved by the European Medicines Agency (EMA) to treat NPC. This drug represents the first specific treatment for the disease and gives a reduction in the progression of the disease. However, miglustat has no significant effect on the systemic features of the disease. (Vanier, 2010)

Treatment of NPC is mostly symptomatic. Table 1-2 gives an overview of some of the clinical features and the administered drugs. Combination drug therapy has also been tested. However, up till now, no therapy has alleviated both neurological and visceral symptoms. Despite that, some of these treatments can extend the lifespan and slow the disease progression. (Maass et al., 2015; Vanier, 2010; Williams et al., 2014)

Table 1-2 The symptomatic treatment of the clinical features of NPC (Vanier, 2010)

Clinical feature	Drugs
Seizures	Anti-epileptic drugs
Cataplexy	Clomipramine, protriptyline, modafinil
Dystonia, tremor	Anticholinergic drugs
Spasticity, contractures	Physiotherapy
Inflammation	Non-steroidal anti-inflammatory drugs

Also, some specific treatments have been tested. A regression in the hepatosplenomegaly and lung infiltration by macrophages has been observed after a bone marrow transplantation. However, no improvement of the neurological features is reported. Also, liver transplantation does not improve neurodegeneration. (Vanier, 2010)

At the time of writing this thesis, ten clinical trials were running or recruiting subjects. This means a lot of research is being done but underlines the fact that NPC is a complex disease to find a cure for. (U.S. National Library of Medicine, n.d.)

2 NPC1 mouse model

Several mouse models are available to investigate the effects of NPC1 in mice. Some examples are *Npc1*$_{spm}$ mice, *Npc1*$_{nih}$ mice (also known as *Npc1*$_{m1N}$ mice) and *Npc1*$_{nmf164}$ mice. For this project, BALB/c *Npc1*$_{nih}$ mice (also known as BALB/c Nctr-*Npc1*$_{m1N}$/J mice) (Figure 2-1) are used. This model has a slower and less severe loss of Purkinje cells than *Npc1*$_{spm}$ mice. BALB/c Nctr-*Npc1*$_{m1N}$/J mice are also a better model for the early onset of the disease compared to C57BL/6J *Npc1*$_{nmf164}$ mice, which are mostly used to investigate the late onset forms. Compared to C57BL/6J *Npc1*$_{m1N}$ mice, BALB/c Nctr-*Npc1*$_{m1N}$/J mice show a later onset of clinical features, avoiding premature death and giving researchers time to investigate the consequences of these features. (Maue et al., 2012; The Jackson Laboratory, 2020a, 2020b, 2020c)

Figure 2-1 A healthy BALB/c mouse (A) and a BALB/c Npc1$_{nih}$ mouse (B). Mouse B shows obvious signs of illness such as gait ataxia and lower body weight.

BALB/c *Npc1*$_{nih}$ is a mouse strain that has a transposon inserted into the ninth exon of the *Npc1* gene. This insertion results in a truncated NPC1 protein deleting eleven out of thirteen transmembrane domains. Mice of this strain manifest clinical features similar to those mentioned in 1.4. Based on increased levels of microglia in the used model, it can be concluded that this strain also suffers from deficiencies in the innate immune system. These deficiencies can be caused by lower levels of chemoattractant or impaired transport of molecules needed for activation of immune cells. The average lifespan of these mice is estimated at 9 to 11 weeks (Speak et al., 2012; The Jackson Laboratory, 2020b; Williams et al., 2014)

3 Methodology

This bachelor project investigates the anti-inflammatory effect of MSC-EVs on NPC1 pathology. The principles of the used techniques are explained below.

3.1 Experimental design

For this experiment, *Npc1*$^{+/+}$ and *Npc1*$^{-/-}$ mice are used. Two separate groups of *Npc1*$^{-/-}$ mice are treated with MSC-EVs fraction 16.3 or MSC-EVs fraction 41.5, delivered by an external lab (from the University Hospital of Essen). The *Npc1*$^{+/+}$ mice are treated with platelet-derived EVs (EV PL) or buffer (also referred to as vehicle). Another two groups of *Npc1*$^{-/-}$ mice are also treated with EV PL or vehicle. How EVs can be derived from platelets or MSCs, will be explained in 3.2.

Four intravenous injections are given to mice that are genotyped as *Npc1*$^{-/-}$ starting on the fourth week after birth. Two of the injections are given between five and six weeks of age and the other two between six and seven weeks of age. Before each injection, the mice are weighed. On the seventh week of age, the mice are sacrificed and sampled to perform several read-outs that are described below. (Figure 3-1)

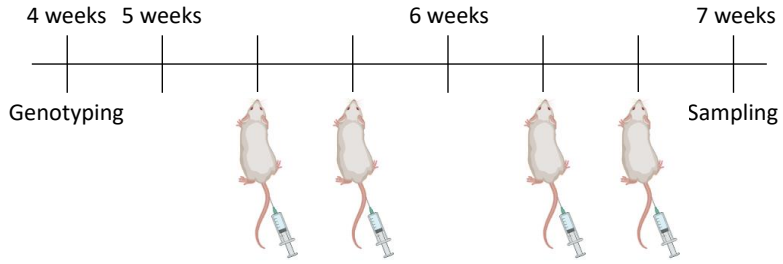

Figure 3-1 Experimental design (Biorender.com is used)

For the experiments, the brain is divided into different brain regions, including the prefrontal cortex (PFC), olfactory bulb (OB), cerebellum (CB), hippocampus and *corpus striatum*. An overview of these brain regions is given in Figure 3-2.

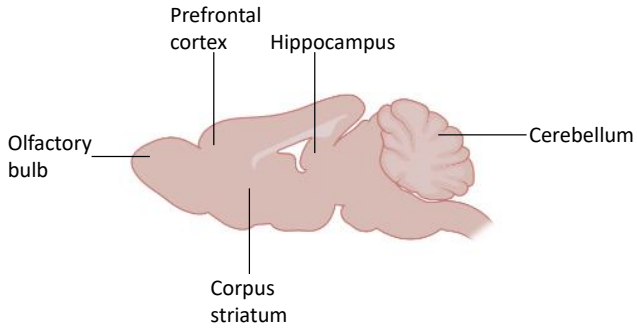

Figure 3-2 Overview of the investigated brain regions with indications of the prefrontal cortex, olfactory bulb, cerebellum, hippocampus and corpus striatum (Biorender.com is used)

3.2 Isolation and purification of extracellular vesicles

EVs are small (< 1 µm) vesicular bodies secreted from cells and tissues. Studies have shown that these are important in intercellular communication, but also can be used for diagnostics or as therapeutic delivery vectors. EVs are able to modulate protein expression. The interest in EVs for preclinical studies have grown in the last years. (NanoView Biosciences, n.d.)

A first step in the analysis of EVs is sample preparation and purification to obtain purified EVs. However, this step has many challenges because other contaminants (such as lipoproteins) can be co-purified. EVs are also very small and are mostly found surrounded by a complex matrix. Several techniques are used for purification. These techniques can be based on density (ultracentrifugation or density gradient centrifugation), size (size exclusion chromatography) or characteristics of the EVs (precipitation or immunocapture). For this experiment, size-exclusion chromatography is used. Hereby, a column packed with a gel with pores of approximately 70 nm is used. Contaminating proteins enter the pores and take a longer time to elute, while EVs cannot enter the pores and elute immediately. (Bio-Rad Laboratories Inc., 2013, p. 20; IZON Science LTD, 2021; Vandendriessche, 2021)

Quality control is performed to make sure purified EVs were obtained. This quality control comprises western blot, nanoparticle tracking analysis (ZetaView), ExoView and electron microscopy. This was already done before starting this thesis. (Vandendriessche, 2021)

3.3 Bio-Plex

Chemo- and cytokines are (glyco-)proteins or peptides secreted by immune cells and are therefore markers for inflammation. Bio-Plex is an immunoassay presented by Bio-Rad. This kit enables to determine the expression of chemokines and cytokines. (Bio-Rad Laboratories Inc., n.d.-c; Sokol & Luster, 2015)

The principle behind Bio-Plex (Figure 3-3) is very similar to the principle of sandwich enzyme-linked immunosorbent assay (ELISA). Capture antibodies against the chemo- or cytokine of interest are covalently bound to a magnetic bead on the bottom of a well. After adding the prepared sample and possible binding with the capture antibody, a biotinylated detection antibody against the same chemo- or cytokine is added. Afterwards, streptavidin labelled with a fluorescent reporter is added. Data can be acquired using a Bio-Plex 200 reader. (Bio-Rad Laboratories Inc., n.d.-c)

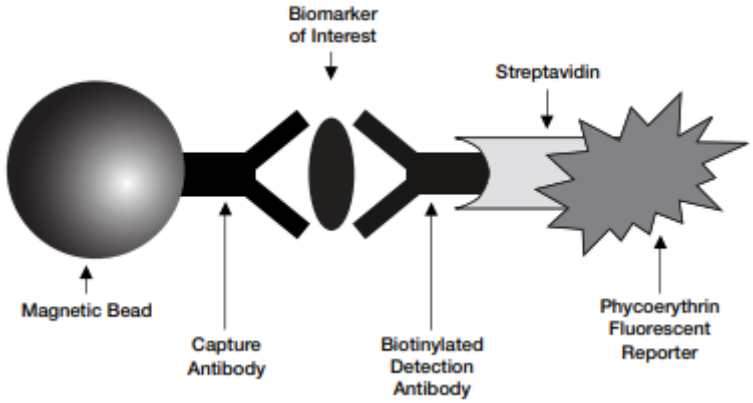

Figure 3-3 Principle of Bio-Plex by Bio-Rad (Bio-Rad Laboratories Inc., n.d.-c)

During this experiment, Bio-Plex is used to determine the concentration of several chemo- and cytokines. The functions of the investigated inflammation markers are listed in Table 3-1.

Table 3-1 Overview of investigated chemo- and cytokines using Bio-Plex. (Idriss & Naismith, 2000; Justiz Vaillant & Qurie, 2021; Ottum et al., 2015; Sokol & Luster, 2015)

Chemo-/cytokine	Function
IL-12	Induction of T-cells and interferon-gamma (IFN_γ) production by T-cells and natural killer (NK)-cells.
TNF	Role in cellular processes leading to apoptosis and necrosis.
Keratinocytes-derived chemokine (KC)	Chemoattractant for neutrophils.
IFN_γ	Induction of the expression of chemokines, neuroprotection, T-cell activation

3.4 Gene expression analysis using quantitative polymerase chain reaction

DNA is not the best marker to investigate gene expression as DNA only reveals whether a particular gene is present or not. The first step in gene expression is the transcription of DNA to mRNA. The more mRNA, the more transcription took place. That makes RNA the best marker to look at the expression of genes. However, to perform quantitative polymerase chain reaction (qPCR), DNA is needed. Reverse transcription can be used to form complementary DNA (cDNA), which in turn can be used for qPCR. The steps that need to take place are illustrated in Figure 3-4.

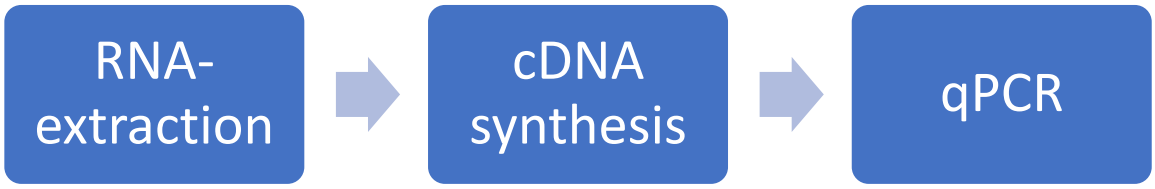

Figure 3-4 Roadmap to perform gene expression analysis.

3.4.1 RNA-extraction

The first step in the extraction of RNA is to lyse the tissue. In this project, TRIzol is used. TRIzol is a solution that consists of phenol and guanidinium isothiocyanate. The solution denatures proteins and solubilizes biological material. Guanidinium isothiocyanate is also a protective reagent for nucleic acids. The addition of chloroform and centrifugation induces the formation of three phases. RNA is present in the upper, aqueous phase. Proteins are present in the organic phase and DNA is present in the separating layer between the organic and aqueous phase. (Rio et al., 2010)

This project uses Aurum™ Total RNA Mini Kit by Bio-Rad for the extraction of mRNA. Solid-phase extraction is performed on the aqueous layer that forms after centrifugation. The aqueous solution is brought onto a silica-based column that can bind a maximum of 100 µg of purified RNA. Under certain conditions, RNA can bind to the silica in the column. Wash steps are inserted into the protocol to remove several contaminants such as proteins. DNase I is used to cleave DNA that may have bound to the column. The final step is to add an elution solution to the column. This solution either destroys the forces that created the binding of RNA and silica or creates a better environment for RNA to be in. Either way, RNA is eluted.(Bio-Rad Laboratories Inc., n.d.-b, n.d.-a; Christiaens et al., 2019)

3.4.2 cDNA synthesis

Using reverse transcription PCR (RT-PCR), cDNA can be synthesized from RNA. Just like a normal PCR reaction, primers and enzymes are needed to succeed the reaction. Hexamer and anchored oligo(dT) primers are used. The latter one binds specifically to the poly-A-tail of mRNA.(Meridian, 2018; Thermo Fisher Scientific, n.d.)

RT-PCR uses reverse transcriptase to convert RNA to cDNA. The enzyme binds to the primers that annealed to the RNA transcript and adds nucleotides in the 5'→3' direction. That way, a double-stranded RNA-cDNA hybrid is synthesized. (Pray, 2008)

The PCR program can be divided into different steps with different temperatures. The first step is primer annealing. The optimal temperature for this step differs from primer to primer and depends on the melting temperature. In this case, the optimal annealing temperature is 25 °C. In the next step, the reverse transcription, the temperature is raised to 42 °C as this is the optimal working temperature for reverse transcriptase. To inactivate the enzyme, the temperature is raised to 85 °C. That way, qPCR won't be inhibited by reverse transcriptase. The cDNA needs to be stored at 4 °C (short period) or -20 °C (longer period) to preserve the cDNA. (IRC VIB-UGent Lab Vandenbroucke, 2021; Thermo Fisher Scientific, n.d.)

3.4.3 qPCR

The final step in the gene expression analysis is qPCR. Different kits with qPCR reagents, such as SensiFAST™ SYBR® No-ROX Kit by Meridian Bioscience, are available. In this kit, a mastermix containing SYBR® Green dye, deoxynucleotide triphosphates, stabilizers and enhancers are included. The final qPCR mix consists of this mastermix together with primers and cDNA. (Meridian, n.d.)

Just like a classic PCR reaction, a qPCR reaction can be divided into different steps forming one cycle. The first step is denaturation at 95 °C. During this step, the double-stranded cDNA will be denatured using heat. The next step is the primer annealing at 60 °C. The primers are targeted to a specific gene of interest that will be amplified. The extension at 72 °C is the third step. DNA polymerase has a critical role in this step as this enzyme binds to the 3' end of the primer and adds nucleotides complementary to the original strand to extend the primer. After this step, the cycle is completed and the next cycle can start. As DNA and reagents are abundant at the beginning of a qPCR reaction, the DNA concentration increases exponentially (Figure 3-5). The reagents will become lacking as the cycles progress, leading to a non-exponential increase of DNA until no amplification can occur anymore (Figure 3-5). (Pestana et al., 2009; Roche Life Science, n.d.)

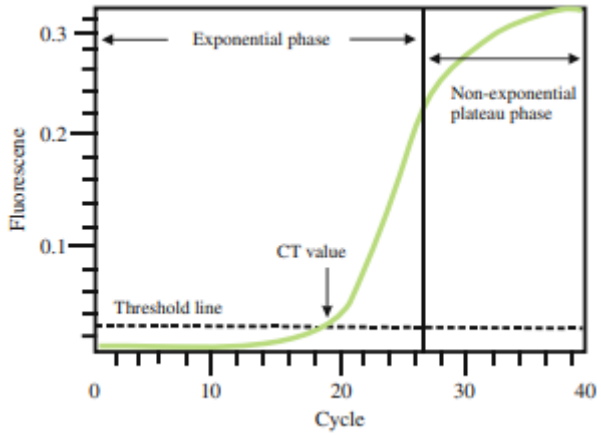

Figure 3-5 Amplification plot of qPCR (Pestana et al., 2009)

SYBR® Green is a fluorescent dye that shows a high increase in fluorescence when bound to double-stranded DNA. The amount of double-stranded DNA increases each qPCR cycle, and so does the fluorescence due to SYBR® Green. The number of cycles that is needed to detect the fluorescence of SYBR® Green above the background fluorescence is called the threshold cycle (C_t)-value. The C_t-value is a relative measure for the amount of DNA in a sample. There are more cycles needed to detect fluorescence above the background fluorescence when the original DNA concentration is lower. (Pestana et al., 2009; Thermo Fisher Scientific, 2016)

qPCR is a PCR reaction with which the relative concentration of DNA in a sample can be determined. As in this thesis cDNA derived from RNA is used, qPCR enables to determine the expression of different genes in the sample. To avoid any errors due to pipetting faults, the DNA levels need to be normalised using housekeeping genes (HKGs). By equating the expression of the HKG in all conditions and multiplying the expression of the other genes with the same factor, the expression can be normalised and conditions can be compared. In this thesis, glyceraldehyde-3-phosphate dehydrogenase (*Gadph*), ribosomal protein L (*Rpl*), hypoxanthine-guanine phosphoribosyltransferase (*Hprt*) and ubiquitin C (*Ubc*) are used as HKGs.(Decuyper, 2020; Panina et al., 2018)

The expression of multiple genes is investigated during this experiment. An overview of these genes and their function is given in Table 3-2. The function of *Tnf* is already listed in Table 3-1.

Table 3-2 Overview of the genes (and their function) that are investigated using qPCR (Anavi & Tirosh, 2020; Justiz Vaillant & Qurie, 2021; Liu et al., 2011; Perkins & Gilmore, 2006; Sokol & Luster, 2015; Vázquez et al., 2012)

Gene	Function
Il-1β	Activation of lymphocytes, hypothalamus and macrophages.
Il-4	Growth factor for B-cells, differentiation of Th2 helper cells, proliferation of mast cells.
Il-6	Differentiation of B-cells.
Ccl2	Chemoattractant for monocytes.
Ccl3	Stimulation of macrophages and NK-cells to migrate.
Ccl5	Chemoattractant for macrophages and NK-cells.
C-X-C motive chemokine ligand 10 kDa (*Cxcl10*)	Induction of apoptosis, proliferation, cell growth, angiogenesis and chemotaxis of multiple immune cells. Induced by IFN_{γ}.
Inducible nitric oxide synthase (*Inos*)	Marker for oxidative stress, supplying immune cells with glucose.
Nuclear factor of kappa light polypeptide gene enhancer in B-cells inhibitor, alfa (*Iκba*)	Induction of apoptosis and reduction of the expression of chemo- and cytokines.

3.5 Immunohistochemistry staining

The general principle of immunohistochemistry (IHC) stainings is to detect antigens or cellular structures in tissues. Several steps have to be performed to make this possible. These steps are extensively described below. (Im et al., 2019)

First of all, the tissue needs to be fixated in order to preserve tissue integrity during the IHC procedure. Fixation can occur in different ways: (i) by using chemicals that create crosslinks between proteins (aldehydes) or (ii) by precipitating proteins (acetone) or (iii) by freezing the tissue in optimal cutting temperature (OCT) compound. For bigger tissues or if multiple organs from the same animal need to be preserved, it is recommended to perfuse the animal with the chemical (e.g. paraformaldehyde). That way, the fixative reaches every part of the tissue in contrast to the immersion of the tissue into the fixative. (Gage et al., 2012; VIB Bioimaging core, n.d.)

After the fixation step, the tissue is often embedded in paraffin. Importantly, as the tissues contain water, they need to be dehydrated first. This can be done using a concentration gradient of ethanol (99 %, 90 % and 70 %) followed by treatment of the tissue with xylene. Finally, the tissue is embedded in paraffin to be able to cut the tissue. (Defever et al., 2019; Lemeire, 2021)

After cutting sections from the tissues, IHC can be performed. When using paraffin sections, the first step is deparaffinization. This can be done by using the same reagents as used for dehydration but this time in the reverse order. As antigens are crosslinked, antibodies can't bind with the antigen. Consequently, antigen retrieval needs to be done. There are two kinds of antigen retrieval: (i) Protease-Induced Epitope Retrieval (PIER) and (ii) Heat-Induced Epitope Retrieval (HIER). For this thesis, HIER is performed. HIER uses high temperature and pressure in combination with a buffered solution, such as citric acid, to unmask the antigens. The mechanism behind HIER is still unknown. (Im et al., 2019; Lemeire, 2021)

Next, the tissue is treated with a blocking solution to prevent aspecific binding of the antibody. For this, a combination of normal serum and protein blocking solution is used. The normal serum is derived from the same species as the secondary antibody. Protein blocking solution consists of proteins, such as bovine serum albumin (BSA), that bind to other proteins in the sample. This means that the primary antibody needs to compete to bind with the antigen, which leads to more specific binding. When peroxidase is used as a detection method, the tissue needs to be treated with hydrogen peroxide (H_2O_2) to prevent the endogenous enzymes to interfere with the detection. (Im et al., 2019; Proteintech group, Inc., n.d.)

There are two kinds of immunofluorescence (IF) staining: direct and indirect IF. For this thesis, indirect IF (Figure 3-6) is used. A primary antibody against the antigen of interest is added to the tissue. Afterwards, a fluorophore labelled secondary antibody (derived from a different species than the primary antibody) is added. This secondary antibody binds to the primary antibody. The location of the primary antibody and so the antigen can be determined using a fluorescence microscope. A secondary antibody can also be labelled with an enzyme. When adding a suitable substrate, a colour can develop. That colour can be observed with a light microscope. Between the different steps, the slices are washed with phosphate-buffered saline (PBS) to remove the unbound antibodies. (Im et al., 2019)

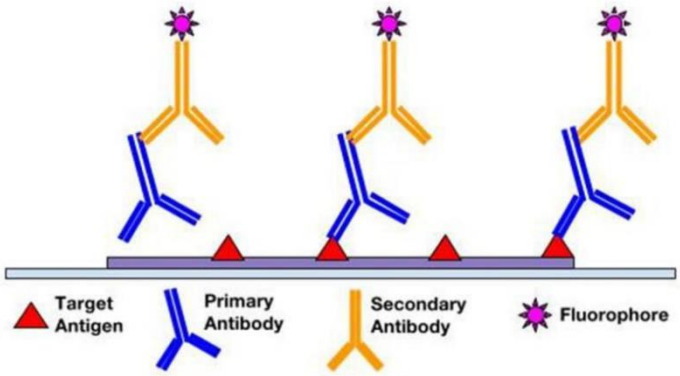

Figure 3-6 Principle of indirect IF staining (Im et al., 2019)

Signal amplification (Figure 3-7) is needed when the signal is too low to detect. This is mostly the case in stainings using horseradish peroxidase. For this step, kits are commercially available (e.g. avidin-biotin complex (ABC) kit by Thermo Fisher Scientific). In this latter kit, the polyclonal secondary antibodies are labelled with biotin which shows a big affinity towards tetravalent avidin carrying enzymes or fluorophores. In this way, a bigger signal can be created for one single primary antibody. (Im et al., 2019; Thermo Fisher Scientific, 2018)

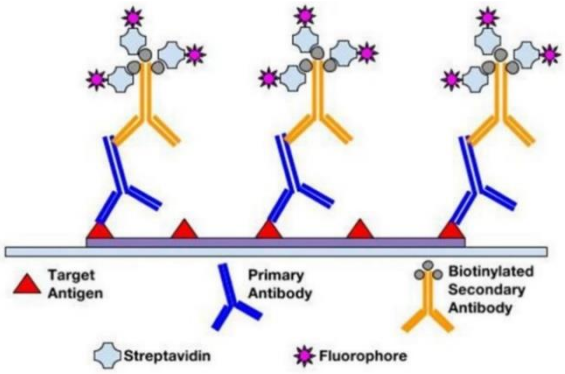

Figure 3-7 Principle of signal amplification(Im et al., 2019)

Several stainings are performed in this experiment. A general overview of these stainings is given in Table 3-3.

Table 3-3 Overview of the performed stainings for the experiment (Ayanlaja et al., 2017; Balthazart & Ball, 2014; Brenner, 2014; Mattei et al., 2006; Ohsawa et al., 2000)

Staining	Marker for	Primary antibody	Secondary antibody
Ionized calcium-binding adapter molecule 1 (Iba1)	Microglia and macrophages	Rabbit anti-Iba1	Goat anti-rabbit (GAR)
Glial fibrillary acidic protein (GFAP)	Glial cells	Rabbit anti-GFAP	
Doublecortin (DCX)	Neurogenesis and neuronal development	Anti-DCX	Anti-rabbit biotin
Apoptosis-linked gene-2 interacting protein X (Alix)	Apoptosis	Anti-Alix	

4 Materials and methods

To find an answer to the research questions, several experiments are conducted. The protocols of the experiments are provided in this chapter. A list of the materials and reagents and their companies is given in Addendum 1.

4.1 Bio-Plex

Materials:

- 96-well flat-bottom plate
- 96-well plate provided by Bio-Rad
- Aluminium foil
- Bio-Plex 200 reader
- Bio-Plex Pro Mouse Cytokine 23-Plex Assay
- Microplate washer
- MilliQ
- Pipettes with tips
- Plate shaker

All the reagents are provided by the kit.

Solutions and dilutions:

- **Bead solution:** Make a 1/10 dilution of the bead of interest in assay buffer with a total volume of 25 µl.
- **Detection antibody dilution:** Make a 1/20 dilution of the detection antibody of interest in assay buffer.
- **Steptavidin solution:** Make a 1/100 dilution of streptavidin in assay buffer. Make enough to add 25 µl to each well.

Methods:

1 Sample preparation for serum:
   - Collect blood into collection tubes with an anticoagulant.
   - Allow to clot at room temperature.
   - Centrifuge for 15 minutes at 1000 g at 4 °C.
   - Transfer the upper layer to a polypropylene tube
   - Centrifuge for 10 minutes at 10 000 g at 4 °C.
   - Isolate the upper layer.

2 Sample preparation for CSF:
   - Collect CSF into collection tubes.
   - Centrifuge for 10 minutes at 10 000 g at 4 °C.
   - Isolate the upper layer.

3 Prepare the microplate washer by running MilliQ and wash buffer through the machine.

4 Add 15 µl of the sample/standard to the well of a 96-well plate.

5 Add 15 µl 0,5 % albumin in diluent to samples without carrier proteins (such as BSA).

6 Add 15 µl of diluent to samples with carrier proteins.

7 Add 30 µl of diluent to a well as a negative control.
8 Put the plate on a shaker to make sure all fluids are on the bottom of the well.
9 Let incubate at room temperature for 20 minutes.
10 Add 25 µl of the bead solution to the wells of a 96-well plate from Bio-Rad.
11 Put the plate on a shaker for a few minutes to make sure all beads are on the bottom of the well.
12 Wash the plate using the microplate washer.
13 Add 25 µl of the sample in the wells with the beads.
14 Incubate at room temperature for 30 minutes while shaking the plate. Protect from light.
15 Wash the plate using the microplate washer.
16 Add 25 µl of the detection antibody dilution against the chemo- or cytokine of interest.
17 Incubate at room temperature for 30 minutes while shaking the plate. Protect from light.
18 Wash the plate using the microplate washer.
19 Add 25 µl of streptavidin solution.
20 Incubate at room temperature for 30 minutes while shaking the plate. Protect from light.
21 Wash the plate using the microplate washer.
22 Add 25 µl assay buffer to each well.
23 Measure the signal using the Bio-Plex 200-machine.

4.2 Gene expression analysis: qPCR

The protocol used to extract RNA and synthesize cDNA is added in Addendum 2 and Addendum 3.

Materials:

- 1,5 ml Eppendorf tubes
- 384-well plate
- cDNA samples
- Centrifuge
- Nuclease-free water
- PCR compatible stickers
- Pipettes
- Primers of interest
- qPCR compatible stickers
- qPCR machine
- SYBR Green Mix

The sequences of the used primers are given in Addendum 4.

Solutions and dilutions:

- **cDNA samples (500 ng):** Dilute with a factor of 10 using nuclease-free water.
- **Primer solutions:** Dilute 1000 µM primer solutions with a factor of 1000 so that one solution contains 1 µM of both forward and reverse primer.
- **Mastermix (for one reaction):** Mix 3 µl of primer solution and 5 µl SYBR Green Mix.

Method:

1. Dilute cDNA samples with 180 µl nuclease-free water.
2. Add 2 µl of cDNA of interest in the wells.
3. Seal the plate with a PCR compatible sticker.
4. Spin down the plate.
5. Add 8 µl mastermix of interest in the wells.
6. Seal the plate with a qPCR compatible sticker.
7. Spin down the plate.
8. Put the plate in the qPCR machine or store in the fridge at 4 °C protected from light.

Analysis of the results:

See Addendum 6.

4.3 Immunohistochemistry: Immunofluorescence staining

The protocol used to cut paraffin- and cryosections is added in Addendum 5.

Materials:

- 100 % methanol
- 10x PBS
- 30 % H_2O_2
- 4',6-diamidino-2-phenylindole (DAPI)
- ABC-kit
- Antigen retriever
- Antigen unmasking solution – citrate buffer
- Boric acid
- Bovine serum albumin (BSA) (Immunoglobulin G-free and protease-free)
- Closable box
- Coverslips
- Distilled water
- Hydrophobic barrier pen
- Microscopic slides with sections of interest
- MilliQ
- Sodium hydroxide
- Normal goat serum (NGS)
- Pipettes
- Poly-vinyl alcohol (PVA) + 1,4-diazabicyclo[2.2.2]octane (DABCO)
- Primary antibody of interest
- Secondary antibody of interest
- Tissues
- Triton X-100
- Tyramide Signal Amplification (TSA)
- Varistain apparatus

Solutions and dilutions:

- **Antigen unmasking solution-citrate buffer:** Dilute with a factor of 100 with distilled water (100 ml per container for the antigen retriever).
- **1x PBS:** Dilute 10x PBS with a factor of 10 with distilled water.
- **3 % H_2O_2:** Dilute 30 % H_2O_2 with a factor of 10 with 100 % methanol.
- **PBS-NGS-Triton (PBT)**: Add 0,5 % (m/V) BSA to PBS with 0,02 % (V/V) Triton X-100.
- **Blocking buffer**: Make a solution of 5% NGS in PBT.
- **Primary antibodies:** Dilute using blocking buffer as diluent. Dilution factors are shown in Table 4-1.

Table 4-1 Dilution factors of the different primary antibodies

Antibody	Dilution factor
Iba1	500
GFAP	1000
DCX	100
Alix	1000

- **Secondary antibodies:** Dilute using PBT as a diluent. The dilution factors are shown in Table 4-2. Protect the dilutions from light by wrapping them in aluminium foil.

Table 4-2 Dilution factors of the different secondary antibodies

Antibody	Dilution factor	Staining
Anti-rabbit biotin	500	DCX and Alix
GAR dylight 633	300	Iba1 and GFAP

- **DAPI:** Dilute DAPI 1/1000 in PBS and protect from light.
- **ABC-solution:** Make a dilution of 1 % solution A and 1 % of solution B in PBS.
- **0,1 M boric acid buffer pH 8,5 (1 l):** Dissolve 6,18 g of boric acid in 1 litre of MilliQ and bring the pH to 8,5 using sodium hydroxide.
- **TSA solution:** Make a 1/20 000 dilution of TSA in 0,1 M boric acid buffer. It is recommended to first make an intermediate 1/20 dilution.
- **Streptavidin-dylight 633 and DAPI:** Make a dilution of 0,1 % streptavidin-dylight 633 and 0,1 % DAPI in PBS. Protect this dilution from light.

Method:

1 Put the microscopic slides into the Varistain device and let them run a dewaxing programme (Table 4-3).

Table 4-3 Dewaxing programme on the Varistain device

Step	Liquid	Duration (minutes)
1	Xylene	5
2	Xylene	5
3	Xylene	5
4	Ethanol 99 %	1
5	Ethanol 99 %	1
6	Ethanol 90 %	1
7	Ethanol 90 %	1
8	Ethanol 70 %	1
9	Destilled water	PASS
10	Haematoxylin	PASS
11	Haematoxylin	PASS
12	Tap water	2

2 After dewaxing the coupes, bring the microscopic slides in a container suitable for the antigen retriever, filled up to ¾ with antigen unmasking solution.

3 Fill the container and bring it into the antigen retriever.

4 After antigen retrieval, wash the microscopic slides three times with PBS for five minutes.

5 Only for DCX and Alix stainings: Bring the microscopic slices in 3 % H_2O_2 for ten minutes.

6 Only for DCX and Alix stainings: Wash the microscopic slices three times with PBS for five minutes.
7 Wipe the microscopic slides around the tissues and remove the tissues that will not be used for staining.
8 Use a hydrophobic barrier pen to make a hydrophobic barrier around the tissue.
9 Add the blocking buffer to the tissues and let it incubate for 30 minutes at room temperature.
10 Remove the blocking buffer to add the primary antibodies to the sections. (Don't remove the blocking buffer of the sections that will be used as negative control).
11 Add the dilution of the primary antibody of interest on the sections (not on the negative control). The volume needed per section depends on the size.
12 Let incubate overnight at 4 °C in a closable box filled with water and tissues.
13 Remove all fluids from the sections and put PBS on them.
14 Wash the microscopic slices three times for five minutes with PBS.
15 Add the dilution of the secondary antibody of interest on the sections, including the negative control.
16 Let incubate for an hour in a closable box.
17 After incubation, wash the microscopic slides three times for five minutes with PBS. Between renewing PBS, protect the microscopic slides from light.

<u>Additional steps for stainings that do not use TSA and peroxidase (Iba1 and GFAP)</u>

1 Put PVA + DABCO at 37 °C.
2 After washing the microscopic slides (step 17), add DAPI to the sections.
3 Let incubate for 30 minutes in a closable box.
4 Wash the microscopic slides three times for five minutes with PBS. Between renewing PBS, protect the microscopic slides from light.
5 Add a few drops of mounting medium (PVA + DABCO) on the microscopic slide.
6 Place a coverslip on the microscopic slide and remove air bubbles.
7 Let the mounting medium dry overnight at room temperature. Protect the microscopic slides from light.
8 Keep the microscopic slides at 4 °C until imaging can be performed.

<u>Addition steps for DCX and Alix stainings</u>

1 Incubate the ABC-solution for 30 minutes at room temperature.
2 After washing the microscopic slides (step 17), add ABC-solution to the sections.
3 Let incubate for 30 minutes in a closable box.
4 Wash the microscopic slides three times for five minutes with PBS.
5 After washing the microscopic slides (step 4), add 1/20 000 dilution of TSA on the sections.
6 Let incubate for ten minutes in a closable box.
7 Wash the microscopic slides three times for five minutes with PBS.
8 Add the streptavidin-DAPI-PBS dilution to the sections.
9 Let incubate for 30 minutes in a closable box.
10 Put PVA at 37 °C.

11 Wash the microscopic slides three times for five minutes with PBS. Between renewing PBS, protect the microscopic slides from light.
12 Add a few drops of mounting medium (PVA+DACBO) on the microscopic slide.
13 Place a coverslip on the microscopic slide and remove air bubbles.
14 Let the mounting medium dry overnight at room temperature. Protect the microscopic slides from light.
15 Keep the microscopic slides at 4 °C until imaging can be performed.

Analysis of the results:
See Addendum 6.

5 Results and discussion

In this chapter, the results of the experiments performed to investigate the effect of MSC-EVs on NPC will be shown and discussed. Discrimination between peripheral organs and the central nervous system is made.

5.1 Effect of MSC-EV treatment on weight gain

The weight of the treated mice is determined at several time points. This data is used to calculate the weight gain compared to the weight at the first injection(Figure 5-1).

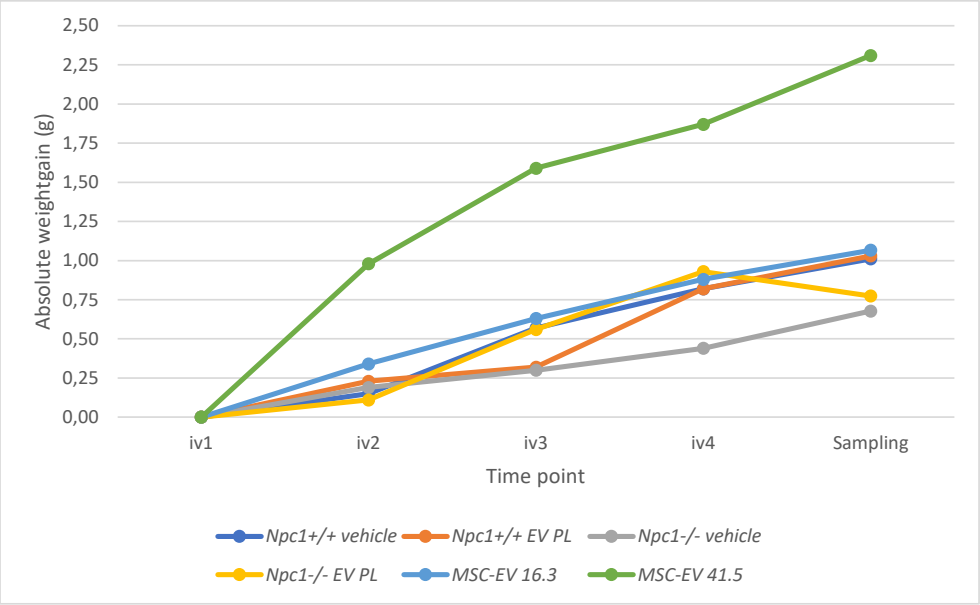

Figure 5-1 Mean absolute weight gain on several time points of the treated mice

All of the treatments, except for MSC-EV 41.5, have a similar effect on the weight gain with a slight increase of 0,68 g up to 1,07 g before sampling compared to the weight at the first injection. However, treatment with MSC-EV 41.5 causes an increase of weight with 1,75 g within the same time. These preliminary results suggest that MSC-EV 41.5 can be able to revert the NPC1 pathology.

5.2 Effect of MSC-EV treatment on peripheral organs

5.2.1 Bio-Plex on serum

Previous studies performed by scientists at Vandenbroucke Lab at IRC-UGent showed differences in certain chemo- and cytokines in serum between *Npc1*$^{+/+}$ and *Npc1*$^{-/-}$ mice. Based on these results, the concentration of KC and IL-12 are determined in serum of mice treated with the different substances described in 3.1 (Figure 5-2). The function of the chemo- and cytokines is described in 3.3. (IRC VIB-UGent Lab Vandenbroecke, 2020)

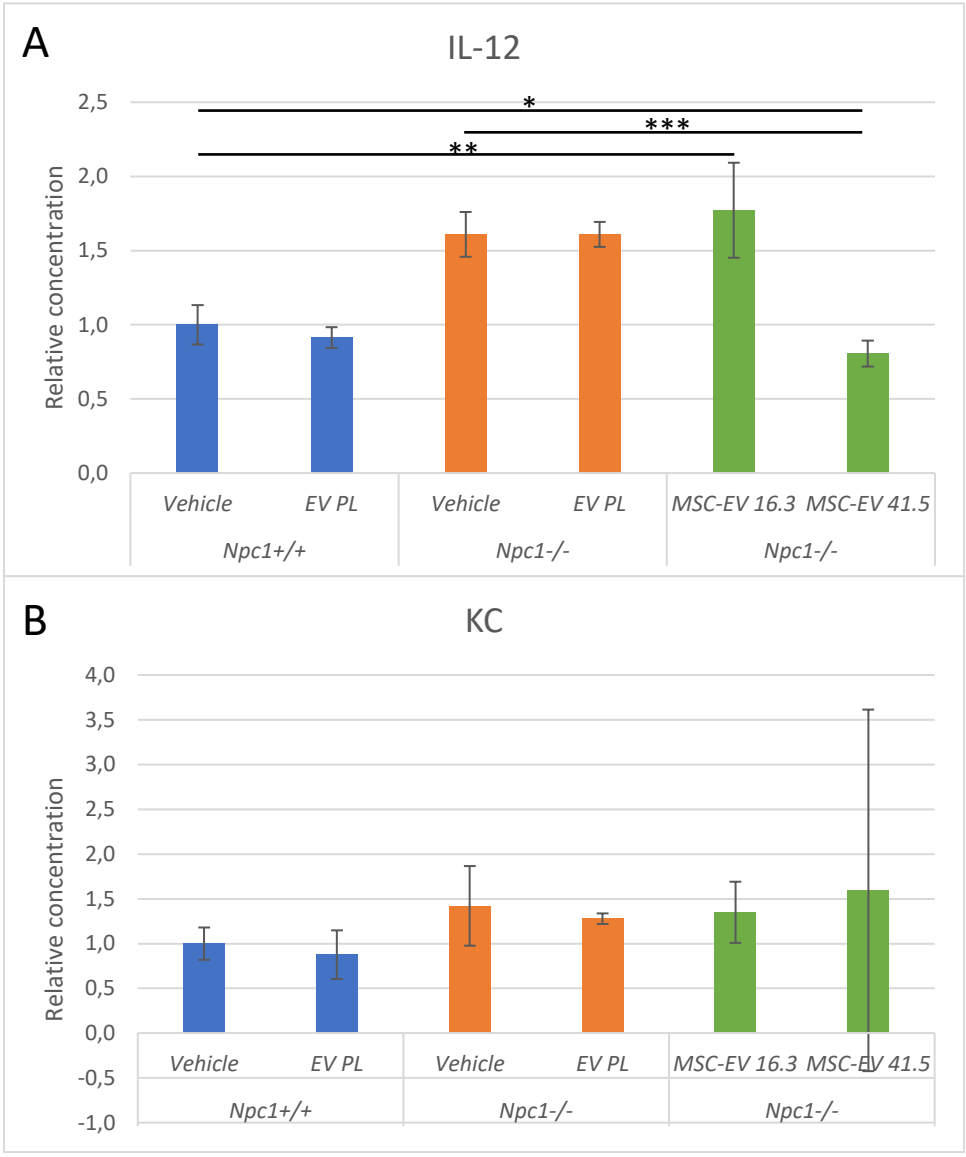

*Figure 5-2 Relative concentration of interleukin-12 (A) and keratinocyte-derived chemokine (B) in serum samples after treatment of mice. Sample size (n) = five per group. The error bars represent the standard deviation. T-test is performed and significancy is indicated: * = p < 0,05; ** = p < 0.01; *** = p < 0.001.*

5.2.2 Liver, lung and spleen

The liver, lung and spleen are peripheral organs that are affected by the NPC1 pathology. For each tissue, RNA is extracted out of 30 samples (five mice per treatment) and is used to synthesize cDNA. This cDNA is used to investigate the expressions of *Tnf and Il-1β* via qPCR (Figure 5-3). The functions of these cytokines are described in 3.3 and 3.4.3.

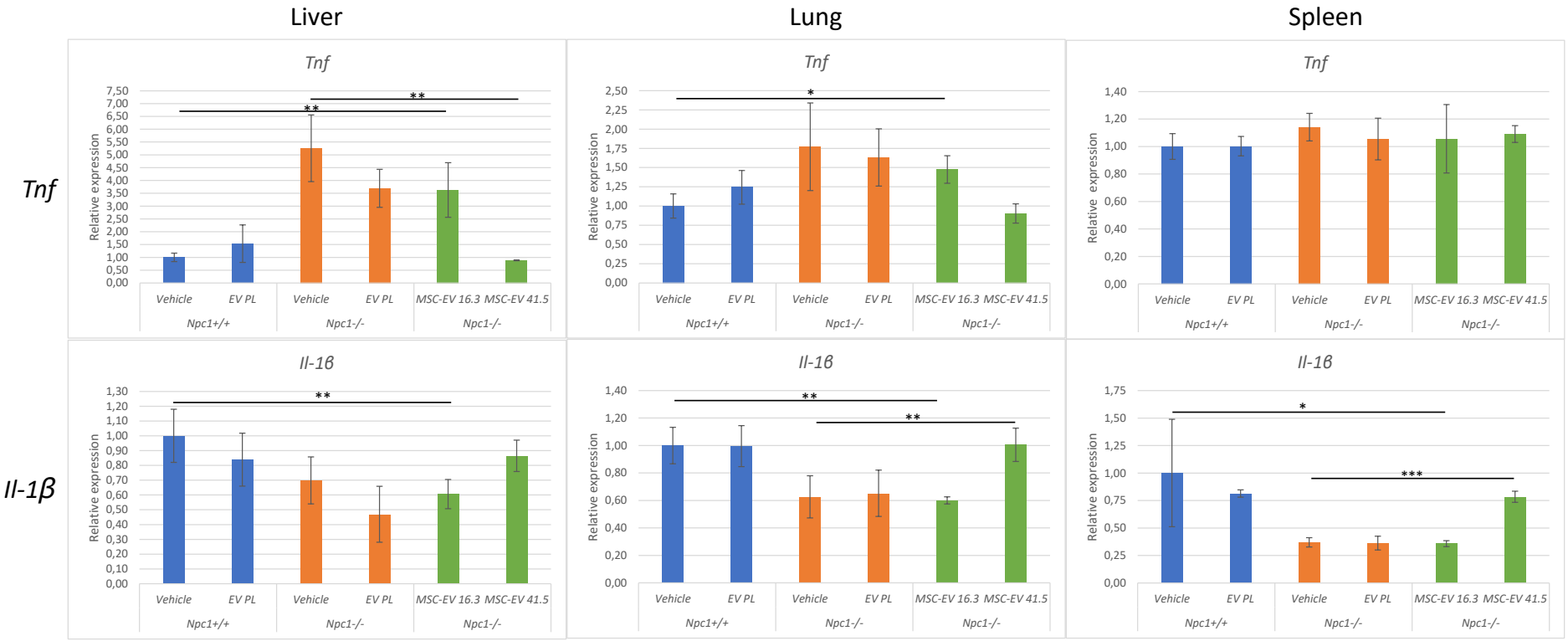

*Figure 5-3 Relative expression of tumour necrosis factor and interleukin-1β in liver, lung and spleen samples after treatment of mice. n = five per group. The error bars represent the standard deviation. T-test is performed and significancy is indicated: * = p < 0,05; ** = p < 0.01; *** = p < 0.001.*

5.2.3 Discussion

During the treatment of the mice, the weight gain is kept in track. *Npc1*$^{-/-}$ mice treated with MSC-EV 41.5 showed a remarkable higher weight gain compared to the other groups of mice. Based on these results, the expectation was that MSC-EV 41.5 would cause an effect on NPC1 pathology.

Bio-Plex showed a significant difference in the concentration of IL-12 between mice treated with MSC-EV 41.5 and mice treated with MSC-EV 16.3. IL-12 is a cytokine that induces T-cells and IFN_γ production, which has a neuroprotective function among other functions. The concentration of IL-12 was lower in the MSC-EV 41.5 group, meaning that fewer inflammation markers are expected in the plasma of these mice. (Justiz Vaillant & Qurie, 2021)

qPCR was performed to determine the expression of several inflammatory genes in tissues. Based on the results, it was possible to make three big groups per tissue. The first group consists of the genes that meet the following criteria:

- The expression levels of the different groups show that MSC-EV 41.5 can revert the NPC1 pathology, while MSC-EV 16.3 can't.
- There is a significant difference between the expression value of mice treated with MSC-EV 41.5 and *Npc1*$^{-/-}$ control mice and also between mice treated with MSC-EV 16.3 and *Npc1*$^{+/+}$ control mice. Furthermore, there isn't a significant difference between mice treated with MSC-EV 41.5 and *Npc1*$^{+/+}$ control mice and also not between mice treated with MSC-EV 16.3 and *Npc1*$^{-/-}$ control mice.

The second group consists of genes that only meet the first criterium, but not the second. Genes are classified in the third group when none of the criteria is met.

Tnf, *Il-1β* and *Cxcl10* can be classified in either the first or the second group. This is not the case for the spleen (*Tnf*). For all three genes, this means that treatment of *Npc1*$^{-/-}$ mice with MSC-EV 41.5 decreases the gene expression to approximately the same level as healthy mice. This conclusion cannot be extended to treatment with MSC-EV 16.3. Based on these results, it can be concluded that administration of MSC-EV 41.5 caused a decrease in apoptosis in NPC1 pathology. Furthermore, fewer lymphocytes and macrophages are expected. (Idriss & Naismith, 2000; Justiz Vaillant & Qurie, 2021; Liu et al., 2011)

Ccl2, *Ccl3* and *Ccl5* are in most of the cases classified in the second group. As these genes encode for chemoattractants, fewer immune cells, such as monocytes, macrophages and NK-cells, are expected in *Npc1*$^{-/-}$ mice after treatment with MSC-EV 41.5. It should be mentioned that there is either not always sufficient significant difference between the groups or a significant difference between the control groups of the same genotype. (Sokol & Luster, 2015)

Finally, treatment of *Npc1*$^{-/-}$ mice with either MSC-EV 16.3 or MSC-EV 41.5 does not have any influence on the expression of *Inos* or *Iκba*. Since no clear pattern can be derived from the expression levels, it can be concluded that *Npc1*$^{-/-}$ mice don't suffer more from oxidative stress compared to *Npc1*$^{+/+}$ mice. (Anavi & Tirosh, 2020; Perkins & Gilmore, 2006; Vázquez et al., 2012)

When these conclusions are combined, there is a decrease of lymphocytes and macrophages in *Npc1*$^{-/-}$ mice after treatment with MSC-EV 41.5. Moreover, less apoptosis and necrosis should be seen. On the other hand, the same or even a higher concentration of these immune cells should be seen after treatment of the mice with MSC-EV 16.3. Based on these results, MSC-EV 41.5 has an anti-inflammatory effect on NPC1 pathology.

As NPC-related hepatitis and pneumonia are associated with an increase of TNF and IL-1β, the expectation was to see a difference between *Npc1*$^{+/+}$ and *Npc1*$^{-/-}$ mice. This is confirmed by the results of the qPCR on the liver and lung. Moreover, studies have shown that NPC is relatable to oxidative stress. The expression pattern of *Inos* doesn't confirm this theory. As apoptosis appears in an inflamed liver or lung, higher levels of *Iκba* were expected in *Npc1*$^{-/-}$ mice. The results, however, don't show this pattern. The expectation for the gene expression analysis on the spleen was that it would be comparable to the liver as both organs are similarly affected by the pathology. However, only IL-1β shows a comparable pattern. This could mean that the spleen is less affected by inflammation than the liver. (Idriss & Naismith, 2000; Justiz Vaillant & Qurie, 2021; Mukhopadhyay et al., 2006; Perkins & Gilmore, 2006; Rimkunas et al., 2009; Vázquez et al., 2012)

The error bars, showing the standard deviation, in some graphs are quite large. This can be due to several causes. A first explanation is that there could be variation between the mice within one group. Another explanation could be pipetting faults during qPCR, although this risk is reduced by including technical replicates. As there is a long process before qPCR (treatment of the mice, sampling, RNA extraction and cDNA syntheses), there could be a lot more explanations why the standard deviation is large.

5.3 Central nervous system

5.3.1 Bio-Plex on CSF

Previous studies performed by scientists at Vandenbroucke Lab at IRC-UGent showed differences in certain chemo- and cytokines in serum between *Npc1*$^{+/+}$ and *Npc1*$^{-/-}$ mice. Based on these results, the concentration of IFN_γ, KC and TNF was determined in CSF of mice treated with the different substances described in 3.1 (Figure 5-4). The function of the investigated chemo- and cytokines are described in 3.3. (IRC VIB-UGent Lab Vandenbroecke, 2020)

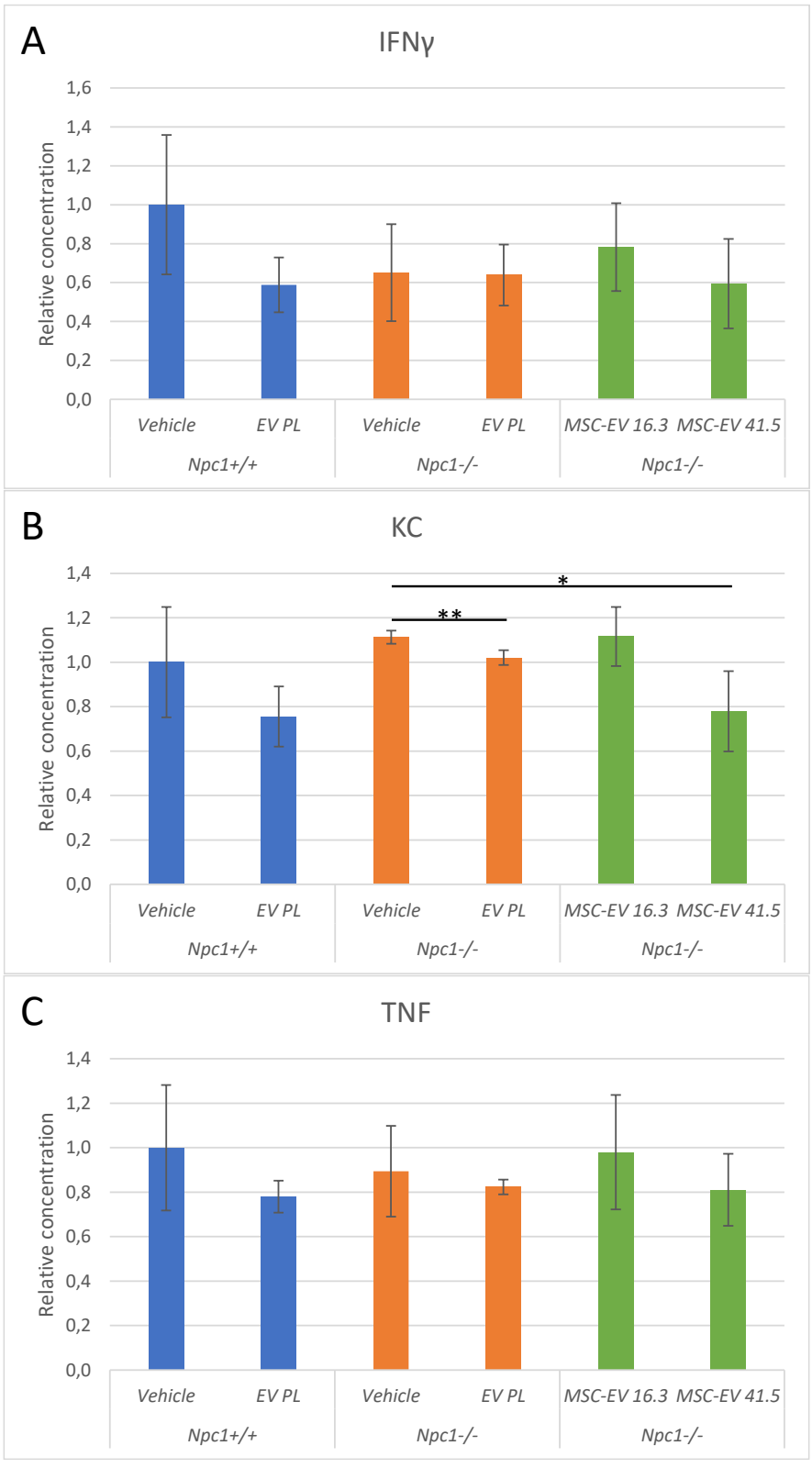

*Figure 5-4 Relative concentration of interferon-gamma (A), keratinocyte-derived chemokine (B) and tumour necrosis factor (C) in cerebrospinal fluid samples after treatment of mice. n = 5 per group. The error bars represent the standard deviation. T-test is performed and significancy is indicated: * = p < 0,05; ** = p < 0.01; *** = p < 0.001.*

5.3.2 (Pre-frontal) Cortex

5.3.2.1 qPCR

To investigate the effect of treatment of NPC1 with MSC-EVs in the brain, the organ is parted into five big regions. The prefrontal cortex (PFC) is one of these regions. In the PFC, the expressions of *Tnf*, *Il-1β*, *Inos*, *Iκba*, *Il-4*, *Il-6*, *Ccl2*, *Ccl3*, *Ccl5* and *Cxcl10* (Figure 5-5, Figure 5-6 and Addendum 7) are investigated. cDNA that was synthesized out of RNA that was extracted out of 30 PFC samples is used. The functions of the genes of interest are described in 3.3 and 3.4.3.

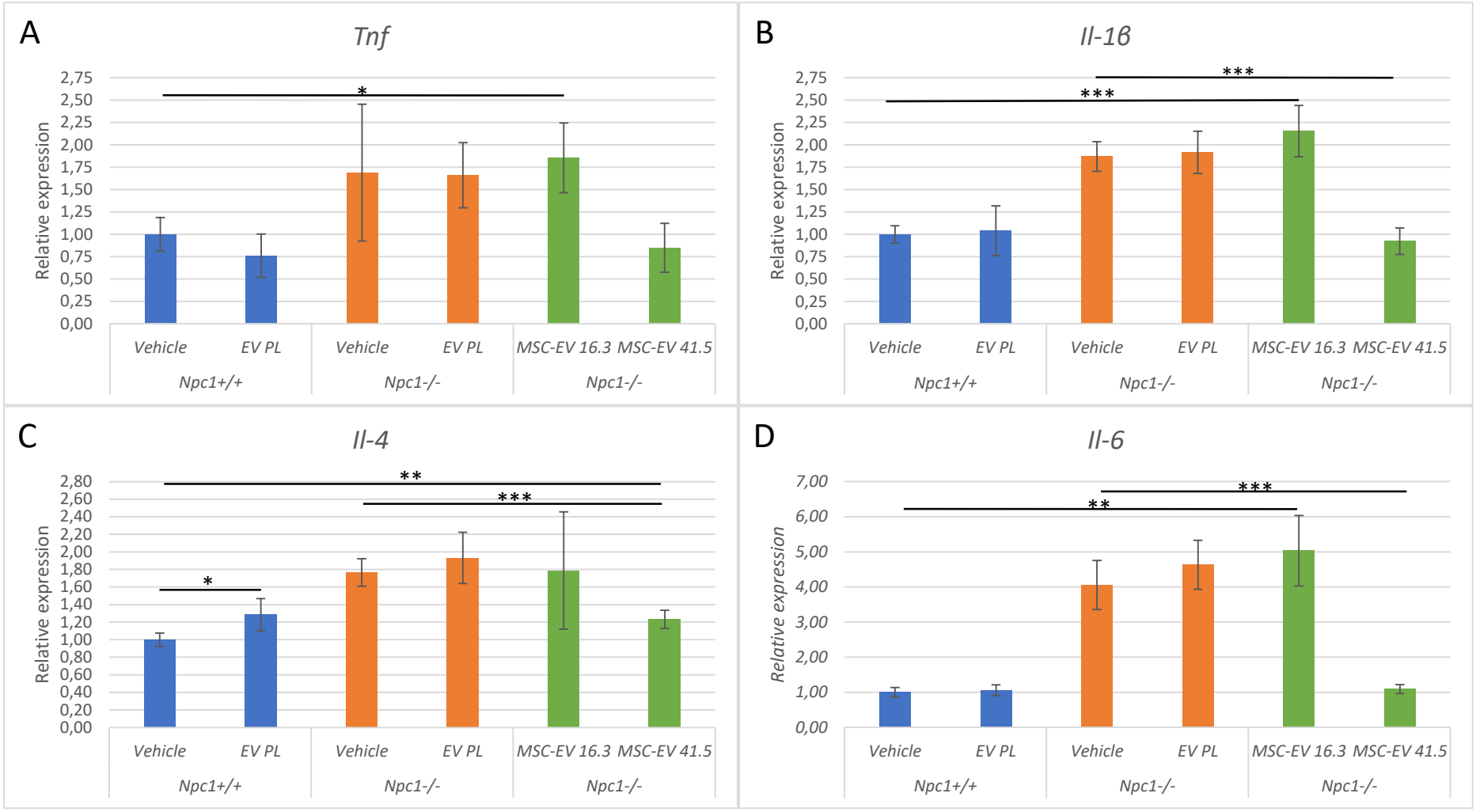

*Figure 5-5 Relative expression of tumour necrosis factor (A), interleukin-1β (B), interleukin-4 (C), interleukin-6 (D) in prefrontal cortex samples after treatment of mice. n = five per group. The error bars represent the standard deviation. T-test is performed and significancy is indicated: * = p < 0,05; ** = p < 0.01; *** = p < 0.001.*

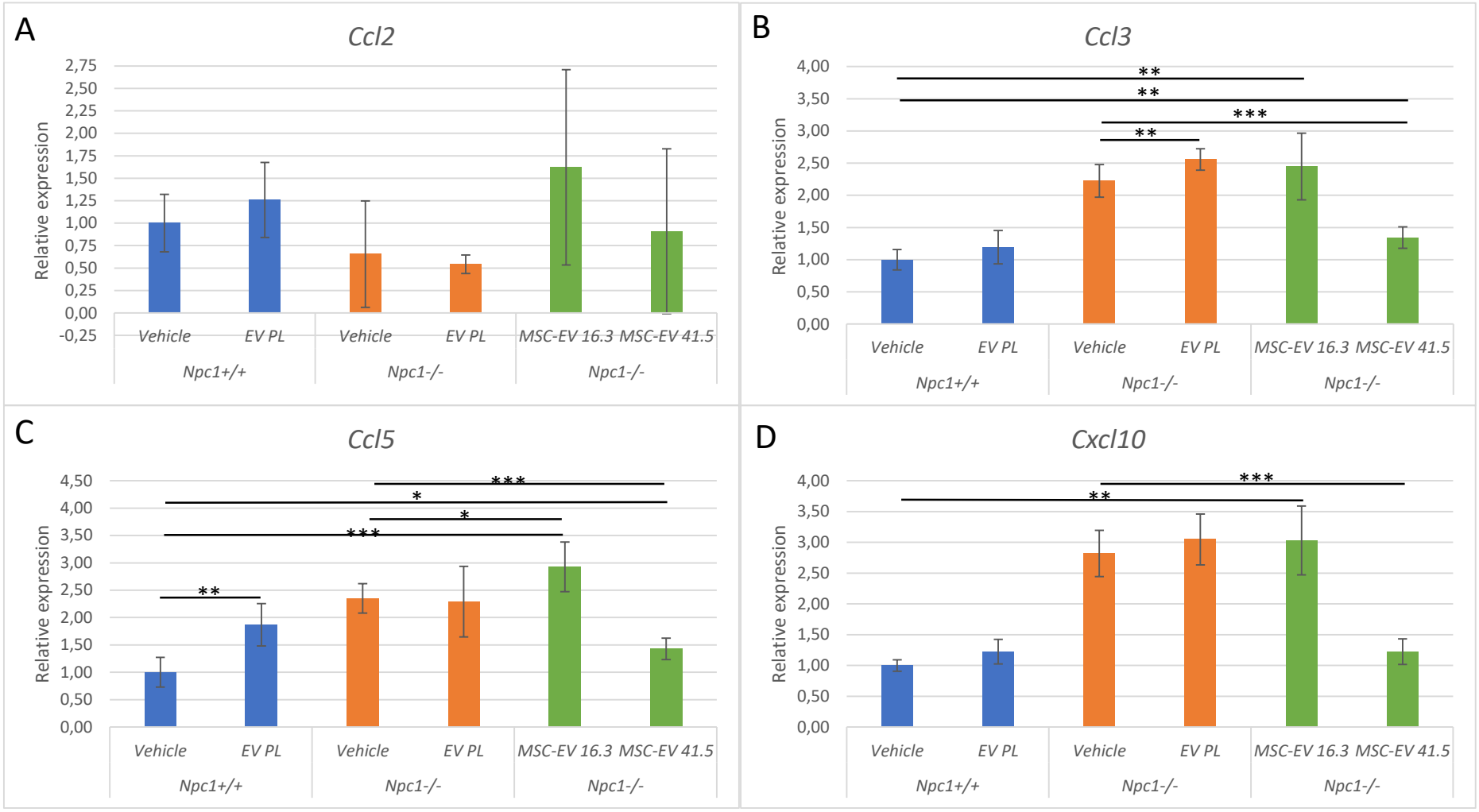

*Figure 5-6 Relative expression of C-C motif chemokine ligand 2 (A), C-C motif chemokine ligand 3 (B), C-C motif chemokine ligand 5 (C) and C-X-C motif chemokine ligand 10 (D) in prefrontal cortex samples after treatment of mice. n = five per group. The error bars represent the standard deviation. T-test is performed and significancy is indicated: * = p < 0,05; ** = p < 0.01; *** = p < 0.001.*

5.3.2.2 Immunohistochemistry

Iba1-, GFAP-, DCX- and Alix-stainings are performed on the cortex (Figure 5-7). The corresponding graphs are presented in Figure 5-8.
These stainings are performed to detect certain structures or cellular processes that are described in 3.5.

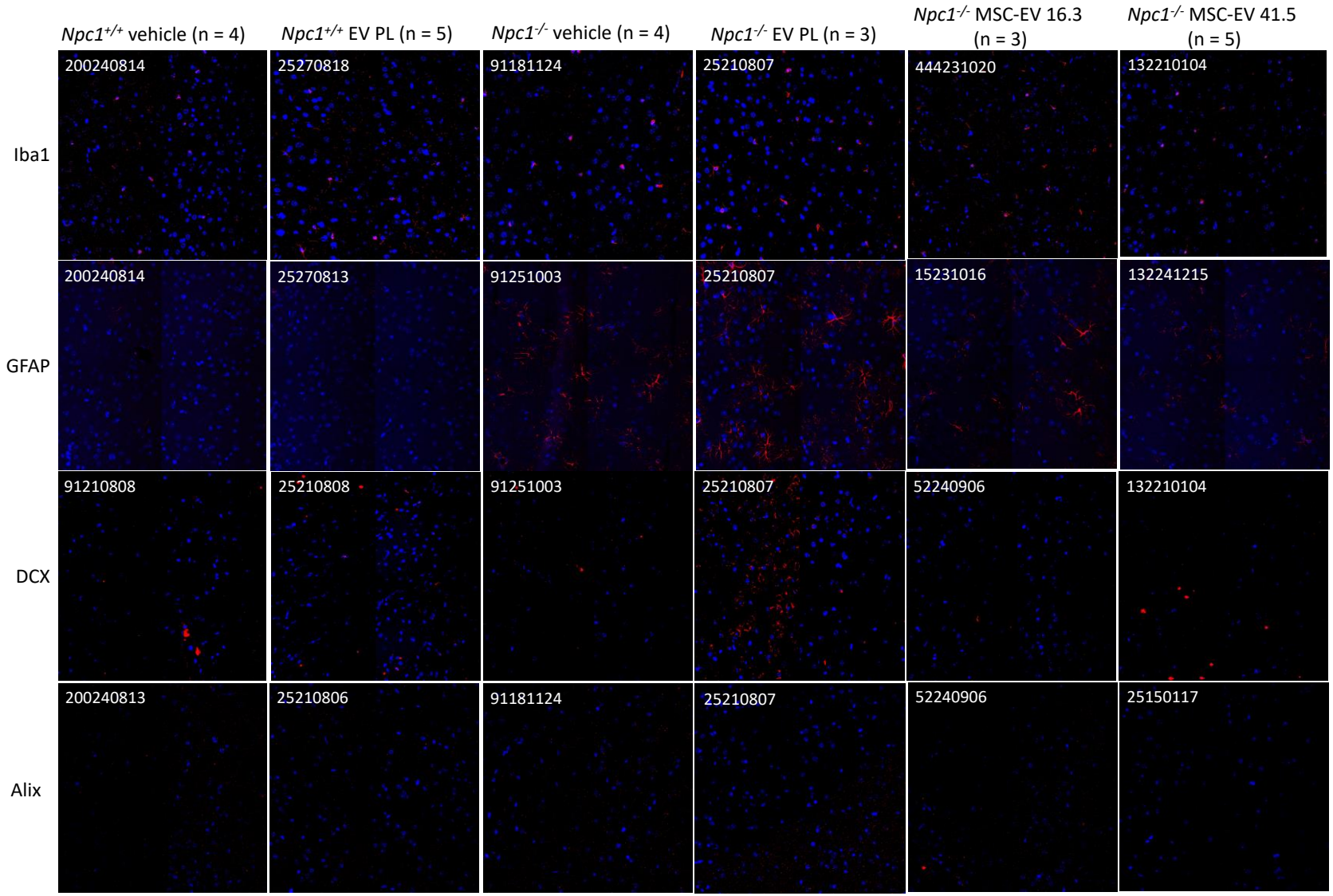
Npc1$^{+/+}$ vehicle (n = 4)
Npc1$^{+/+}$ EV PL (n = 5)
Npc1$^{-/-}$ vehicle (n = 4)
Npc1$^{-/-}$ EV PL (n = 3)
Npc1$^{-/-}$ MSC-EV 16.3 (n = 3)
Npc1$^{-/-}$ MSC-EV 41.5 (n = 5)
Iba1
GFAP
DCX
Alix
200240814
25270818
91181124
25210807
444231020
132210104
200240814
25270813
91251003
25210807
15231016
132241215
91210808
25210808
91251003
25210807
52240906
132210104
200240813
25210806
91181124
25210807
52240906
25150117

Figure 5-7 Representative images of the performed stainings on the cortex. Each image represents three up to five images of samples from the same group. The eartag of the mouse is shown in the upper left corner. Magnification = 40x

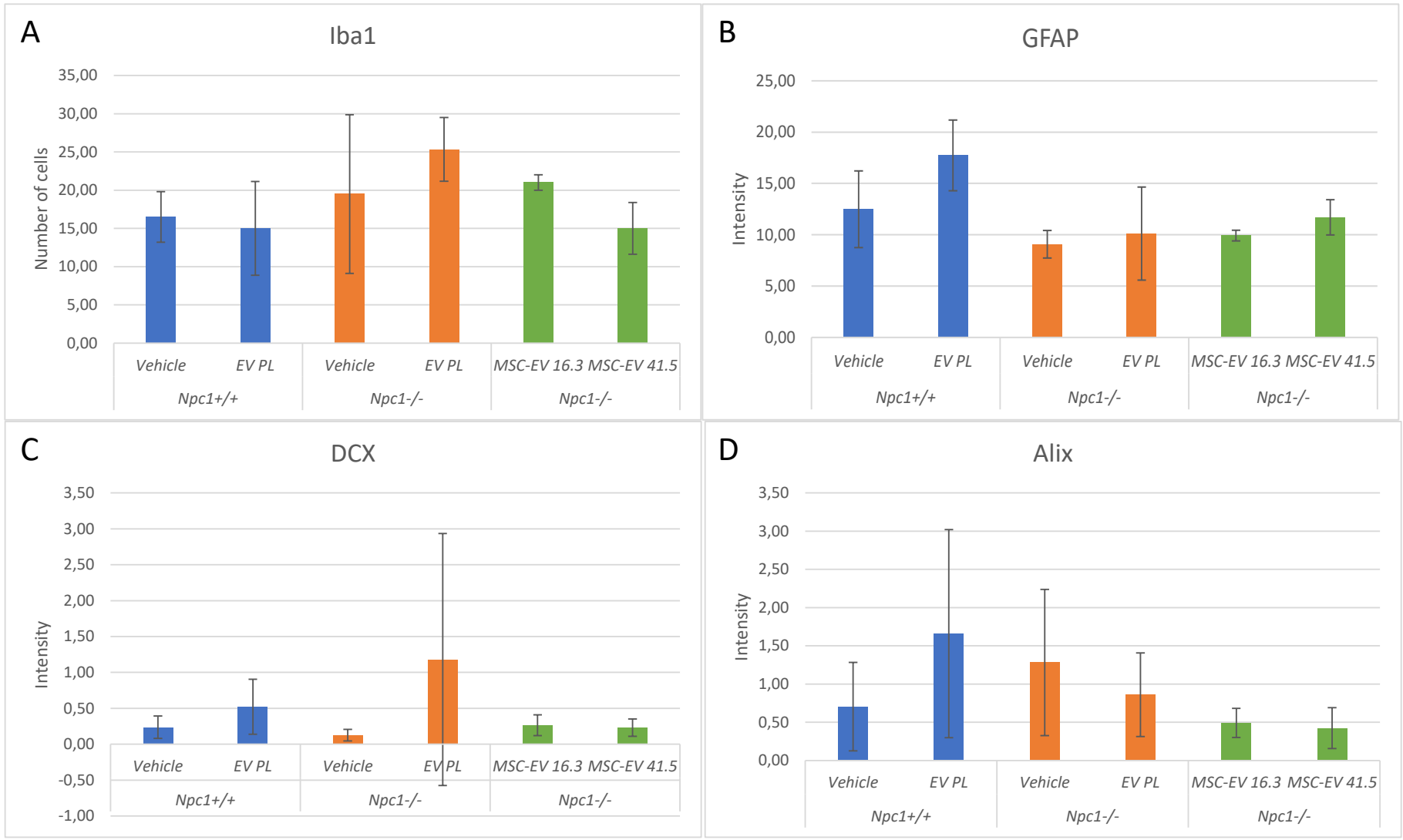

*Figure 5-8 The number of positive cells or the intensity of the signal for the different stainings on the cortex. A = ionized calcium-binding adapter molecule 1; B = glial fibrillary acidic protein; C = doublecortin and D = apoptosis-linked gene-2 interacting protein X. The error bars represent the standard deviation. T-test is performed and significancy is indicated: * = p < 0,05; ** = p < 0,01; *** = p < 0,001.*

5.3.3 Olfactory bulb

5.3.3.1 qPCR

The olfactory bulb (OB) is another brain region that is investigated. RNA is extracted out of 30 OB samples to synthesize cDNA out of it. This cDNA is used to perform qPCR to investigate the expressions of *Tnf*, *Il-1β*, *Inos*, *Iκba*, *Il-4*, *Il-6*, *Ccl2*, *Ccl3*, *Ccl5* and *Cxcl10* (Figure 5-9, Figure 5-10 and Addendum 7). In 3.3 and 3.4.3, the functions of these genes are described.

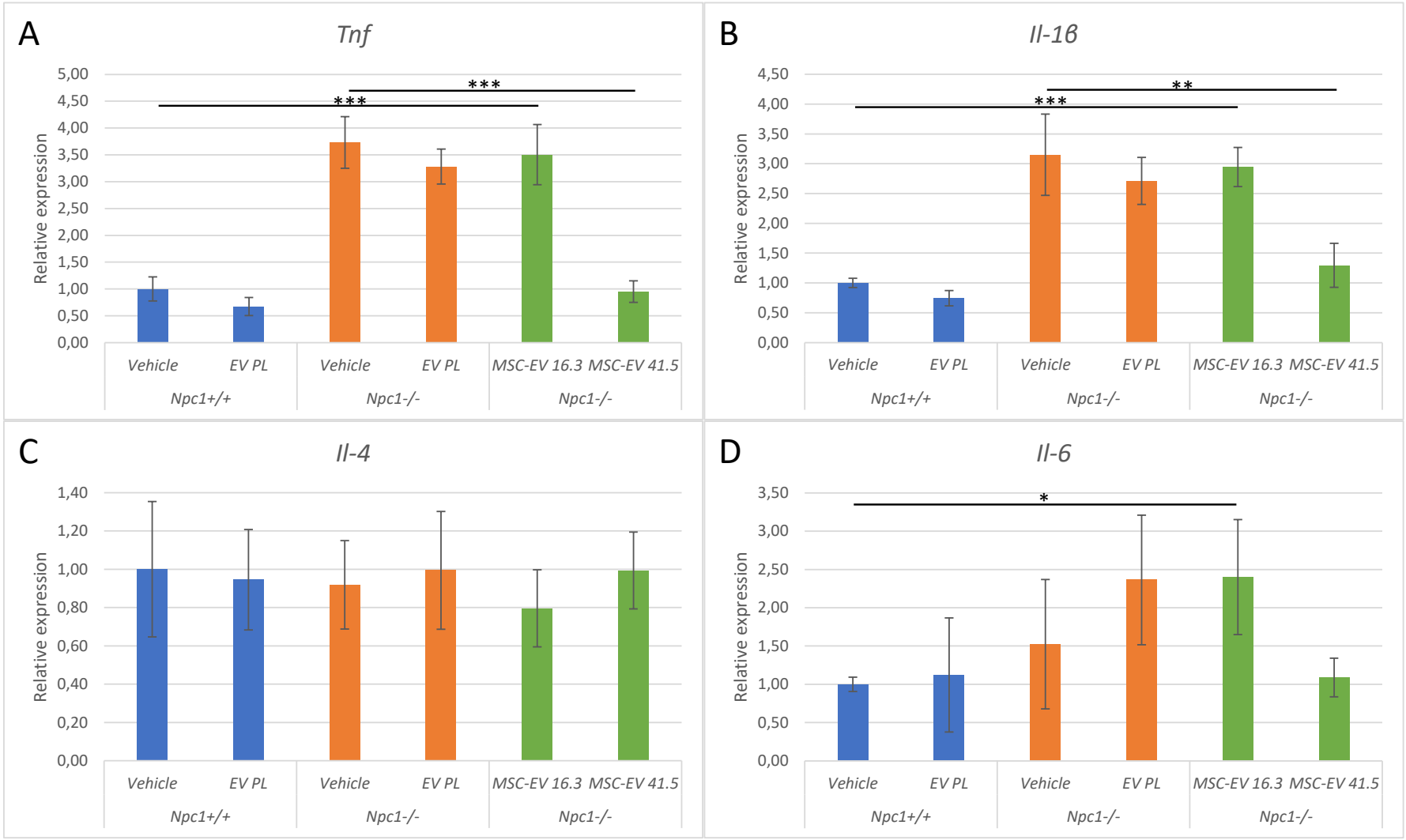

*Figure 5-9 Relative expression of tumour necrosis factor (A), interleukin-1β (B), interleukin-4 (C), interleukin-6 (D) in olfactory bulb samples after treatment of mice. n = five per group. The error bars represent the standard deviation. T-test is performed and significancy is indicated: * = p < 0,05; ** = p < 0.01; *** = p < 0.001.*

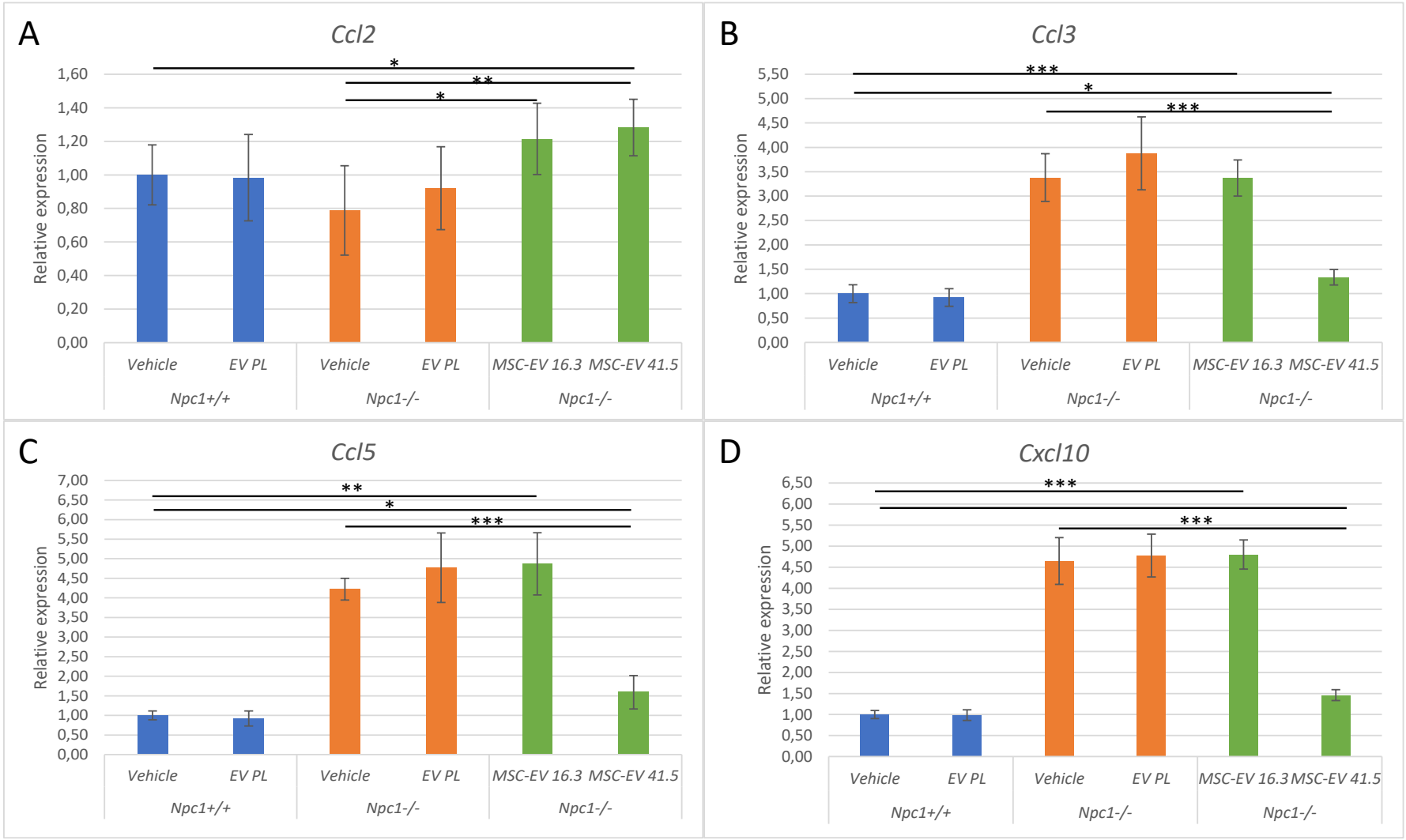

*Figure 5-10 Relative expression of C-C motif chemokine ligand 2 (A), C-C motif chemokine ligand 3 (B), C-C motif chemokine ligand 5 (C) and C-X-C motif chemokine ligand 10 (D) in olfactory bulb samples after treatment of mice. n = five per group. The error bars represent the standard deviation. T-test is performed and significancy is indicated: * = p < 0,05; ** = p < 0.01; *** = p < 0.001.*

5.3.4 Cerebellum

5.3.4.1 qPCR

A third part of the brain that is investigated is the cerebellum (CB). qPCR is performed using cDNA that is synthesized out of RNA that is extracted out of 30 CB samples. The expression of *Tnf*, *Il-1β*, *Inos*, *Iκba*, *Il-4*, *Il-6*, *Ccl2*, *Ccl3*, *Ccl5* and *Cxcl10* is investigated (Figure 5-11, Figure 5-12 and Addendum 7). Table 3-1 and Table 3-2 are dedicated to the functions of these chemo- and cytokines.

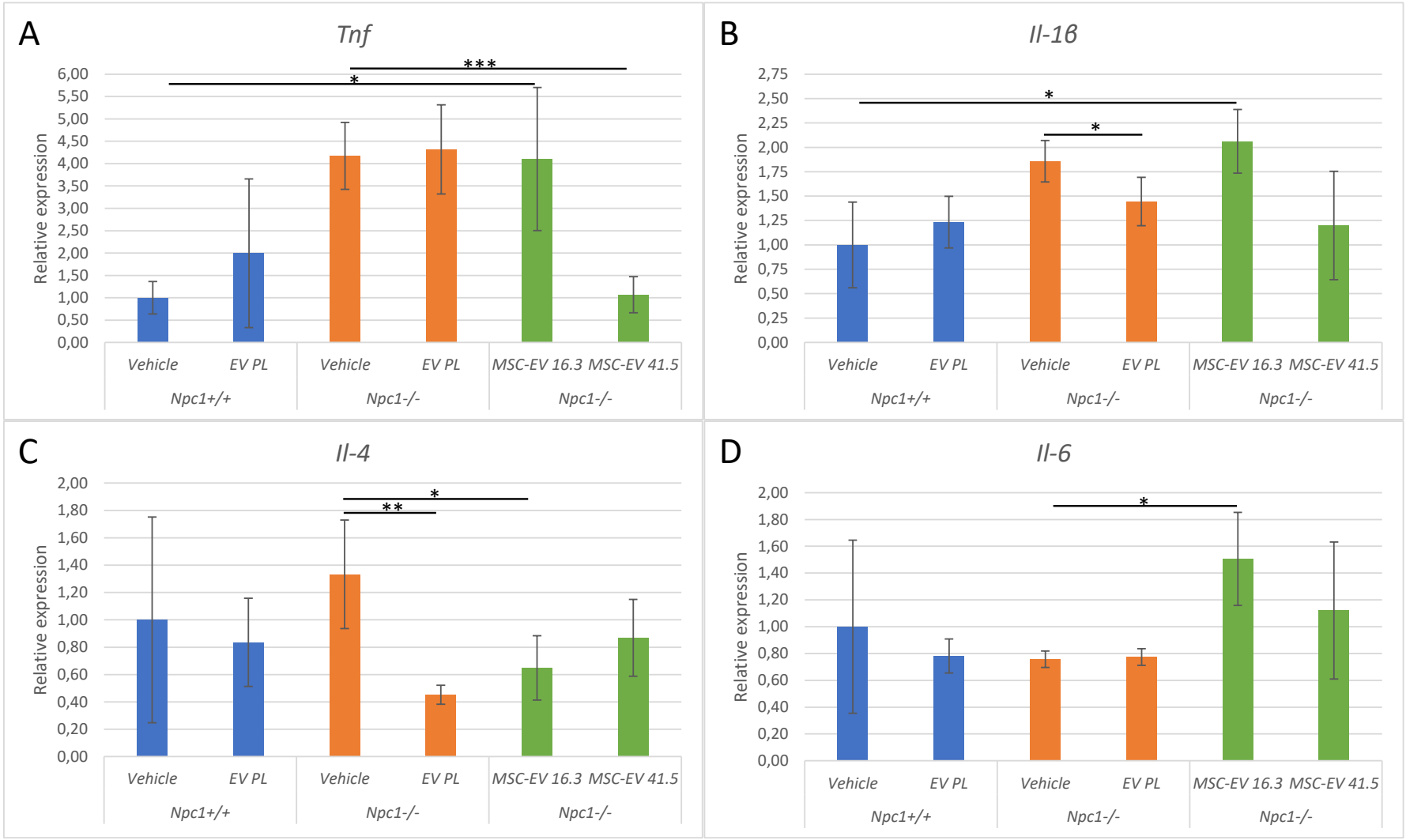

*Figure 5-11 Relative expression of tumour necrosis factor (A), interleukin-1β (B), interleukin-4 (C), interleukin-6 (D) in cerebellum samples after treatment of mice. n = five per group. The error bars represent the standard deviation. T-test is performed and significancy is indicated: * = p < 0,05; ** = p < 0.01; *** = p < 0.001.*

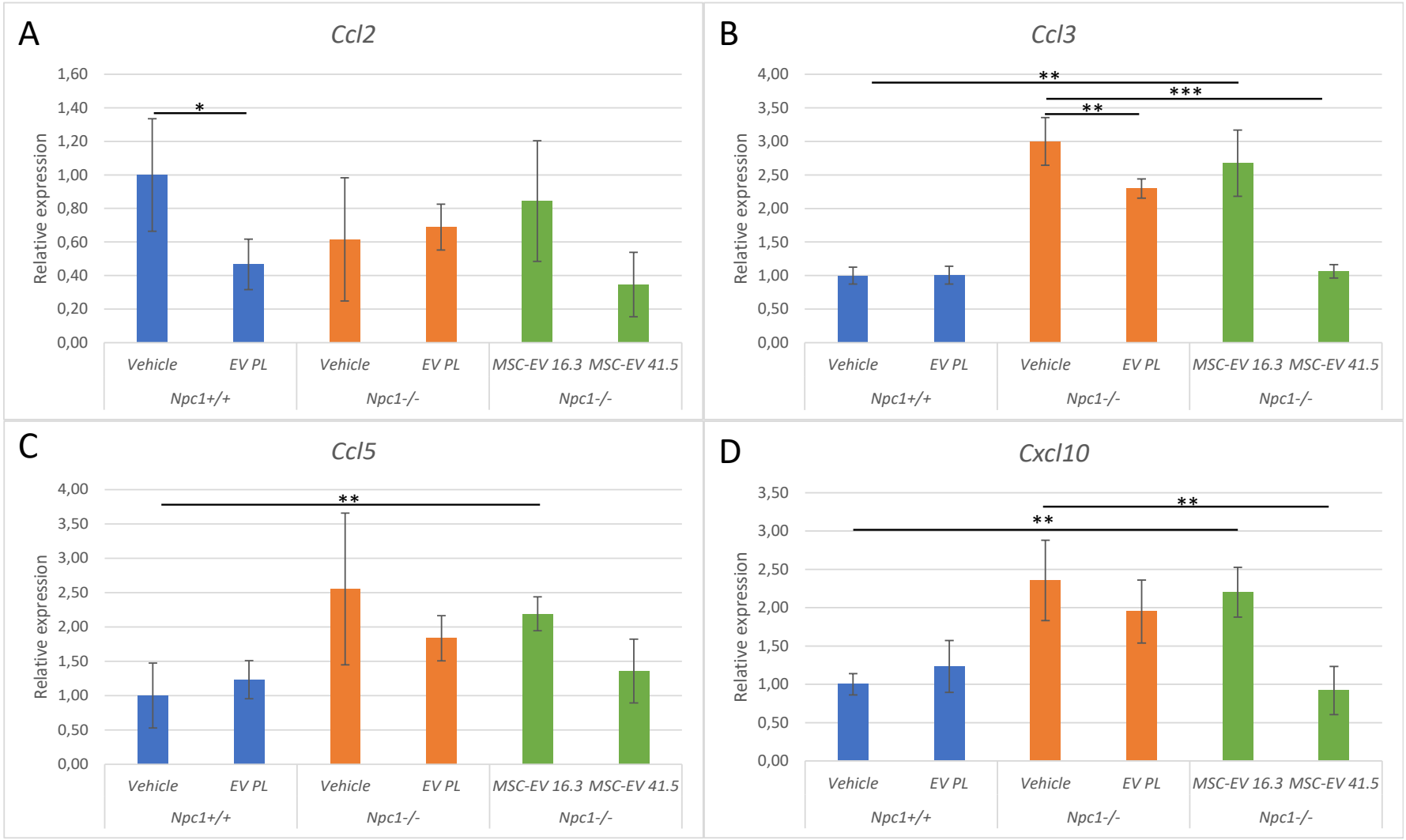

*Figure 5-12 Relative expression of C-C motif chemokine ligand 2 (A), C-C motif chemokine ligand 3 (B), C-C motif chemokine ligand 5 (C) and C-X-C motif chemokine ligand 10 (D) in cerebellum samples after treatment of mice. n = five per group. The error bars represent the standard deviation. T-test is performed and significancy is indicated: * = p < 0,05; ** = p < 0.01; *** = p < 0.001.*

5.3.4.2 Immunohistochemistry

Several IF-stainings are performed on the cerebellum. An overview of the most representative images within one treated group is given in Figure 5-13. The graphs (Figure 5-14) can be used to make a comparison between the groups. The principle of these stainings is described in 3.5.

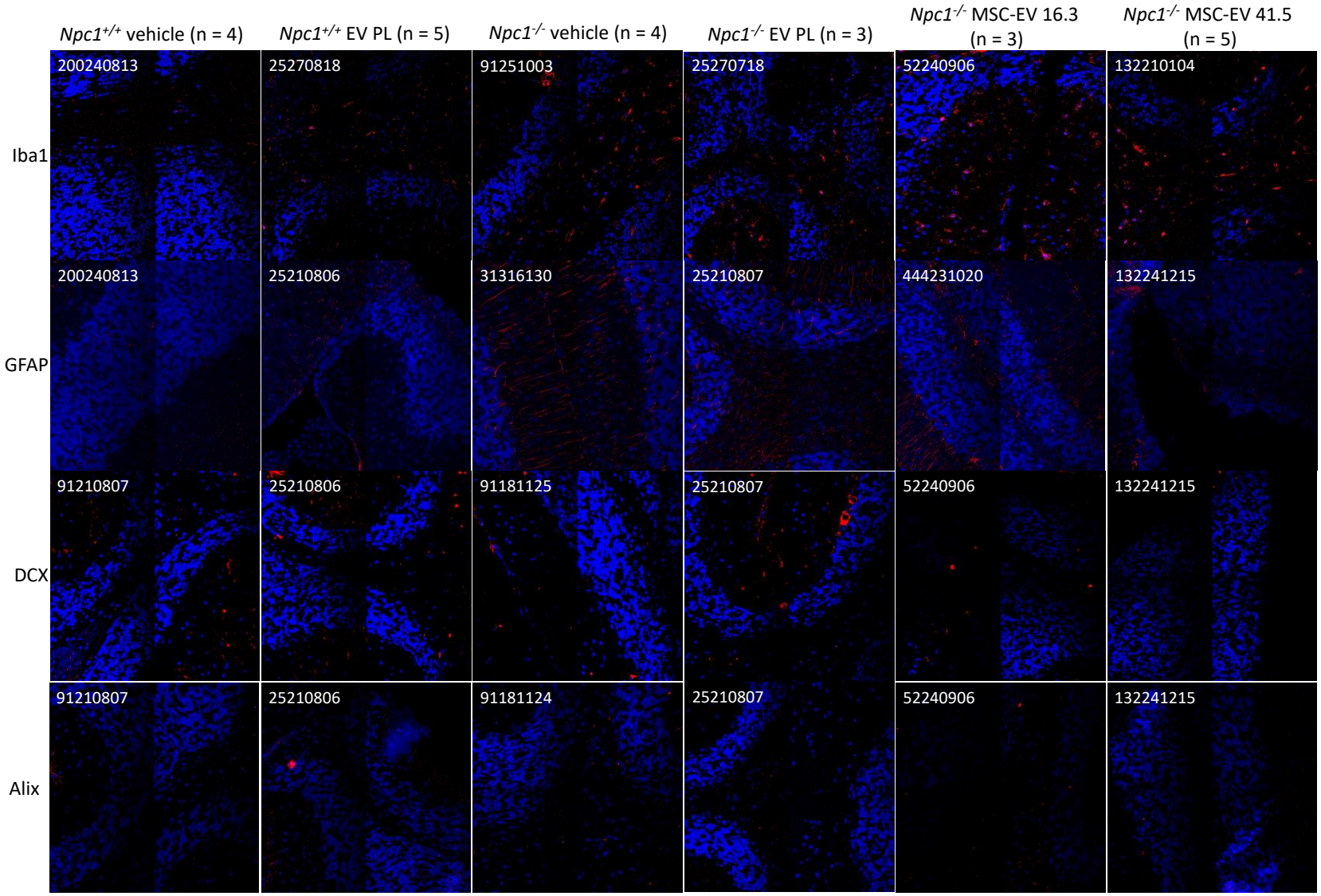

Figure 5-13 Representative images of the performed staining on the cerebellum. Each image represents three up to five images of samples from the same group. The eartag of the mouse is shown in the upper left corner. Magnification = 40x

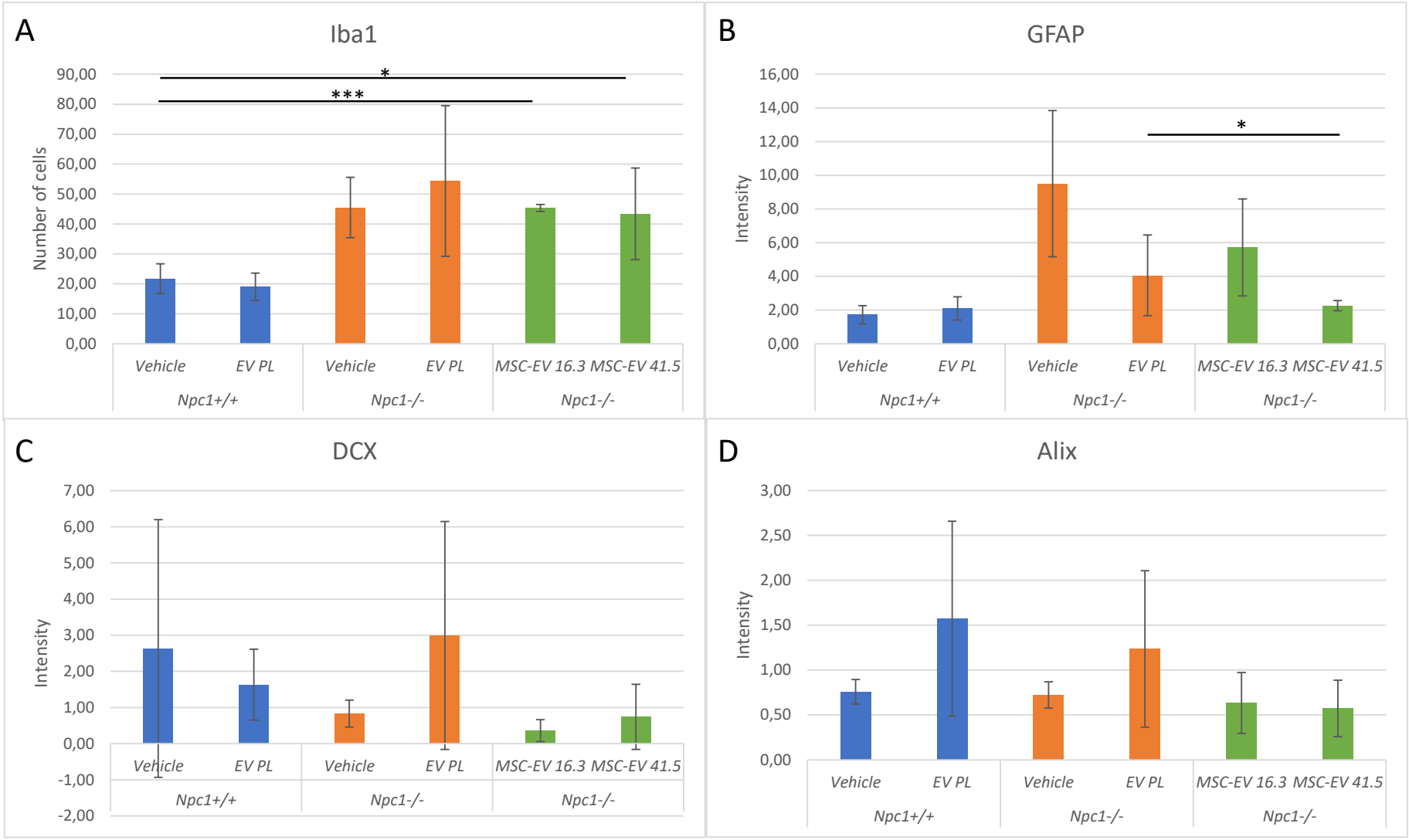

*Figure 5-14 The number of positive cells or the intensity of the signal for the different stainings on the cerebellum. A = ionized calcium-binding adapter molecule 1; B = glial fibrillary acidic protein; C = doublecortin and D = apoptosis-linked gene-2 interacting protein X. The error bars represent the standard deviation. T-test is performed and significancy is indicated: * = p < 0,05; ** = p < 0,01; *** = p < 0,001.*

5.3.5 Hippocampus

5.3.5.1 qPCR

The hippocampus is the fourth brain region that is investigated. Again, RNA is extracted to synthesize cDNA. This cDNA is used to perform qPCR to investigate the expressions of *Tnf*, *Il-1β*, *Inos*, *Iκba*, *Il-4*, *Il-6*, *Ccl2*, *Ccl3*, *Ccl5* and *Cxcl10* (Figure 5-15 and Figure 5-16). These genes have specific functions that are described in 3.3 and 3.4.3.

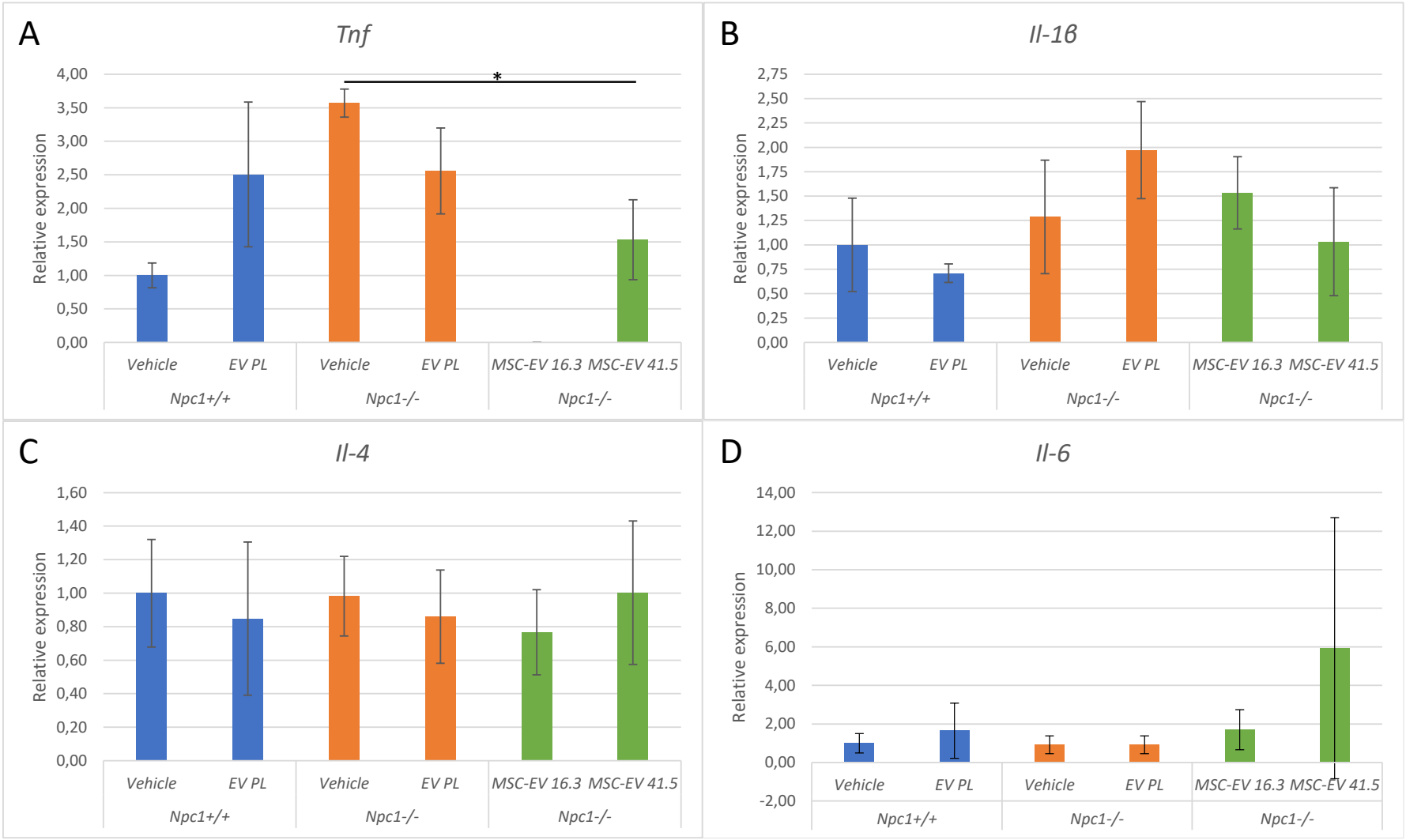

*Figure 5-15 Relative expression of tumour necrosis factor (A), interleukin-1β (B), interleukin-4 (C), interleukin-6 (D) in hippocampus samples after treatment of mice. n = five per group. The error bars represent the standard deviation. T-test is performed and significancy is indicated: * = p < 0,05; ** = p < 0.01; *** = p < 0.001.*

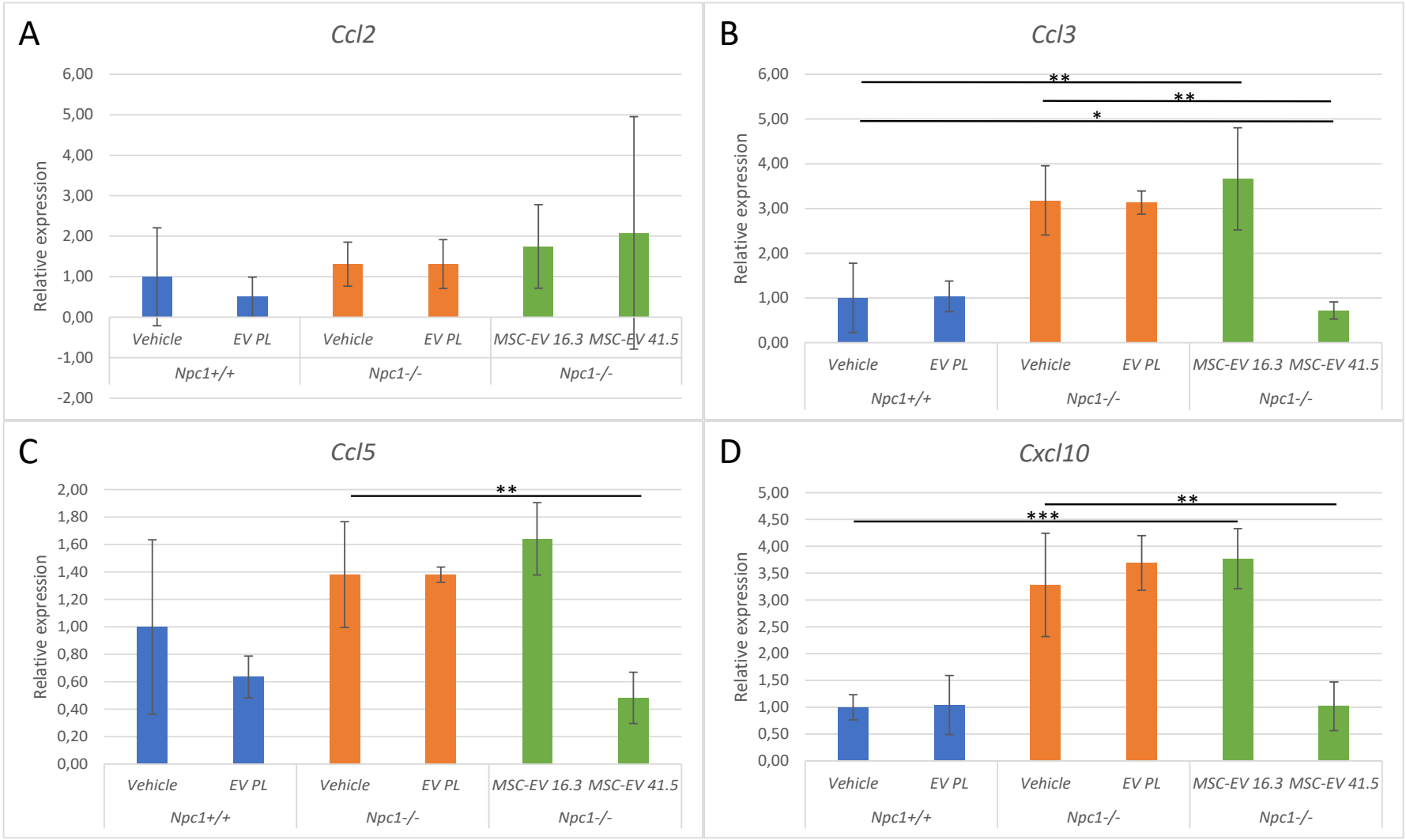

*Figure 5-16 Relative expression of C-C motif chemokine ligand 2 (A), C-C motif chemokine ligand 3 (B), C-C motif chemokine ligand 5 (C) and C-X-C motif chemokine ligand 10 (D) in hippocampus samples after treatment of mice. n = five per group. The error bars represent the standard deviation. T-test is performed and significancy is indicated: * = p < 0,05; ** = p < 0.01; *** = p < 0.001.*

5.3.5.2 Immunohistochemistry

Also on the hippocampus, IF stainings are performed (Figure 5-17). An overview of what these stainings stain for is given in 3.5. The results are shown in Figure 5-18.

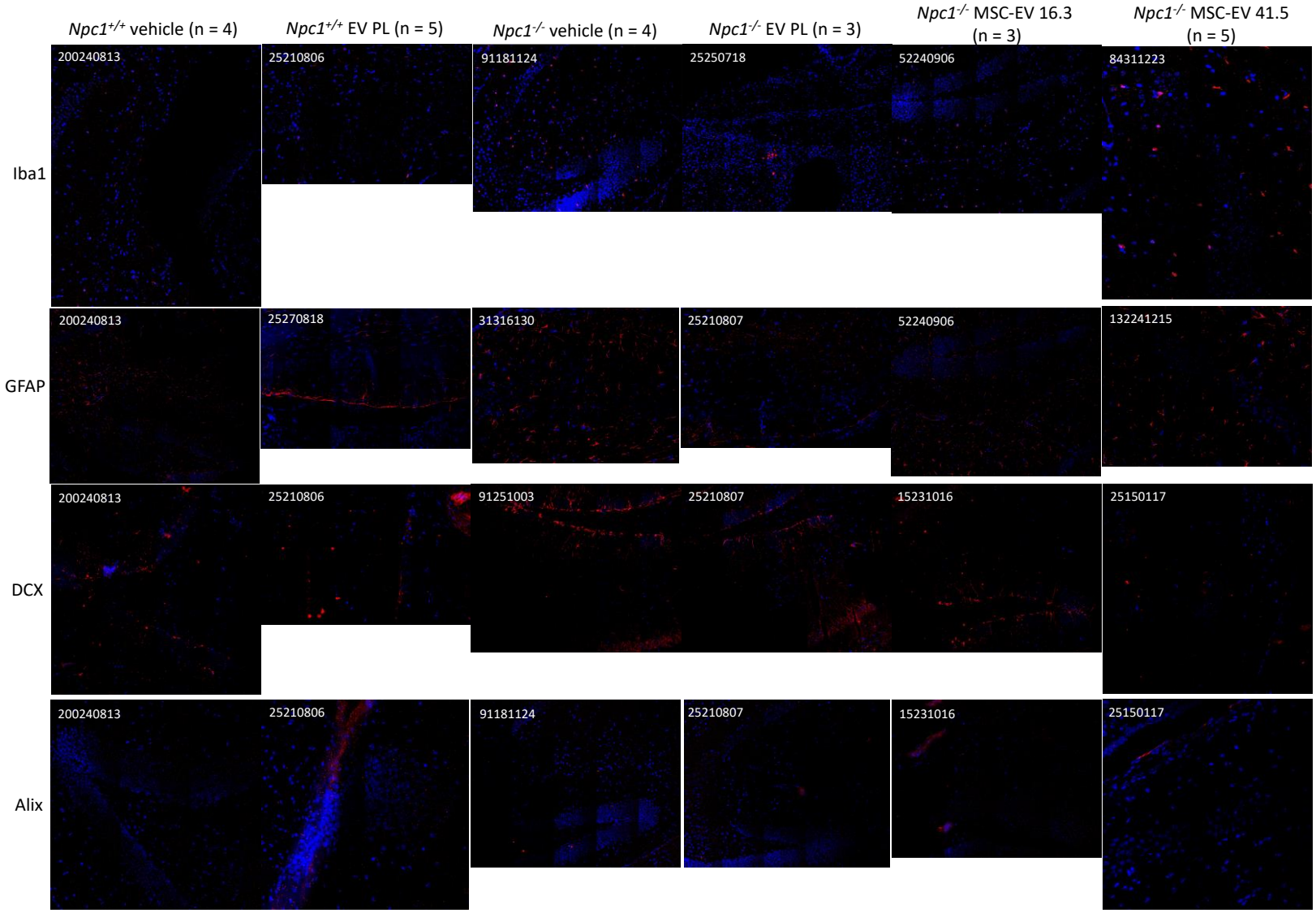

Figure 5-17 Representative images of the performed staining on the hippocampus. Each image represents three up to five images of samples from the same group. The eartag of the mouse is shown in the upper left corner. Magnification = 40x

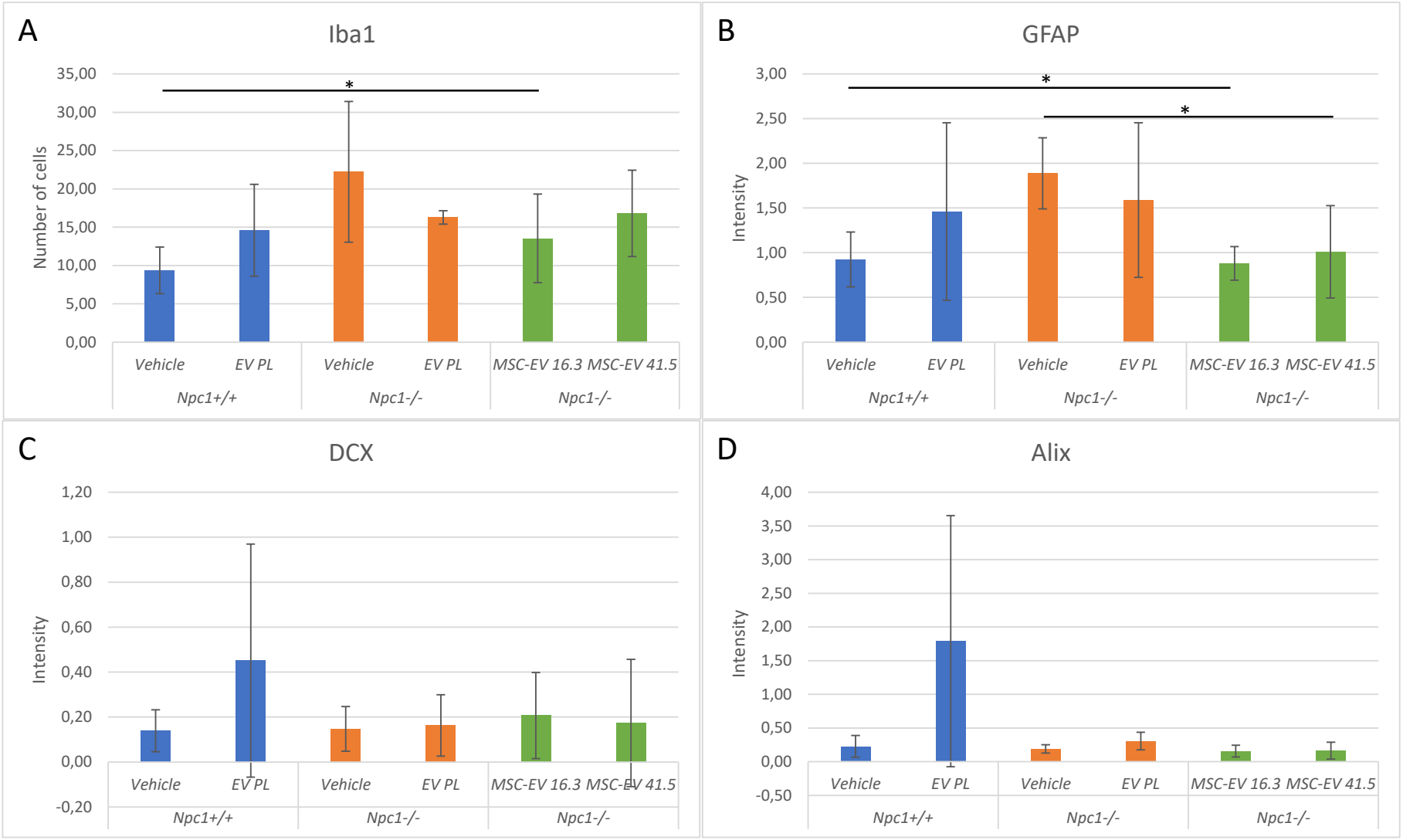

*Figure 5-18 The number of positive cells or the intensity of the signal for the different stainings on the hippocampus. A = ionized calcium-binding adapter molecule 1; B = glial fibrillary acidic protein; C = doublecortin and D = apoptosis-linked gene-2 interacting protein X. The error bars represent the standard deviation. T-test is performed and significancy is indicated: * = p < 0,05; ** = p < 0,01; *** = p < 0,001.*

5.3.6 Corpus striatum

IF is also performed on the *corpus striatum* (Figure 5-19). The results are given in Figure 5-20. The principle behind these stainings can be found in 3.5.

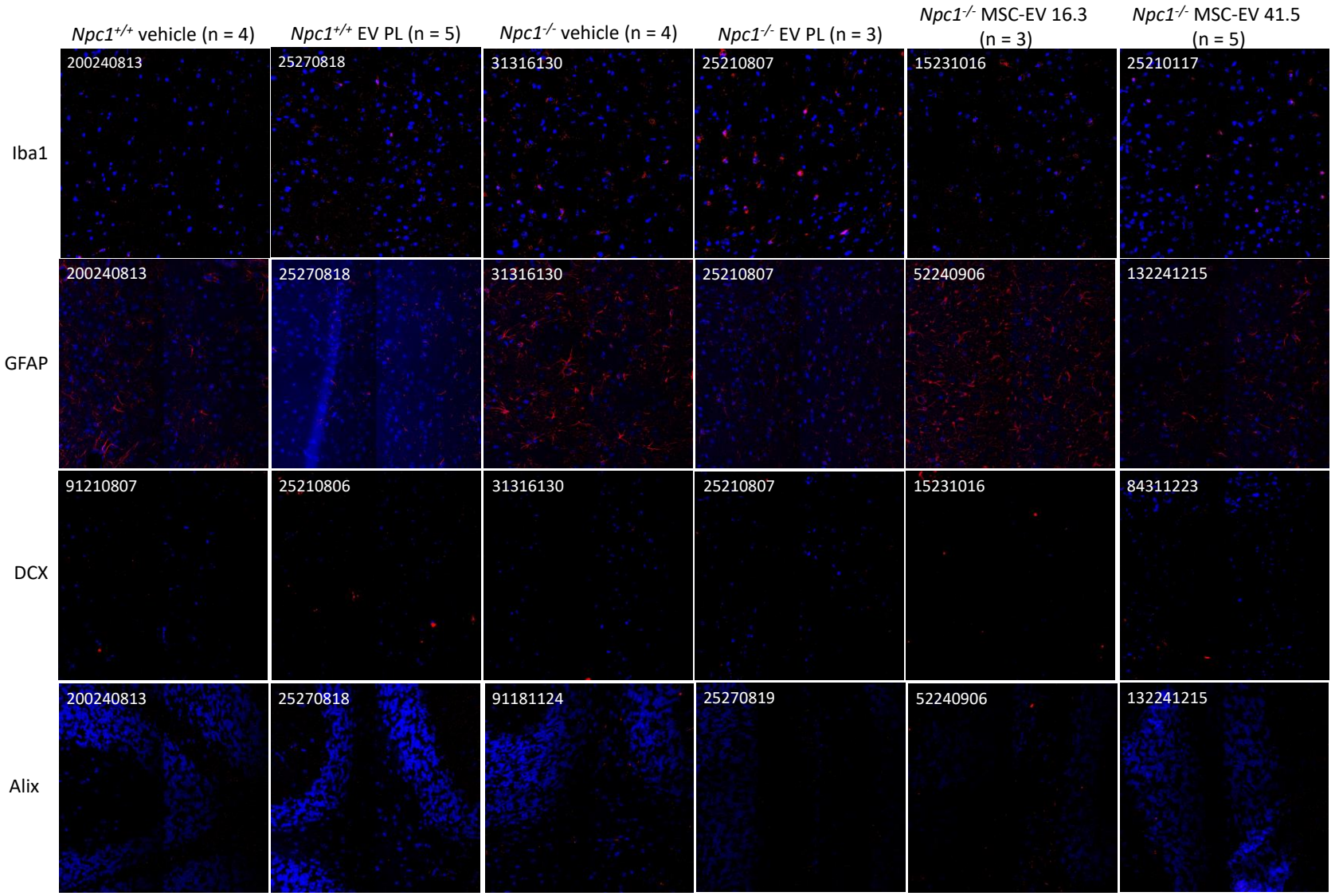

Figure 5-19 Representative images of the performed staining on the corpus striatum. Each image represents three up to five images of samples from the same group. The eartag of the mouse is shown in the upper left corner. Magnification = 40x.

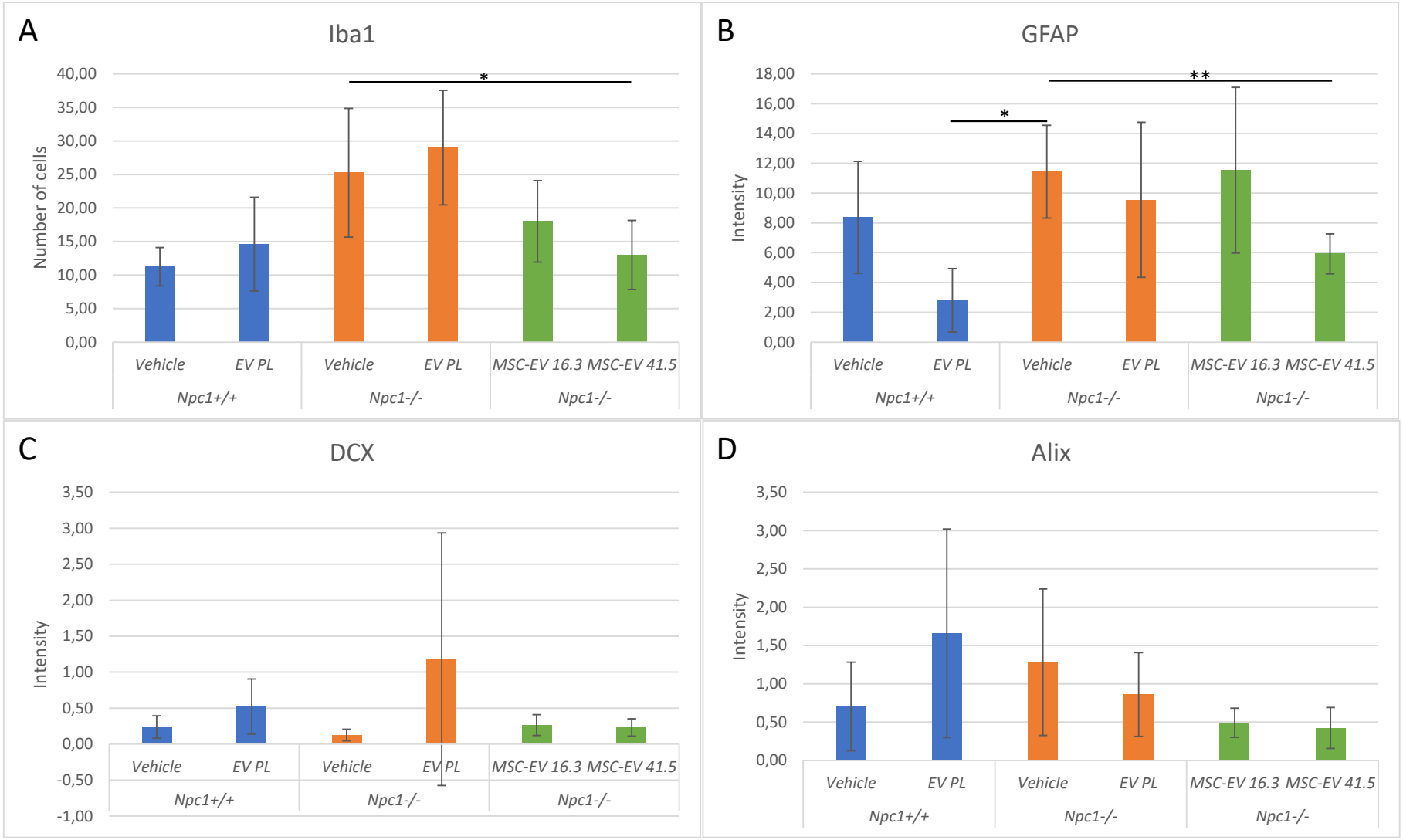

*Figure 5-20 The number of positive cells or the intensity of the signal for the different stainings on the corpus striatum. A = ionized calcium-binding adapter molecule 1; B = glial fibrillary acidic protein; C = doublecortin and D = apoptosis-linked gene-2 interacting protein X. The error bars represent the standard deviation. T-test is performed and significancy is indicated: * = p < 0,05; ** = p < 0,01; *** = p < 0,001.*

5.3.7 Discussion

Besides the peripheral organs, this thesis also focuses on the central nervous system, with the brain in particular. To get an overview of this part of the body, Bio-Plex is performed on CSF. This experiment shows a significant decrease in KC levels after treatment with MSC-EV 41.5 whereby the same levels as in *Npc1*$^{+/+}$ control mice are registered. Studies about the relationship between KC and NPC1 pathology are scarce. The hypothesis is that the neutrophils that are attracted by KC play an important role in the inflammation reaction caused by the pathology. However, in normal conditions neutrophils can't pass the BBB. Vandenbroucke lab is currently studying whether NPC1 pathology affects the CP and therefore the BBB and BCSF. Nevertheless, the decrease in the concentration of KC after administration of MSC-EV 41.5 proves that less neuroinflammation occurs. Also, TNF levels are determined using Bio-Plex, but no significant differences are seen. These findings correspond with earlier studies where also no significant differences in TNF levels are determined. Studies on IFN_{γ}-levels in CSF are also scarce. The original hypothesis was that IFN_{γ} would be increased in *Npc1*$^{-/-}$ mice since these cytokines have a neuroprotective function. However, the results don't show any difference. A possible explanation for that is not found yet. (Cologna et al., 2014; Manda-Handzlik & Demkow, 2019; Ottum et al., 2015)

qPCR is performed to determine the expression of several inflammatory genes while IHC is performed to detect particular markers in tissues. Therefore the brain is divided into different regions including (pre-frontal) cortex, OB, CB, hippocampus and *corpus striatum*. Just like described in 5.2.3, the genes can be divided into different groups based on their expression pattern. In the cerebellum, all investigated genes (except for *Inos* and *Ikba*) are covered by either the first or the second group, stating that MSC-EVs 41.5 have an anti-inflammatory effect in the prefrontal cortex. The overall functions of the genes include activation of macrophages, lymphocytes and T- and B-cells, attraction of monocytes, macrophages and NK-cells and induction of apoptosis. Therefore, the expectation is that IHC will show clear differences between the different groups. However, the findings of the qPCR cannot be extended to these of IHC. In general, no significant differences nor similar patterns as in qPCR are seen. Nevertheless, for Iba1- and GFAP-staining, there is a difference between *Npc1*$^{-/-}$ control mice and *Npc1*$^{+/+}$ control mice. This proves that neuroinflammation does occur in NPC1 pathology. (Brenner, 2014; Idriss & Naismith, 2000; Justiz Vaillant & Qurie, 2021; Liu et al., 2011; Ohsawa et al., 2000; Sokol & Luster, 2015)

Since NPC is relatable with oxidative stress, the hypothesis is to see an increase of *Inos* in *Npc1*$^{-/-}$ mice. The results of this thesis don't confirm this theory as no pattern can be derived from the expression analysis of *Inos.* Also, no pattern can be derived from the expression analysis of *Ikba*. The suggestion is that there is no IκBα-associated apoptosis in NPC1 pathology. (Anavi & Tirosh, 2020; Perkins & Gilmore, 2006; Vázquez et al., 2012)

The same qPCR findings are generally seen in the OB. A difference is that the expression of *Il-4* and *Ccl2* don't show any pattern and thus these genes are placed in the third group. This means that there is no clear difference in differentiation in B- and T-cells between *Npc1*$^{+/+}$ and *Npc1*$^{-/-}$ mice in the olfactory bulb. Moreover, treatment with MSC-EV 41.5 does not have an influence on the chemoattraction of monocytes in the olfactory bulb. In the CB, *Inos*, *Iκba*, *Il-4* and *Il-6* are also placed in the third group while all the other genes show a pattern stating that MSC-EV 41.5 can revert the NPC1 pathology. Furthermore, GFAP-staining on the CB shows a decrease of glial cells after treatment with MSC-EV 41.5 to a level comparable to healthy mice. (Justiz Vaillant & Qurie, 2021; Sokol & Luster, 2015)

In the hippocampus, only *Ccl3*, *Ccl5* and *Cxcl10* show a pattern that confirms the anti-inflammatory effect of MSC-EV 41.5. More specifically, fewer macrophages and NK-cells are expected in that brain region. Since *Cxcl10* is induced by IFN_Y and no significant differences were observed in CSF, the expectation is that MSC-EV 41.5 wouldn't influence the expression of *Cxcl10*. The other investigated genes don't show a pattern at all. For the IF stainings, only GFAP shows a pattern stating that MSC-EV 41.5 has an anti-inflammatory effect. On the *corpus striatum*, only IHC is performed. Here, only Iba1- and GFAP-staining show a decrease in inflammation (more specific microglia, macrophages and glial cells) after treatment with MSC-EV 41.5. This confirms the decrease in expression of *Ccl3* and *Ccl5*. (Brenner, 2014; Liu et al., 2011; Sokol & Luster, 2015)

As described above, the results of the qPCRs don't correspond with the results of the stainings. A first explanation is that there is a big variation between mice of the same group. Furthermore, the mice may be offered too soon after the treatments so that the expected effect on the immune cells didn't have time to develop.

The results of this thesis confirm the results of the paper of Cologna *et al*., where an increase of *Tnf*, *Il-1β*, *Ccl3*, *Ccl5* and *Cxcl10* is reported. The increase of GFAP in *Npc1*$^{-/-}$ mice that is described in the paper of Karten *et al.* is not always visible on the IF stainings that are performed for this thesis. However, the increase of expression of *Il-6* as a consequence of the increase of reactive astrocytes is observable in the PFC and OB. Furthermore, Karten *et al.* also described an increase in the expression of *Ccl2*, which is also confirmed by this thesis. (Cologna et al., 2014; Karten et al., 2009)

Studies have shown an increase in microglia in *Npc1*$^{-/-}$ mice in several brain regions. The difference between *Npc1*$^{+/+}$ and knock-out mice is visible with the Iba1-staining, but no differences have been detected between mice treated with MSC-EV 16.3 or 41.5. DCX, which is a marker for neurogenesis, should be more present in *Npc1*$^{+/+}$ mice, but no big differences between *Npc1*$^{+/+}$ and *Npc1*$^{-/-}$ mice are seen and so no effect after treatment with one of the two MSC-EVs. Also, no differences are seen with the Alix-staining, while the signal should be more intense in *Npc1*$^{-/-}$ mice since more apoptosis has been reported in these mice. A possible explanation for the divergent results of this thesis is that the mice are sacrificed too soon after the treatment to see the expected differences. (Mattei et al., 2006; Peake et al., 2011)

6 Conclusion

As many researchers confirmed, NPC1 pathology can be associated with inflammation that can occur both visceral as neurological. Furthermore, MSC-EVs have promising qualities in the therapeutic field. This bachelor thesis aims to investigate whether MSC-EVs have an anti-inflammatory effect on NPC1 pathology. (NanoView Biosciences, n.d.; Vanier, 2010)

The first experiment whereby the weight gain in the different groups was determined, shows preliminary yet promising results for treatment with MSC-EVs fraction 41.5. For most of the genes and tissues, qPCR and Bio-Plex confirm these findings, whereby a decrease in pro-inflammatory substances is noted after treatment with MSC-EVs 41.5 compared to MSC-EVs 16.3. However, IHC gives results that don't correspond with earlier findings in this thesis. This could be because the mice are sacrificed approximately two weeks after the first treatment and the effect on the immune cells wasn't completely developed yet.

The final answer to the research question is that of the two MSC-EV fractions that are investigated, only MSC-EV fraction 41.5 has an anti-inflammatory effect in NPC1 pathology. Further investigation can include counting the cells that show a positive signal in the immunofluorescence stainings (as for most of the stainings the intensity was determined in this thesis). This experiment could also be repeated but the sampling could take place a few weeks later so that possible changes in immune cells have time to develop. Next, flowcytometry could be performed to determine changes in immune cells both peripheral as neurological. Ultimately, IHC could be performed on the peripheral organs to see whether MSC-EV 41.5 can normalize the morphology.

Bibliography

Anavi, S., & Tirosh, O. (2020). INOS as a metabolic enzyme under stress conditions. *Free Radical Biology and Medicine*, *146*, 16–35. https://doi.org/10.1016/j.freeradbiomed.2019.10.411

Ayanlaja, A. A., Xiong, Y., Gao, Y., Ji, G., Tang, C., Abdikani Abdullah, Z., & Gao, D. (2017). Distinct Features of Doublecortin as a Marker of Neuronal Migration and Its Implications in Cancer Cell Mobility. *Frontiers in Molecular Neuroscience*, *10*. https://doi.org/10.3389/fnmol.2017.00199

Balboa, E., Castro, J., Pinochet, M.-J., Cancino, G. I., Matías, N., José Sáez, P., Martínez, A., Álvarez, A. R., Garcia-Ruiz, C., Fernandez-Checa, J. C., & Zanlungo, S. (2017). MLN64 induces mitochondrial dysfunction associated with increased mitochondrial cholesterol content. *Redox Biology*, *12*, 274–284. https://doi.org/10.1016/j.redox.2017.02.024

Balthazart, J., & Ball, G. F. (2014). Doublecortin is a highly valuable endogenous marker of adult neurogenesis in canaries. *Brain, Behavior and Evolution*, *84*(1), 1–4. https://doi.org/10.1159/000362917

Bi, X., & Liao, G. (2010). Cholesterol in Niemann–Pick Type C disease. *Sub-Cellular Biochemistry*, *51*, 319–335. https://doi.org/10.1007/978-90-481-8622-8_11

Bio-Rad Laboratories Inc. (n.d.-a). *Aurum™ Total RNA Mini Kit*. https://www.bio-rad.com/en-be/product/aurum-total-rna-mini-kit?ID=eb91e411-d011-4032-95e0-cdb29691d4d3

Bio-Rad Laboratories Inc. (n.d.-b). *Aurum™ Total RNA Mini Kit: Instruction Manual*.

Bio-Rad Laboratories Inc. (n.d.-c). *Bio-Plex Pro Cytokine, Chemokine, and Growth Factor Assays—Instruction Manual*.

Bio-Rad Laboratories Inc. (2013, November 20). *Introduction to Size Exclusion Chromatography*. https://www.bio-rad.com/en-be/applications-technologies/introduction-size-exclusion-chromatography?ID=MWHAXJKG4#:~:text=ID%3DMWHAS7E8Z-,Size%20exclusion%20chromatography%20(SEC)%20separates%20molecules%20based%20on%20their%20size,by%20filtration%20through%20a%20gel.&text=within%20the%20matrix.-,Small%20molecules%20diffuse%20into%20the%20pores%20and%20their%20flow%20through,in%20the%20column's%20void%20volume.

Brenner, M. (2014). Role of GFAP in CNS injuries. *Neuroscience Letters*, *565*, 7–13. https://doi.org/10.1016/j.neulet.2014.01.055

Burda, J. E., & Sofroniew, M. V. (2014). Reactive gliosis and the multicellular response to CNS damage and disease. *Neuron*, *81*(2), 229–248. https://doi.org/10.1016/j.neuron.2013.12.034

Chang, T.-Y., Reid, P. C., Sugii, S., Ohgami, N., Cruz, J. C., & Chang, C. C. Y. (2005). Niemann-Pick type C disease and intracellular cholesterol trafficking. *The Journal of Biological Chemistry*, *280*(22), 20917–20920. https://doi.org/10.1074/jbc.R400040200

Christiaens, C., Defever, J., & Quartier, B. (2019). *Instrumentele technieken*. Howest Biomedische Laboratoriumtechnologie.

Cologna, S. M., Cluzeau, C. V. M., Yanjanin, N. M., Blank, P. S., Dail, M. K., Siebel, S., Toth, C. L., Wassif, C. A., Lieberman, A. P., & Porter, F. D. (2014). Human and Mouse Neuroinflammation Markers in Niemann-Pick Disease, type C1. *Journal of Inherited Metabolic Disease*, *37*(1). https://doi.org/10.1007/s10545-013-9610-6

Dardis, A., Zampieri, S., Gellera, C., Carrozzo, R., Cattarossi, S., Peruzzo, P., Dariol, R., Sechi, A., Deodato, F., Caccia, C., Verrigni, D., Gasperini, S., Fiumara, A., Fecarotta, S., Carecchio, M., Filosto, M., Santoro, L., Borroni, B., Bordugo, A., … Bembi, B. (2020). Molecular Genetics of Niemann–Pick Type C Disease in Italy: An Update on 105 Patients and Description of 18 NPC1 Novel Variants. *Journal of Clinical Medicine*, *9*(3), 679. https://doi.org/10.3390/jcm9030679

Decuyper, J. (2020). *FBT04—Werken in een dry lab*. Howest Farmaceutical and Biological Laboratory Science.

Defever, J., Quartier, B., & Van Oostveldt, K. (2019). *Syllabus BLT15 Immunology*. Howest Biomedical Laboratory Science.

Dipharma SA. (n.d.). *Niemann Pick C*. Retrieved 28 February 2021, from https://www.dipharma.ch/science-innovation/metabolic-diseases/niemann-pick-c/

Du, X., Kumar, J., Ferguson, C., Schulz, T. A., Ong, Y. S., Hong, W., Prinz, W. A., Parton, R. G., Brown, A. J., & Yang, H. (2011). A role for oxysterol-binding protein-related protein 5 in endosomal cholesterol trafficking. *The Journal of Cell Biology*, *192*(1), 121–135. https://doi.org/10.1083/jcb.201004142

Fiorenza, M. T., Moro, E., & Erickson, R. P. (2018). The pathogenesis of lysosomal storage disorders: Beyond the engorgement of lysosomes to abnormal development and neuroinflammation. *Human Molecular Genetics*, *27*(R2), R119–R129. https://doi.org/10.1093/hmg/ddy155

Gabandé-Rodríguez, E., Boya, P., Labrador, V., Dotti, C. G., & Ledesma, M. D. (2014). High sphingomyelin levels induce lysosomal damage and autophagy dysfunction in Niemann Pick disease type A. *Cell Death and Differentiation*, *21*(6), 864–875. https://doi.org/10.1038/cdd.2014.4

Gage, G. J., Kipke, D. R., & Shain, W. (2012). Whole Animal Perfusion Fixation for Rodents. *Journal of Visualized Experiments : JoVE*, *65*. https://doi.org/10.3791/3564

Geberhiwot, T., Moro, A., Dardis, A., Ramaswami, U., Sirrs, S., Marfa, M. P., Vanier, M. T., Walterfang, M., Bolton, S., Dawson, C., Héron, B., Stampfer, M., Imrie, J., Hendriksz, C., Gissen, P., Crushell, E., Coll, M. J., Nadjar, Y., Klünemann, H., … Patterson, M. (2018). Consensus clinical management guidelines for Niemann-Pick disease type C. *Orphanet Journal of Rare Diseases*, *13*. https://doi.org/10.1186/s13023-018-0785-7

Greer, W. L., Riddell, D. C., Gillan, T. L., Girouard, G. S., Sparrow, S. M., Byers, D. M., Dobson, M. J., & Neumann, P. E. (1998). The Nova Scotia (Type D) Form of Niemann-Pick Disease Is Caused by a G3097→T Transversion in NPC1. *The American Journal of Human Genetics*, *63*(1), 52–54. https://doi.org/10.1086/301931

Hammond, N., Munkacsi, A. B., & Sturley, S. L. (2019). The complexity of a monogenic neurodegenerative disease: More than two decades of therapeutic driven research into Niemann-Pick type C disease. *Biochimica Et Biophysica Acta. Molecular and Cell Biology of Lipids*, *1864*(8), 1109–1123. https://doi.org/10.1016/j.bbalip.2019.04.002

Hildreth, A., Wigby, K., Chowdhury, S., Nahas, S., Barea, J., Ordonez, P., Batalov, S., Dimmock, D., & Kingsmore, S. (2017). Rapid whole-genome sequencing identifies a novel homozygous NPC1 variant associated with Niemann–Pick type C1 disease in a 7-week-old male with cholestasis. *Cold Spring Harbor Molecular Case Studies*, *3*(5). https://doi.org/10.1101/mcs.a001966

Höglinger, D., Burgoyne, T., Sanchez-Heras, E., Hartwig, P., Colaco, A., Newton, J., Futter, C. E., Spiegel, S., Platt, F. M., & Eden, E. R. (2019). NPC1 regulates ER contacts with endocytic organelles to mediate cholesterol egress. *Nature Communications*, *10*. https://doi.org/10.1038/s41467-019-12152-2

Hovakimyan, M., Meyer, A., Lukas, J., Luo, J., Gudziol, V., Hummel, T., Rolfs, A., Wree, A., & Witt, M. (2013). Olfactory Deficits in Niemann-Pick Type C1 (NPC1) Disease. *PLoS ONE*, *8*(12). https://doi.org/10.1371/journal.pone.0082216

Idriss, H. T., & Naismith, J. H. (2000). TNF alpha and the TNF receptor superfamily: Structure-function relationship(s). *Microscopy Research and Technique*, *50*(3), 184–195. https://doi.org/10.1002/1097-0029(20000801)50:3<184::AID-JEMT2>3.0.CO;2-H

Im, K., Mareninov, S., Diaz, M. F. P., & Yong, W. H. (2019). An introduction to Performing Immunofluorescence Staining. *Methods in Molecular Biology (Clifton, N.J.)*, *1897*, 299–311. https://doi.org/10.1007/978-1-4939-8935-5_26

IRC VIB-UGent Lab Vandenbroecke. (2020, August 7). *NPC1 project: Overview*.

IRC VIB-UGent Lab Vandenbroucke. (2021). *CDNA synthesis (Sensifast cDNA kit)*.

Irun, P., Mallén, M., Dominguez, C., Rodriguez-Sureda, V., Alvarez-Sala, L. A., Arslan, N., Bermejo, N., Guerrero, C., Perez de Soto, I., Villalón, L., Giraldo, P., & Pocovi, M. (2013). Identification of seven novel SMPD1 mutations causing Niemann-Pick disease types A and B. *Clinical Genetics*, *84*(4), 356–361. https://doi.org/10.1111/cge.12076

IZON Science LTD. (2021). *IZON: qEV Isolation*. QEV Overview. https://www.izon.com/qev/overview

Justiz Vaillant, A. A., & Qurie, A. (2021). Interleukin. In *StatPearls*. StatPearls Publishing. http://www.ncbi.nlm.nih.gov/books/NBK499840/

Karten, B., Peake, K. B., & Vance, J. E. (2009). Mechanisms and consequences of impaired lipid trafficking in Niemann-Pick type C1-deficient mammalian cells. *Biochimica Et Biophysica Acta*, *1791*(7), 659–670. https://doi.org/10.1016/j.bbalip.2009.01.025

Kattner, E., Schäfer, A., & Harzer, K. (1997). Hydrops fetalis: Manifestation in lysosomal storage diseases including Farber disease. *European Journal of Pediatrics*, *156*(4), 292–295. https://doi.org/10.1007/s004310050603

KEGG PATHWAY: TNF signaling pathway—Reference pathway. (n.d.). Retrieved 12 May 2021, from https://www.kegg.jp/kegg-bin/highlight_pathway?scale=1.0&map=map04668&keyword=TNF

Kumagai, T., Terashima, H., Uchida, H., Fukuda, A., Kasahara, M., Kosuga, M., Okuyama, T., Tsunoda, T., Inui, A., Fujisawa, T., Narita, A., Eto, Y., & Kubota, M. (2019). A case of Niemann-Pick disease type C with neonatal liver failure initially diagnosed as neonatal hemochromatosis. *Brain and Development*, *41*(5), 460–464. https://doi.org/10.1016/j.braindev.2019.01.004

Lamri, A., Pigeyre, M., Garver, W. S., & Meyre, D. (2018). The Extending Spectrum of NPC1-Related Human Disorders: From Niemann-Pick C1 Disease to Obesity. *Endocrine Reviews*, *39*(2), 192–220. https://doi.org/10.1210/er.2017-00176

Lemeire, K. (2021, February 25). *Microtomy training*.

Li, X., Lu, F., Trinh, M. N., Schmiege, P., Seemann, J., Wang, J., & Blobel, G. (2017). 3.3 Å structure of Niemann–Pick C1 protein reveals insights into the function of the C-terminal luminal domain in cholesterol transport. *Proceedings of the National Academy of Sciences*, *114*(34), 9116–9121. https://doi.org/10.1073/pnas.1711716114

Lima, H., Jacobson, L. S., Goldberg, M. F., Chandran, K., Diaz-Griffero, F., Lisanti, M. P., & Brojatsch, J. (2013). Role of lysosome rupture in controlling Nlrp3 signaling and necrotic cell death. *Cell Cycle (Georgetown, Tex.)*, *12*(12), 1868–1878. https://doi.org/10.4161/cc.24903

Liu, M., Guo, S., Hibbert, J. M., Jain, V., Singh, N., Wilson, N. O., & Stiles, J. K. (2011). CXCL10/IP-10 in infectious diseases pathogenesis and potential therapeutic implications. *Cytokine & Growth Factor Reviews*, *22*(3), 121–130. https://doi.org/10.1016/j.cytogfr.2011.06.001

Maass, F., Petersen, J., Hovakimyan, M., Schmitt, O., Witt, M., Hawlitschka, A., Lukas, J., Rolfs, A., & Wree, A. (2015). Reduced cerebellar neurodegeneration after combined therapy with cyclodextrin/allopregnanolone and miglustat in NPC1: A mouse model of Niemann-Pick type C1 disease. *Journal of Neuroscience Research*, *93*(3), 433–442. https://doi.org/10.1002/jnr.23509

Maeda, Y., Motoyama, K., Nishiyama, R., Higashi, T., Onodera, R., Nakamura, H., Takeo, T., Nakagata, N., Yamada, Y., Ishitsuka, Y., Kondo, Y., Irie, T., Era, T., & Arima, H. (2019). In vivo Efficacy and Safety Evaluation of Lactosyl-β-cyclodextrin as a Therapeutic Agent for Hepatomegaly in Niemann-Pick Type C Disease. *Nanomaterials*, *9*(5), 802. https://doi.org/10.3390/nano9050802

Manda-Handzlik, A., & Demkow, U. (2019). The Brain Entangled: The Contribution of Neutrophil Extracellular Traps to the Diseases of the Central Nervous System. *Cells*, *8*(12). https://doi.org/10.3390/cells8121477

Martello, A., Platt, F. M., & Eden, E. R. (2020). Staying in touch with the endocytic network: The importance of contacts for cholesterol transport. *Traffic*, *21*(5), 354–363. https://doi.org/10.1111/tra.12726

Mattei, S., Klein, G., Satre, M., & Aubry, L. (2006). Trafficking and developmental signaling: Alix at the crossroads. *European Journal of Cell Biology*, *85*(9), 925–936. https://doi.org/10.1016/j.ejcb.2006.04.002

Maue, R. A., Burgess, R. W., Wang, B., Wooley, C. M., Seburn, K. L., Vanier, M. T., Rogers, M. A., Chang, C. C., Chang, T.-Y., Harris, B. T., Graber, D. J., Penatti, C. A. A., Porter, D. M., Szwergold, B. S., Henderson, L. P., Totenhagen, J. W., Trouard, T.

P., Borbon, I. A., & Erickson, R. P. (2012). A novel mouse model of Niemann-Pick type C disease carrying a D1005G-Npc1 mutation comparable to commonly observed human mutations. *Human Molecular Genetics*, *21*(4), 730–750. https://doi.org/10.1093/hmg/ddr505

McCauliff, L. A., Xu, Z., Li, R., Kodukula, S., Ko, D. C., Scott, M. P., Kahn, P. C., & Storch, J. (2015). Multiple Surface Regions on the Niemann-Pick C2 Protein Facilitate Intracellular Cholesterol Transport. *The Journal of Biological Chemistry*, *290*(45), 27321–27331. https://doi.org/10.1074/jbc.M115.667469

McGovern, M. M., Dionisi-Vici, C., Giugliani, R., Hwu, P., Lidove, O., Lukacs, Z., Eugen Mengel, K., Mistry, P. K., Schuchman, E. H., & Wasserstein, M. P. (2017). Consensus recommendation for a diagnostic guideline for acid sphingomyelinase deficiency. *Genetics in Medicine*, *19*(9), 967–974. https://doi.org/10.1038/gim.2017.7

Mengel, E., Klünemann, H.-H., Lourenço, C. M., Hendriksz, C. J., Sedel, F., Walterfang, M., & Kolb, S. A. (2013). Niemann-Pick disease type C symptomatology: An expert-based clinical description. *Orphanet Journal of Rare Diseases*, *8*, 166. https://doi.org/10.1186/1750-1172-8-166

Meridian. (n.d.). *SensiFAST SYBR No ROX Kit—Manual*.

Meridian. (2018, November 27). *SensiFAST™ cDNA Synthesis Kit*. https://www.bioline.com/sensifast-cdna-synthesis-kit.html

Mukhopadhyay, S., Hoidal, J. R., & Mukherjee, T. K. (2006). Role of TNFα in pulmonary pathophysiology. *Respiratory Research*, *7*(1), 125. https://doi.org/10.1186/1465-9921-7-125

NanoView Biosciences. (n.d.). *NanoView—The Guide to Analysis of Extracellular Vesicles*.

Niemann-Pick disease: MedlinePlus Genetics. (2020, August 18). Niemann-Pick Disease. https://medlineplus.gov/genetics/condition/niemann-pick-disease/

Ohsawa, K., Imai, Y., Kanazawa, H., Sasaki, Y., & Kohsaka, S. (2000). Involvement of Iba1 in membrane ruffling and phagocytosis of macrophages/microglia. *Journal of Cell Science*, *113*(17), 3073–3084. https://doi.org/10.1242/jcs.113.17.3073

Ottum, P. A., Arellano, G., Reyes, L. I., Iruretagoyena, M., & Naves, R. (2015). Opposing Roles of Interferon-Gamma on Cells of the Central Nervous System in Autoimmune Neuroinflammation. *Frontiers in Immunology*, *6*. https://doi.org/10.3389/fimmu.2015.00539

Pacheco, C. D., & Lieberman, A. P. (2008). The pathogenesis of Niemann-Pick type C disease: A role for autophagy? *Expert Reviews in Molecular Medicine*, *10*, e26. https://doi.org/10.1017/S146239940800080X

Panina, Y., Germond, A., Masui, S., & Watanbe, T. M. (2018). *Validation of Common Housekeeping Genes as Reference for qPCR Gene Expression Analysis During iPS Reprogramming Process*. https://doi.org/10.1038/s41598-018-26707-8

Peake, K. B., Campenot, R. B., Vance, D. E., & Vance, J. E. (2011). Niemann-Pick Type C1 deficiency in microglia does not cause neuron death in vitro. *Biochimica et Biophysica Acta (BBA) - Molecular Basis of Disease*, *1812*(9), 1121–1129. https://doi.org/10.1016/j.bbadis.2011.06.003

Perkins, N. D., & Gilmore, T. D. (2006). Good cop, bad cop: The different faces of NF-kappaB. *Cell Death and Differentiation*, *13*(5), 759–772. https://doi.org/10.1038/sj.cdd.4401838

Pestana, E. A., Belak, S., Diallo, A., Crowther, J. R., & Viljoen, G. J. (2009). Real-Time PCR – The Basic Principles. In E. Pestana, S. Belak, A. Diallo, J. R. Crowther, & G. J. Viljoen, *Early, rapid and sensitive veterinary molecular diagnostics—Real time PCR applications* (pp. 27–46). Springer Netherlands. https://doi.org/10.1007/978-90-481-3132-7_3

Piano, S., Tonon, M., & Angeli, P. (2018). Management of ascites and hepatorenal syndrome. *Hepatology International*, *12*(Suppl 1), 122–134. https://doi.org/10.1007/s12072-017-9815-0

Pick, L. (1926). Der Morbus Gaucher und die ihm ähnlichen krankheiten (die lipoidzellige Splenohepatomegalie Typus Niemann und die diabetische Lipoidzellenhypoplasie der Milz. *Ergebnisse der Inneren Medizin und Kinderheilkunde (Berlin)*, *29*, 519–627.

Pick, L. (1927). Über lipoidzellige Splenomegalie Typus Niemann-Pick als Stoffwechselerkrankung. *Med. Klinik*, *39*.

Pick, L. (1933). *II. NIEMANN-PICK'S DISEASE AND OTHER FORMS OF SO-CALLED XANTHOMATOSIS*. https://doi.org/10.1097/00000441-193305000-00001

Platt, N., Speak, A. O., Colaco, A., Gray, J., Smith, D. A., Williams, I. M., Wallom, K.-L., & Platt, F. M. (2016). Immune dysfunction in Niemann-Pick disease type C. *Journal of Neurochemistry*, *136 Suppl 1*, 74–80. https://doi.org/10.1111/jnc.13138

Pray, L. A. (2008). *The Biotechnology Revolution: PCR and the Use of Reverse Transcriptase to Clone Expressed Genes*.

Proteintech group, Inc. (n.d.). *IHC blocking*. Retrieved 11 April 2021, from https://www.ptglab.com/support/immunohistochemistry-protocol/ihc-blocking/#

Rimkunas, V. M., Graham, M. J., Crooke, R. M., & Liscum, L. (2009). TNF-α plays a role in hepatocyte apoptosis in Niemann-Pick type C liver disease. *Journal of Lipid Research*, *50*(2), 327–333. https://doi.org/10.1194/jlr.M800415-JLR200

Rio, D. C., Ares, M., Hannon, G. J., & Nilsen, T. W. (2010). Purification of RNA using TRIzol (TRI reagent). *Cold Spring Harbor Protocols*, *2010*(6), pdb.prot5439. https://doi.org/10.1101/pdb.prot5439

Roche Life Science. (n.d.). *LightCycler® 480 Software*.

Roszell, B. R., Tao, J.-Q., Yu, K. J., Gao, L., Huang, S., Ning, Y., Feinstein, S. I., Vite, C. H., & Bates, S. R. (2013). Pulmonary abnormalities in animal models due to Niemann-Pick type C1 (NPC1) or C2 (NPC2) disease. *PloS One*, *8*(7), e67084. https://doi.org/10.1371/journal.pone.0067084

Roszell, B. R., Tao, J.-Q., Yu, K. J., Huang, S., & Bates, S. R. (2012). Characterization of the Niemann-Pick C pathway in alveolar type II cells and lamellar bodies of the lung. *American Journal of Physiology - Lung Cellular and Molecular Physiology*, *302*(9), L919–L932. https://doi.org/10.1152/ajplung.00383.2011

Sokol, C. L., & Luster, A. D. (2015). The Chemokine System in Innate Immunity. *Cold Spring Harbor Perspectives in Biology*, *7*(5). https://doi.org/10.1101/cshperspect.a016303

Speak, A. O., Platt, N., Salio, M., te Vruchte, D. T., Smith, D. A., Shepherd, D., Veerapen, N., Besra, G., Yanjanin, N. M., Simmons, L., Imrie, J., Wraith, J. E., Lachmann, R., Hartung, R., Runz, H., Mengel, E., Beck, M., Hendriksz, C. J., Porter, F. D., … Platt, F. M. (2012). Invariant Natural Killer T cells are not affected by lysosomal storage in patients with Niemann-Pick disease type C. *European Journal of Immunology*, *42*(7), 1886–1892. https://doi.org/10.1002/eji.201141821

Staretz-Chacham, O., Aviram, M., Morag, I., Goldbart, A., & Hershkovitz, E. (2018). Pulmonary involvement in Niemann-Pick C type 1. *European Journal of Pediatrics*, *177*(11), 1609–1615. https://doi.org/10.1007/s00431-018-3219-6

The Jackson Laboratory. (2020a). *002760—C57BLKS/J-Npc1spm/J*. https://www.jax.org/strain/003092

The Jackson Laboratory. (2020b). *003092—BALB/cNctr-Npc1m1N/J*. https://www.jax.org/strain/003092

The Jackson Laboratory. (2020c). *004817—C57BL/6J-Npc1nmf164/J*. https://www.jax.org/strain/003092

Thermo Fisher Scientific. (n.d.). *Basic Principles of RT-qPCR*. https://www.thermofisher.com/be/en/home/brands/thermo-scientific/molecular-biology/molecular-biology-learning-center/molecular-biology-resource-library/spotlight-articles/basic-principles-rt-qpcr.html

Thermo Fisher Scientific. (2016). *Real-time PCR: understanding Ct*.

Thermo Fisher Scientific. (2018). *Ultra-Sensitive ABC Peroxidase Staining Kits*.

Tsiapalis, D., & O'Driscoll, L. (2020). Mesenchymal Stem Cell Derived Extracellular Vesicles for Tissue Engineering and Regenerative Medicine Applications. *Cells*, *9*(4). https://doi.org/10.3390/cells9040991

U.S. National Library of Medicine. (n.d.). *Clinical Trials* [Database]. Retrieved 13 May 2021, from https://clinicaltrials.gov/ct2/home

Vandenbroucke Lab Research | VIB Labs. (n.d.). Retrieved 28 February 2021, from https://vib.be/labs/vandenbroucke-lab/research

Vandendriessche, C. (2021, May 6). *Extracellular vesicles*.

Vanier, M. T. (2010). Niemann-Pick disease type C. *Orphanet Journal of Rare Diseases*, *5*, 16. https://doi.org/10.1186/1750-1172-5-16

Vanier, M. T. (2013). Niemann-Pick diseases. *Handbook of Clinical Neurology*, *113*, 1717–1721. https://doi.org/10.1016/B978-0-444-59565-2.00041-1

Vázquez, M. C., Balboa, E., Alvarez, A. R., & Zanlungo, S. (2012). Oxidative stress: A pathogenic mechanism for Niemann-Pick type C disease. *Oxidative Medicine and Cellular Longevity*, *2012*, 205713. https://doi.org/10.1155/2012/205713

VIB Bioimaging core. (n.d.). *Guidelines For Best Practice in Fixation*.

von Ranke, F. M., Pereira Freitas, H. M., Mançano, A. D., Rodrigues, R. S., Hochhegger, B., Escuissato, D., Araujo Neto, C. A., da Silva, T. K. B., & Marchiori, E. (2016). Pulmonary Involvement in Niemann-Pick Disease: A State-of-the-Art Review. *Lung*, *194*(4), 511–518. https://doi.org/10.1007/s00408-016-9893-0

Walterfang, M., Chien, Y.-H., Imrie, J., Rushton, D., Schubiger, D., & Patterson, M. C. (2012). Dysphagia as a risk factor for mortality in Niemann-Pick disease type C:

Systematic literature review and evidence from studies with miglustat. *Orphanet Journal of Rare Diseases*, *7*(1), 76. https://doi.org/10.1186/1750-1172-7-76

Williams, I. M., Wallom, K.-L., Smith, D. A., Al Eisa, N., Smith, C., & Platt, F. M. (2014). Improved neuroprotection using miglustat, curcumin and ibuprofen as a triple combination therapy in Niemann–Pick disease type C1 mice. *Neurobiology of Disease*, *67*, 9–17. https://doi.org/10.1016/j.nbd.2014.03.001

Xu, Y., Zhang, Q., Tan, L., Xie, X., & Zhao, Y. (2019). The characteristics and biological significance of NPC2: Mutation and disease. *Mutation Research/Reviews in Mutation Research*, *782*, 108284. https://doi.org/10.1016/j.mrrev.2019.108284

Addenda

Addendum 1 – List of materials and reagents
Addendum 2 – Protocol for RNA-extraction using Aurum™ Total RNA Mini Kit by Bio-Rad
Addendum 3 – Protocol for cDNA synthesis
Addendum 4 – Primer sequences
Addendum 5 – Protocol for cutting paraffin sections
Addendum 6 – Analysis of the results
Addendum 7 - Graphs expression of *Inos* and *Iκba* in several tissues

Addendum 1

Table 8-1 Alphabetical list of the materials and their companies

Material	Company
Antigen retriever	BioVendor
Aurum™ Total RNA Mini Kit	Bio-Rad
Bio-Plex 200 reader	Bio-Rad
Centrifuge	Eppendorf
Centrifuge (4 °C)	Eppendorf
Coverslips	Menzel-Gläzer
Fluorescence microscope	ZEISS
Hydrophobic barrier pen	ImmunoEdge
Microplate washer	BioTek
Discussion microscope	Olympus
Microscopic slides	Klinipath
Microtome	Microm HM360 #2 - Coolcut Paraffin Microtome Thermo Scientific Rotary Microtome Microm HM340E
NanoDrop	Thermo Scientific NanoDrop 1000
PCR-machine	Bio-Rad C1000 Touch Thermal Cycler
Plate shaker	Heidolph
qPCR machine	Roche
Thermoblock	Eppendorf
TissueLyser	Qiagen
Varistain apparatus	Thermo Shandon Varistain 24-4 -- Robot Stainer

Table 8-2 Alphabetical list of the reagents and their companies

Reagent	Company
100 % ethanol RNase-free	Merck
100 % methanol	VWR chemicals
10x PBS	Sigma-Aldrich
30 % H_2O_2	Sigma-Aldrich
ABC kit	Vector
Alix-antibody	Abcam
Antigen unmasking solution - Citrate buffer	Vector
Aurum™ Total RNA Mini Kit	Bio-Rad
Bio-Plex Pro Mouse Cytokine 23-plex Assay	Bio-Rad
Boric Acid	Merck
Bovine serum albumine	Jackson ImmunoResearch
Chloroform (RNase-free)	Merck
DAPI	DAKO
DCX-antibody	Abcam
GAR dylight 633	Thermo Scientific
GFAP-antibody	Agilent
Goat anti-rabbit biotin	DAKO
HCl 37 %	Merck
Iba1-antibody	Wako Chemicals
Normal goat serum	Thermo Scientific
PVA + DABCO	Sigma-Aldrich
qPCR primers	IDT
RNA-later	Life technologies
SensiFAST™ cDNA Synthesis Kit	Meridian
SensiFAST™ SYBR® No-ROX Kit	Meridian
Streptavidin Dylight 633	Thermo Scientific
Tris(hydroxymethyl)aminomethane	Biosolve
Triton X-100	Roche
TRIzol	Ambion
TSA	R&D systems

Addendum 2

Materials:

- 100 % ethanol (RNase-free)
- Beads
- Bio-rad Aurum Kit
- Centrifuge
- Centrifuge (4 °C)
- Chloroform (RNase-free)
- Eppendorf tubes 2 ml
- Hydrochloric acid (HCl) 37 %
- NanoDrop
- Pipettes
- Samples
- Thermoblock
- TissueLyser
- Tissues
- Tris(hydroxymethyl)-aminomethane
- TRIzol
- Tweezers

Preparation of solutions:

- **60 % ethanol (RNase-free):** Dilute 100 % ethanol (RNase-free) with nuclease-free water.
- **DNase solution:** Add 250 µl Tris (10 mM, pH 7.5) to the lyophilized DNase from the kit. Dilute this solution with a factor of 15 using DNase dilution solution (stored at 4 °C) from the kit.
- **Low stringency wash:** Add 80 ml 100 % ethanol (RNase-free) to the bottle of low stringency wash before the first use.
- **Tris 10 mM, pH 7,5 (1 litre):** Make a solution of 10 mM Tris in 900 ml distilled water and adapt the pH using 37 % HCl. Add distilled water until 1 litre.

Protocol (10 samples per run)

1. Thaw the samples and label the (Eppendorf) tubes.
2. When the sample is preserved in RNA-later, transfer the tissue to an empty tube.
3. Add 800 µl TRIzol.
4. Make sure the tissue is submerged in TRIzol.
5. Add beads to the tubes. (one to two beads per tube)
6. Lyse the tissue using the TissueLyser. Put the settings at 20 Hz and five minutes.
7. Add 120 µl RNase-free chloroform to the tubes.
8. Shake the tubes thoroughly by shaking up and down approximately 20 times.
9. Centrifuge at 14 000 g during 15 minutes at 4 °C. In the meantime
    a. Prepare the DNase solution
    b. Transfer elution solution to an Eppendorf tube and keep it at 70 °C in a thermoblock.
    c. Add 600 µl 60 % ethanol in new eppendorf tubes of 2 ml.
10. Transfer the aqueous layer to the Eppendorf tubes with 60 % ethanol.
11. Shake the Eppendorf tubes thoroughly by shaking up and down approximately 20 times.
12. Pipet 700 µl of the homogenized lysate into the RNA binding column placed on a wash tube.

13 Centrifuge at maximum speed for one minute.
14 Discard the filtrate from the wash tube.
15 Pipet the rest of the lysate into the RNA binding column.
16 Centrifuge at maximum speed for one minute.
17 Discard the filtrate from the wash tube.
18 Add 700 µl low stringency wash onto the column.
19 Centrifuge at maximum speed for 30 seconds.
20 Discard the solution from the wash tube.
21 Add 84 µl of DNase solution onto the column and let incubate at room temperature for 20 minutes.
22 Centrifuge at maximum speed for one minute.
23 Discard the filtrate from the wash tube.
24 Add 700 µl high stringency wash onto the column.
25 Centrifuge at maximum speed for 30 seconds.
26 Discard the column from the wash tube.
27 Add 700 µl low stringency wash onto the column.
28 Centrifuge at maximum speed for 30 seconds.
29 Discard the solution from the wash tube.
30 Transfer the column onto a new wash tube.
31 Centrifuge at maximum speed for one minute.
32 Transfer the column onto 1,5 ml Eppendorf tubes.
33 Add 60 µl elution buffer onto the column.
34 Centrifuge at maximum speed for one minute.
35 Remove the column and keep the 1,5 ml Eppendorf tubes for measurement of RNA-concentration using NanoDrop.

Protocol NanoDrop

1 Start the programme on the computer.
2 Open the valve and clean it with a tissue.
3 To calibrate and to blank: add 1 µl of elution buffer and close the valve.
4 Let calibrate and measure blank.
5 Open the valve and clean it with a tissue.
6 Pipet 1 µl of the sample and close the valve.
7 Let measure the concentration, 260 nm/280 nm-ratio and 260 nm/230 nm-ratio.
8 Repeat step 5-7 for every sample.

Addendum 3

Materials:

- 1,5 ml Eppendorf tube
- PCR tubes with lids
- PCR machine
- Pipettes
- SensiFAST™ cDNA Synthesis Kit
- RNase-free water.

Preparation of solutions

PCR mix: Mix 4 µl TransAmp buffer and 1 µl reverse transcriptase per sample.

Protocol:

1 Calculate the amount of sample needed by dividing 500 ng with the RNA-concentration of the sample.
2 Calculate the amount of RNase-free water by subtracting 15 µl with the amount of sample.
3 Add RNase-free water to the PCR tubes.
4 Add sample in the PCR tubes.
5 Add 5 µl PCR mix in the PCR tubes.
6 Mix and spin down.
7 Put in the PCR machine and run the program (**Fout! Verwijzingsbron niet gevonden.**).

Table 8-3 PCR program for cDNA-synthesis

	Temperature (°C)	Duration
Step 1 1: Annealing	25	10 minutes
Step 2: Reverse transcription	42	15 minutes
Step 3: Inactivation	85	5 minutes
Step 4: Storage	4	

8 Store at -20 °C until further usage.

Addendum 4

Table 8-4 Sequences of the qPCR-primers

Gene	Primer	Sequence
Gadph	Forward	TGAAGCAGGCATCTGAGGG
	Reverse	CGAAGGTGGAAGAGTGGGAG
Hprt	Forward	AGTGTTGGATACAGGCCAGAC
	Reverse	CGTGATTCAAATCCCTGAAGT
Rpl	Forward	CCTGCTGCTCTCAAGGTT
	Reverse	TGGTTGTCACTGCCTCGTACTT
Ubc	Forward	AGGTCAAACAGGAAGACAGACGTA
	Reverse	TCACACCCAAGAACAAGCACA
Tnf	Forward	ACCCTGGTATGAGCCCATATAC
	Reverse	ACACCCATTCCCTTCACAGAG
Il-1β	Forward	CACCTCACAAGCAGAGCACAAG
	Reverse	GCATTAGAAACAGTCCAGCCCATAC
Inos	Forward	CAGCTGGGCTGTACAAACCTT
	Reverse	CATTGGAAGTGAAGCGTTTCG
Iκba	Forward	TGAAGGACGAGGAGTACGAGC
	Reverse	TTCGTGGATGATTGCCAAGTG
Il-4	Forward	GGTCTCAACCCCCAGCTAGT
	Reverse	GCCGATGATCTCTCTCAAGTGAT
Il-6	Forward	TAGTCCTTCCTACCCCAATTTCC
	Reverse	TTGGTCCTTAGCCACTCCTTC
Ccl2	Forward	TTAAAAACCTGGATCGGAACCAA
	Reverse	GCATTAGCTTCAGATTTACGGGT
Ccl3	Forward	TTCTCTGTACCATGACACTCTGC
	Reverse	CGTGGAATCTTCCGGCTGTAG
Ccl5	Forward	GCTGCTTTGCCTACCTCTCC
	Reverse	TCGAGTGACAAACACGACTGC
Cxcl10	Forward	GACGGTCCGCTGCAACTG
	Reverse	GCTTCCCTATGGCCCTCATT

Addendum 5

Materials

- Demineralized water
- Microscope
- Microscopic slides
- Microtome
- Pasteur pipettes
- Samples embedded in paraffin
- Tissues

Method:

1 Fill the bath of the microtome with demineralized water until the edge and set the temperature between 40 °C and 45 °C.
2 Put the places of the microtome together to make it ready to use. Let the water flow down the slide into the bath.
3 Set the thickness of trimmed slices at 20 µm and the thickness of cut slices at 5 µm.
4 Label the microscope slide with a pencil. Also mention the chronological number of the slide.
5 Plug the cooling block of the microtome in and put the paraffine embedded sample in the holder.
6 Trim the block until the region of interest is visible on the cut (20 µm).
7 Check under the microscope if the region of interest is visible, if not return to step 6.
8 Cut slices with a thickness of 5 µm.
9 Collect the sections on the microscope slides. Pasteur pipettes can be useful to let the sections flow down the slide into the bath. Torn sections can easily be picked up with a Pasteur pipette.
10 Let the microscope slides dry overnight on a tissue.

Addendum 6

Analysis of qPCR results

The results are analysed using an Excel template made during one of the lessons 'Working in a dry lab' at Howest University of Applied Sciences (Decuyper, 2020). The following steps have proceeded:

1. Look at the melting curves of each gene and write down the wells that differ too much from the curve.
2. Rebuild the format of the qPCR plates in Excel.
3. Remove the wells that differ too much from the melting curve.
4. Remove the wells from the technical replicates if the C_t-value differs more than 1 unit.
5. Calculate the mean of the technical replicates.
6. Make a brief overview of the mean C_t-value of each gene for each condition.
7. Calculate the normalization factor:
    - I Determine the two most stable HKGs by looking at the melting curve. The two HKGs with the most consistent curves should be used.
    - II Determine the lowest C_t-value for each HKG.
    - III Calculate the difference between the lowest C_t-value and the original C_t-value for each condition and each HKG.
    - IV Calculate the quantitative expression value by using the formula 'two by the power of the difference'.
    - V Determine the normalization factor by taking the mean of the quantitative expression value for each condition.
8. Calculate the normalized expression values of the genes of interest:
    - I Determine the lowest C_t-value for each gene of interest.
    - II Calculate the difference between the lowest C_t-value and the original C_t-value for each condition and each gene.
    - III Calculate the quantitative expression value by using the formula 'two by the power of the difference'.
    - IV Normalize the expression by dividing the quantitative expression value by the normalization factor of the same condition.
9. Determine the mean and the standard deviation of the five biological replicates within one group.
10. Perform the F-test between:
    - I *Npc1*$^{-/-}$ EV PL and *Npc1*$^{-/-}$ vehicle
    - II *Npc1*$^{+/+-}$ EV PL and *Npc1*$^{+/+-}$ vehicle
    - III MSC-EV 41.5 and *Npc1*$^{-/-}$ vehicle
    - IV MSC-EV 41.5 and *Npc1*$^{+/+-}$ vehicle
    - V MSC-EV 16.3 and *Npc1*$^{-/-}$ vehicle
    - VI MSC-EV 16.3 and *Npc1*$^{+/+-}$ vehicle

11 Perform the student T-test between:
    I *Npc1*$^{-/-}$ EV PL and *Npc1*$^{-/-}$ vehicle
    II *Npc1*$^{+/+-}$ EV PL and *Npc1*$^{+/+-}$ vehicle
    III MSC-EV 41.5 and *Npc1*$^{-/-}$ vehicle
    IV MSC-EV 41.5 and *Npc1*$^{+/+-}$ vehicle
    V MSC-EV 16.3 and *Npc1*$^{-/-}$ vehicle
    VI MSC-EV 16.3 and *Npc1*$^{+/+-}$ vehicle

    Depending on the p-value of the F-test, the unpaired T-test should be with equal ($p > 0,05$) or unequal ($p < 0,05$) variance.
12 Make graphical representations of the calculated data.

Immunofluorescence stainings

After imaging, the results can be analysed using Fiji and Zen.
When the cells need to be counted:

1 Open the image in Fiji.
2 Split the channels (Image > Color > Split channels).
3 Adapt the brightness and contrast of both channels of the image until the intensity of the signal is as high as possible with as little background signal as possible. (Image > Adjust > Brightness/Contrast)
4 Remove the remaining background signal of both channels. (Image > Adjust > Threshold)
5 Merge the channels (Image > Color > Merge channels).
6 Count the cells with a signal in both channels.
7 Save the image (File > Save as > Jpeg).
8 Make sure the area of the images is equal or correct by implementing a factor correcting the difference in the area.
9 Make a graphic representation of the results.

When the amount of signal needs to be determined:

1 Open all the images in Zen blue.
2 Adapt the brightness, contrast as well as background signal by moving the limits of the histogram.
3 Copy, paste and adapt the histogram on the other images until no image has a background signal left.
4 Save the images as .jpg-files. (File > Save as)
5 Open the .jpg-files in Fiji.
6 Split the channels (Image > Color > Split channels).
7 Analyse the amount of the signal of the channel of the staining of interest (Analyse > Set Measurements > 'Area', 'Mean gray value', 'Integrated density' > OK; Analyse > Measure)
8 Copy and paste the values into an Excel file.

9 Make sure the area of the images is equal or correct the gray value by multiplying by a factor correcting the difference in the area.
10 Make a graphic representation of the results.

Addendum 7

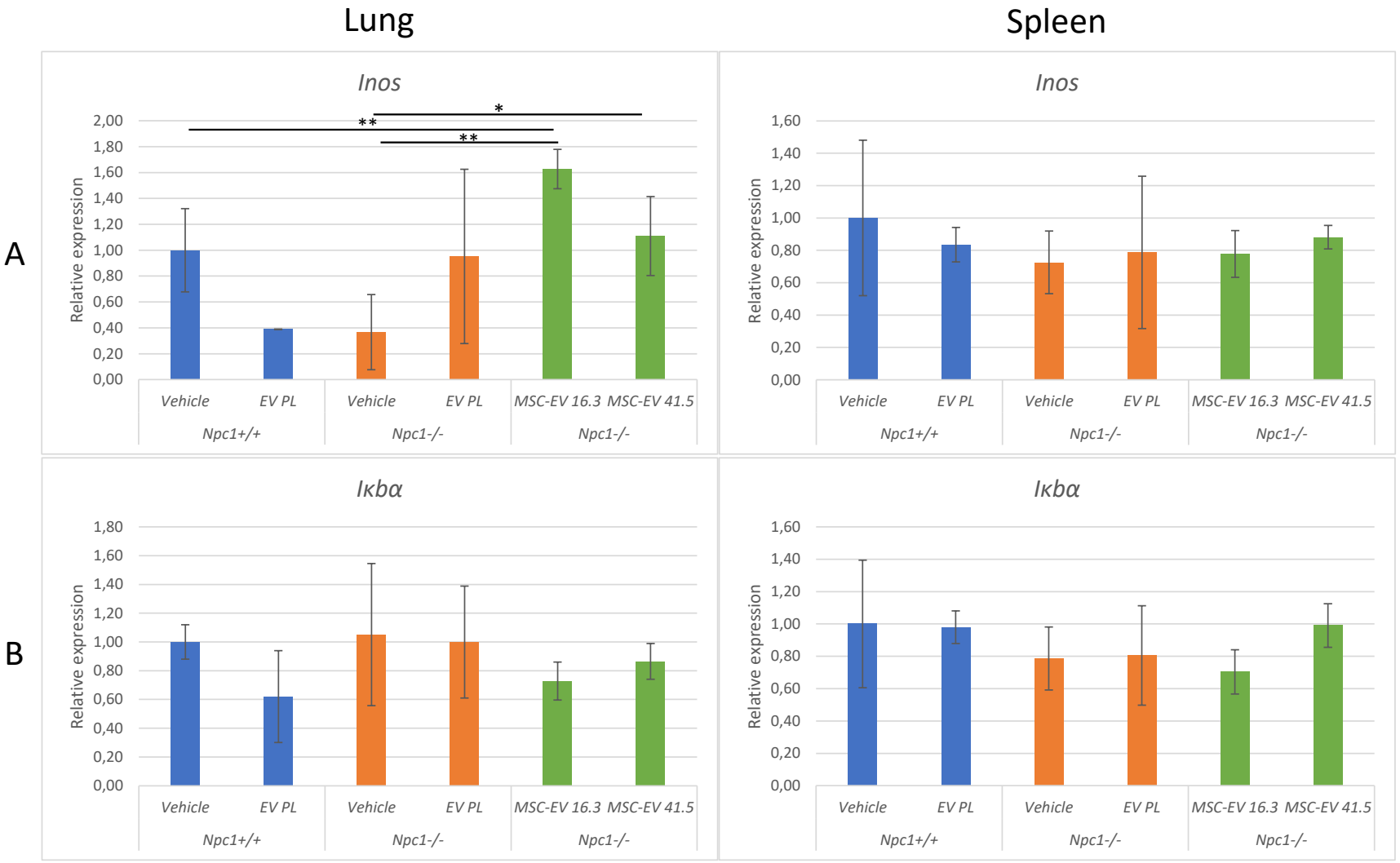

*Figure 8-1 Relative expression of Inos (A) and Iκbα (B) in lung and spleen samples after treatment of mice. T-test is performed and significancy is indicated: * = p < 0,05; ** = p < 0.01; *** = p < 0,001.*

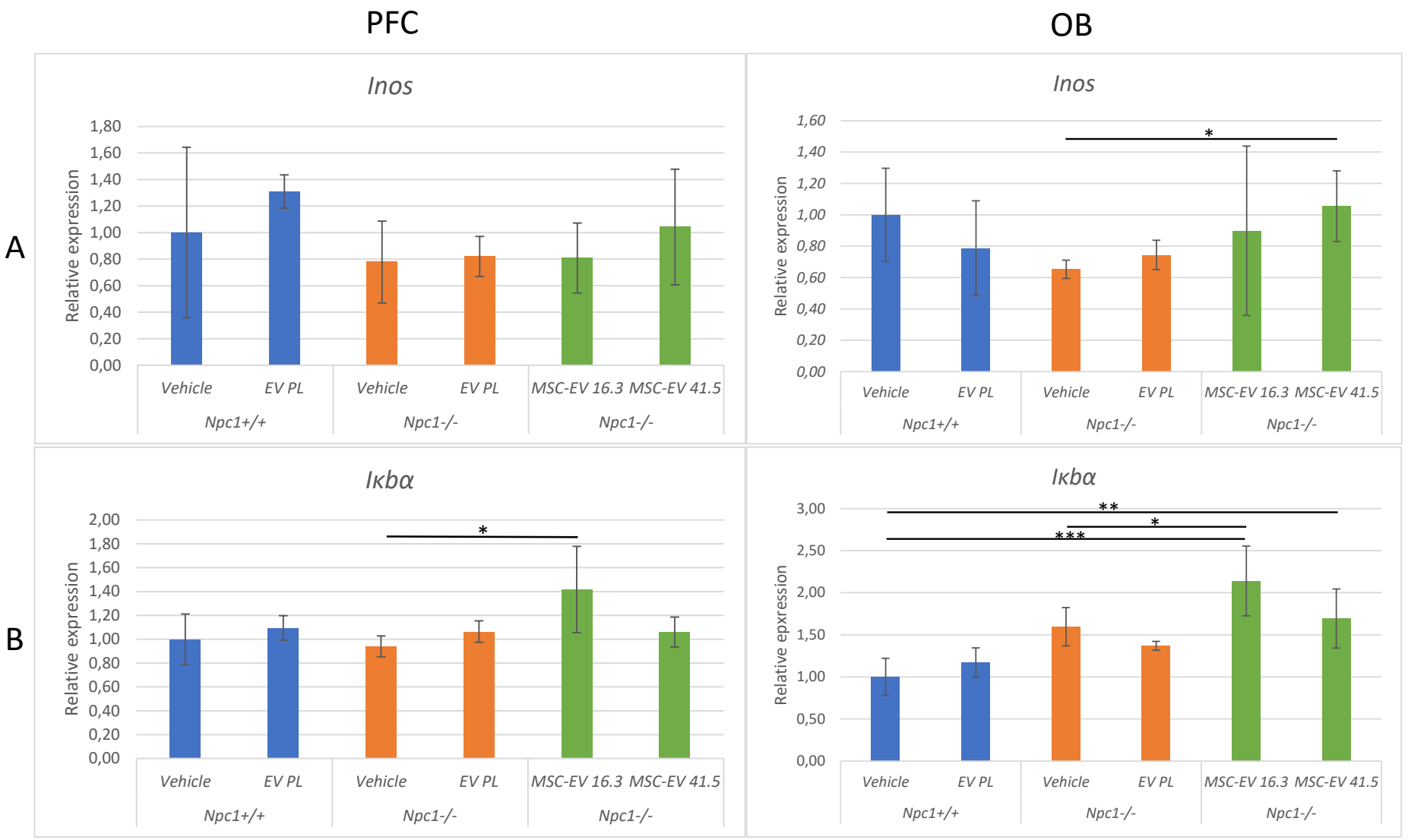

*Figure 8-2 Relative expression of Inos (A) and Iκbα (B) in PFC and OB samples after treatment of mice. T-test is performed and significancy is indicated: * = p < 0,05; ** = p < 0.01; *** = p < 0.001.*

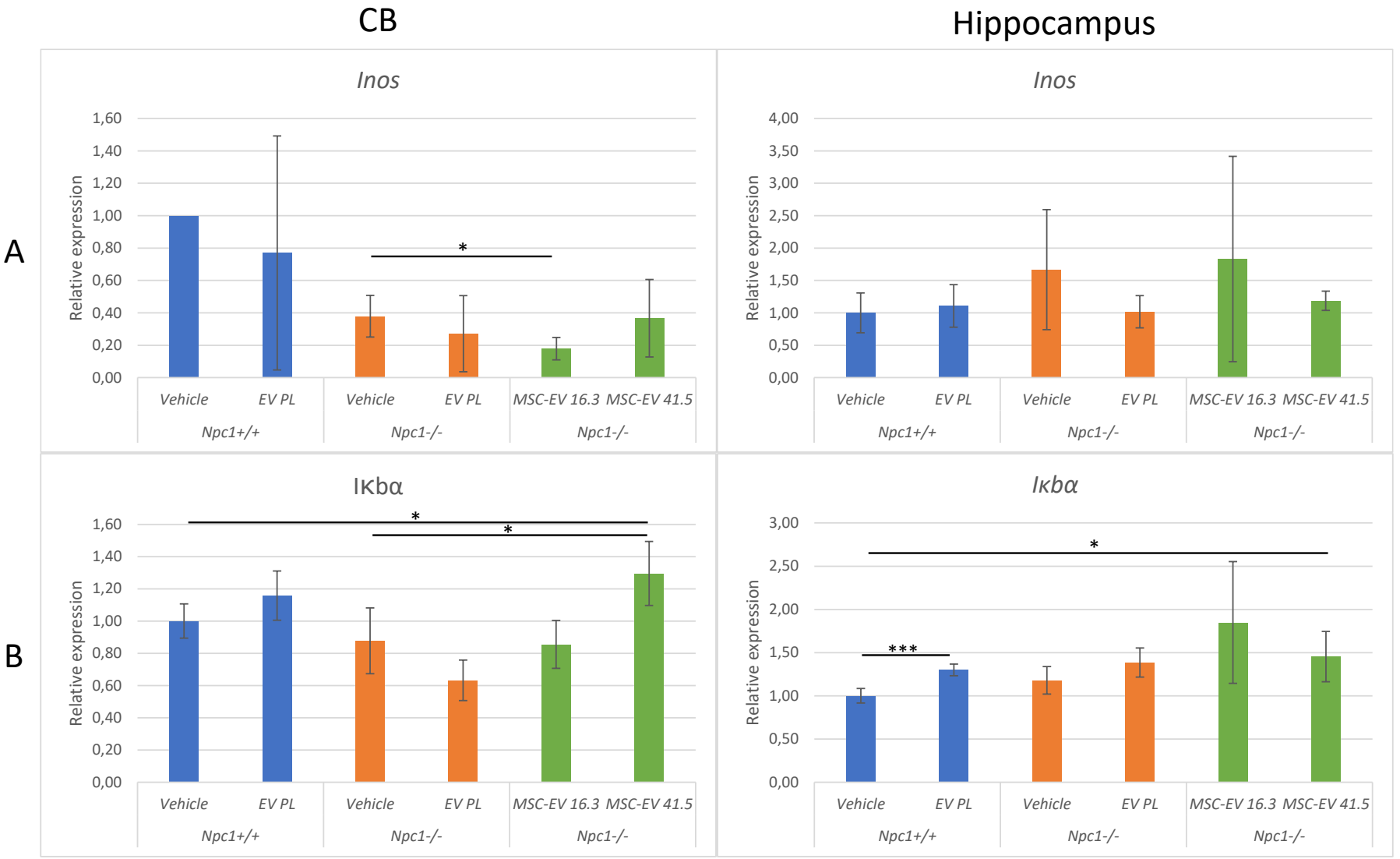

*Figure 8-3 Relative expression of Inos (A) and Iκbα (B) in OB and hippocampus samples after treatment of mice. T-test is performed and significancy is indicated: * = p < 0,05; ** = p < 0.01; *** = p < 0.001.*